THE VULNERABLITY OF AUCKLAND CITY'S BUILDINGS TO TEPHRA HAZARDS

A thesis

submitted in partial fulfilment of the requirements for the degree of

Master of Science in Geology

at

The University of Canterbury

by

George Thomas Williams

University of Canterbury

2016

Frontispiece

Every act of creation is first of all an act of destruction

Pablo Picasso

Abstract

Tephra hazards can cause widespread impacts to buildings which reduce available housing and commercial activities during post-eruption recovery and create a large burden on insurance and construction sectors. Impacts can be reduced by undertaking loss assessments to inform pre-eruption recovery planning but limited understanding of how vulnerable buildings are to certain aspects of tephra hazard makes accurate loss assessments challenging. The objectives of this thesis are to develop quantitative methods to assess building vulnerability to ballistic and tephra fall hazards which can then be used to inform tephra impact assessments in Auckland, New Zealand.

To achieve these objectives building vulnerability has been quantified through the development of fragility and vulnerability functions. These functions can be used to relate hazard intensity (i.e. tephra fall thickness) with what assets are exposed (i.e. residential buildings) to predict impact. Development of new fragility functions has used data from post-eruption building surveys at Mt Ontake and Mt Usu, review of relevant literature, and novel ballistic cannon experiments. A total of 93 experiments were carried out on 4 roof and wall claddings commonly used in New Zealand construction, impacted by dense volcanic rocks moving at up to 39 m/s. The claddings were highly vulnerable to perforation by perpendicular impacts but were able to deflect oblique impacts to receive significantly less damage. The velocity of building material fragments ejected during experiments was also measured with implications for life safety. Conducting and analysing these experiments represents the first known attempt at quantifying building vulnerability to ballistics using fragility functions.

The fragility and vulnerability functions developed from this research were then used in an impact assessment to determine likely building damage and insurance losses for a credible Auckland Volcanic Field (AVF) eruption scenario. The eruption modelled significant damage to buildings located within 3 km of the eruptive centre. In the ballistic impact assessment, over 800 ballistics directly impacted 486 buildings. Most impacts were modelled to have caused cladding perforation (maximum damage), but the overall damaged area on all impacted buildings was small enough that repairs are

likely to be economic. In the tephra impact assessment over 200,000 buildings were impacted by >0.1 mm of ash with repair costs from structural damage estimated at $0.4-1.2 billion. However 97% of buildings impacted did not receive tephra loads sufficient to cause structural damage. Therefore non-structural damage is a large source of uncertainty in the impact assessment.

The results from the literature review, building surveys, experiments and modelling have implications for response (e.g. life safety actions) and recovery planning (e.g. building repairs, building waste disposal) as part of disaster risk reduction in Auckland and globally.

Acknowledgements

Firstly - thanks to my sweet supervisor team: Tom Wilson, Ben Kennedy, Jim Cole and Nick Horspool for all the enthusiasm and support this past year. Tom and Ben, thank you for coming up with such a wicked thesis topic with so many opportunities. Thanks Jim for always asking when you might be able to review my next piece of writing and for always having an open door to your office. Thanks Nick for providing so much intense building data, without which I would not have any models to present.

Huge thanks to my Ballistics Buddy Bec! You've been a big part of all the coolest moments this past year and they wouldn't have been the same without you. You've been such a great mentor and I'm looking forward to working with you in the future.

To the rest of my fellow CoUGARs Alec, Ali, Dan, Heather and Josh. We've shared in many an epic trip this year and it always makes me happy to see you guys are in the office. And to Alec especially - thanks for your patience in helping me this year with anything and everything thesis related. From teaching me the basics of excel through to writing python codes together. You've been a great person to share in the battle through Masters with.

To everyone in office 401 – Thanks for the banter and the reminder not to take work too seriously, whilst also providing many examples of what happens when you leave it all to the last minute! Additionally thank you to the technical staff who have helped this past year, in particular Matt Cockcroft, Chris Grimshaw, Rob Spiers and Sacha Baldwin-Cunningham. And thanks to all the other friendly staff and students who make this place into the great department it is.

This project was supported by funding from the Mason Trust, EQC and the Natural Hazards Research Platform, without which fieldwork would not have been possible.

A big thank you to my Christchurch whanau for being a never ending supply of delicious food and 5 pm Bombay Sapphires. To my mum and my sisters, thanks for all abandoning me this year to go live overseas. Just kidding! Thank you for the supportive, strangely timed skype calls and for the blissful daydream of a future holiday to come visit you. To my father Alan, thank you for being such an incredible role model for me. I've definitely got some of your Williams Workaholic gene but I love what I'm doing right now so I don't mind one bit.

Contents

List of Figures

List of Tables

Chapter 1 Introduction

1.1 Context of the study

Volcanic eruptions are violent, uncontrollable events which produce hazards that can impact on all aspects of society, including buildings. The most destructive volcanic hazards include pyroclastic density currents, volcanogenic tsunamis and lahars which account for 71% of recorded deaths associated with volcanic eruptions (Auker et al., 2013). Tephra fall on the other hand is more of a disruptive hazard, being the most common and geographically widespread volcanic hazard but associated with only 3% of recorded deaths (Simkin et al., 2001; Auker et al., 2013). Due to the widespread nature of this hazard, it has the potential to cause disruption and damage to buildings over large geographic areas, leading to serious societal impacts (Wilson et al., 2012). Fortunately, previous eruptions from around the world have shown that these impacts can be reduced with proactive, pre-event risk management.

Volcanic risk management has successfully reduced the number of deaths associated with volcanic hazards through increased public education and increased volcanic surveillance contributing to more effective warnings and evacuations (ESCAP, 1999). In the past, research into assessing and reducing volcanic risk has typically been focussed on analysis of the hazard itself (Douglas, 2007). This has allowed the implementation of engineering solutions and more thoughtful land use planning prior to eruptions. However, compared to the research on volcanic phenomena which cause hazards, much less attention has been given to the impacts of the hazards to different sectors of society (e.g. critical infrastructure, agriculture and buildings (Green and Rose, 2005; Wilson, 2015)). To evaluate and mitigate the risk to an exposed asset, consideration of hazard alone is not sufficient. Consideration of the asset's vulnerability (propensity to suffer impact) is also required (Figure 1). This has been identified as a critical need to achieve more effective volcanic risk management (Wilson et al., 2014; Maqsood et al., 2015).

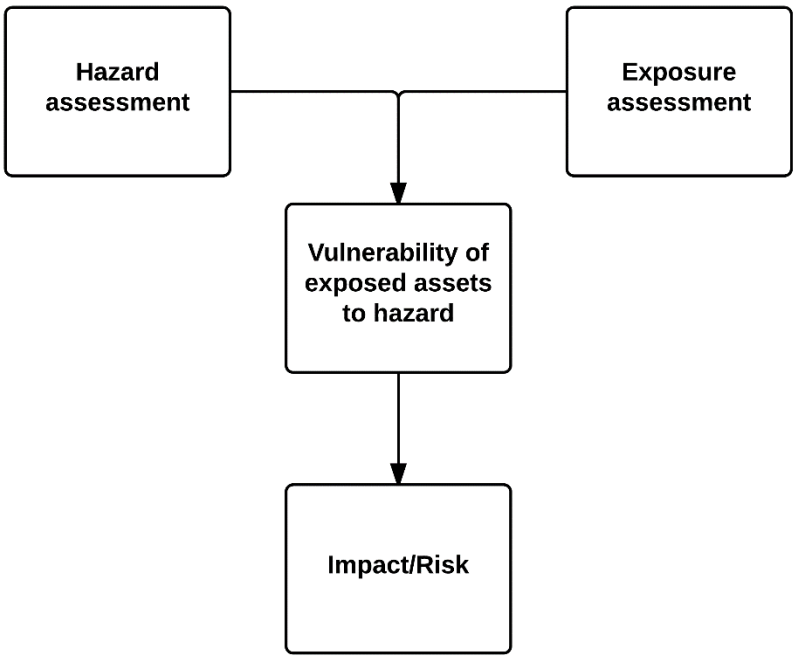

Figure 1: The three key components of risk/impact assessment.

One negative impact which contributes to volcanic disasters are impacts to buildings which can reduce available housing and commercial activities during the post-eruption recovery and place a heavy burden on insurance and construction sectors. Accurately assessing the likely extent of building damage and insurance losses prior to eruption can lessen impacts by informing pre-event recovery planning. Unfortunately there are certain volcanic hazards for which our understanding of building vulnerability is relatively limited, making accurate impact assessments challenging. Not all volcanic hazards require a detailed understanding of how they impact buildings. For example, highly destructive hazards such as lahars and lava flows can be considered to have binary impacts meaning if the hazard is present it will destroy any building it impacts but if the hazard is absent, it will not impact at all . Tephra fall and ballistic hazards can cause a wider variety of impacts. Heavy tephra falls and ballistic projectiles can destroy buildings which are relatively close to the vent but impacts can still occur >100 kilometres away with light tephra falls causing non-structural damage to a larger numbers of exposed buildings (Blong, 1984; Wilson et al., 2012) (Throughout this thesis tephra fall and ballistics are collectively referred to as tephra, with tephra fall pertaining to volcanic ejecta that settles out of an eruption plume and ballistics

pertaining to ejecta that is too large to be convected into a plume and is therefore ejected with a near parabolic, ballistic trajectory).

Most tephra-building impacts research focusses on structural damage caused by heavy tephra fall loads (e.g. Zuccaro et al., 2008; Jenkins and Spence, 2009; Maqsood et al., 2015). This is likely due to situations where there are high building densities in close proximity to active stratovolcanoes (as is the case at Vesuvius or Pinatubo for example (Spence et al., 1996; Zuccaro et al., 2008)). Tephra fall from largescale eruptions in these areas can cause damage or collapse to large numbers of buildings. This is an issue because building repairs can constitute a costly and time consuming stage of recovery following major disasters (e.g. Mount Pinatubo 1991, (Spence et al., 1996); Rabaul 1994, (Blong, 2003) and the Christchurch earthquake sequence 2010-2011,(Doherty, 2011)) and because heavy tephra loads can cause catastrophic roof collapse potentially injuring or killing any sheltering occupants (Pomonis et al., 1999; Spence et al., 2005a).

However for most eruptions, tephra falls are too light to cause widespread structural damage. In the Auckland context for example, tephra falls from AVF eruptions are expected to be relatively light and therefore unlikely to cause extensive structural damage (Magill et al., 2006a; Magill et al., 2006b). Despite this, risk assessments have identified tephra fall as the most significant hazard facing the Auckland region. This is because high building density means heavy tephra falls and ballistics can cause severe impacts close to the vent (Houghton et al., 2006) and because light tephra falls from AVF eruptions or other volcanoes and volcanic centres further afield (e.g. Mt Taranaki, Okataina volcanic centre, Tongariro volcanic centre (Magill and Blong, 2005)) can still cause widespread damage and disruption to non-structural building components. Knowledge on the vulnerability of these components to light tephra falls is largely qualitative and requires further investigation. A second aspect of tephra fall impacts which requires investigation given Auckland's high building density and the unknown location of future eruptive vents, are the impacts associated with relatively short ranged but highly destructive ballistic impacts. These impacts form a large source of uncertainty in Auckland's volcanic risk assessments because little is known about how vulnerable buildings are to ballistics. By undertaking a quantitative assessment of building vulnerability to these aspects of tephra fall impacts, uncertainty

can be reduced resulting in more accurate risk assessments and the adoption of more appropriate risk mitigation measures.

This thesis aims to improve the quantification of tephra-building vulnerability with a focus on quantifying the vulnerability of Auckland's buildings to both tephra fall and ballistic hazards from locally sourced AVF eruptions. Depending on the vent location of the next AVF eruption, many buildings may be damaged or destroyed, leading to significant repair and reconstruction costs during the recovery phase of the disaster. Quantification of building vulnerability can also identify which buildings are the most resilient to impacts and which could benefit most from mitigation measures. This information may be invaluable for anyone forced to shelter-in-place in the event of a short lead in time prior to the next AVF eruption (with minimum times estimated as low as 5 hours (Blake et al., 2006)). Quantification of tephra-building vulnerability can be achieved by following the processes outlined in the risk management framework below.

1.2 Applying a risk management framework to building vulnerability assessment

The following risk management framework is used globally as a common guideline for organisations and research groups seeking to reduce risk in a logical and consistent manner. In the framework set out by Standards New Zealand (2009), risk management may be achieved following risk assessment and treatment. Risk assessment has three stages, these are risk identification, risk analysis and risk evaluation (Figure 2). This framework provides risk managers with a systematic approach as they contribute to volcanic risk management. As such, this thesis will adhere to the framework with a focus on risk assessment by following the three stages: identifying, analysing and evaluating risk for buildings subjected to tephra fall and ballistic impacts.

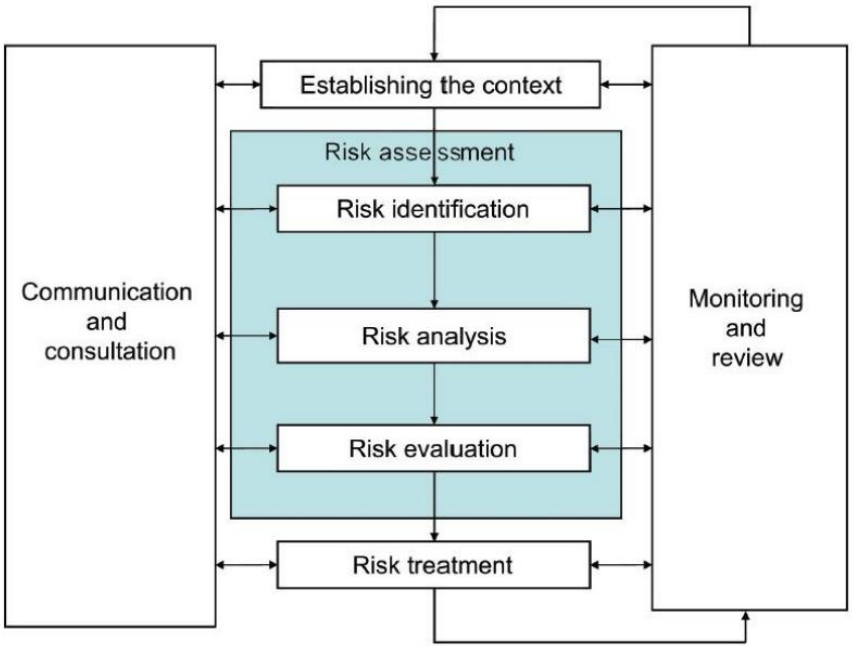

Figure 2: Diagram of the risk management framework (from Standards New Zealand , 2009)

Figure 3 relates terms used in the risk management framework. In this thesis, hazard is defined as the probability of a specific volcanic phenomena occurring with the potential to adversely affect society (e.g. tephra fall on a city) (Blong, 2000). Vulnerability expresses the degree to which elements (e.g. people, buildings, etc.) are likely to be impacted when exposed to hazard (Douglas, 2007). Risk is the combination of these two factors; the probability the hazard will occur and the expected impact to exposed elements.

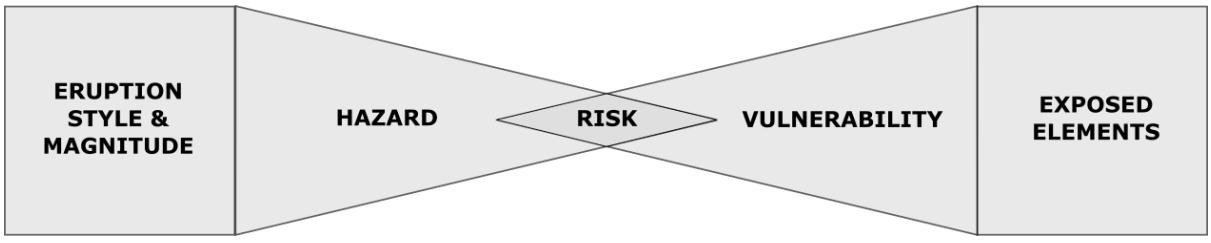

Figure 3: Conceptual relationship between hazard, exposure, vulnerability and risk. After Crozier and Glade (2006).

1.2.1 Establishing the context

To be effective, the risk assessment process first requires establishment of the risk context (Standards New Zealand, 2009). This involves an organization articulating its risk management scope, goals and strategies. This planning is required to identify and

justify the resources that will be used during the risk management process. Establishing the context also helps ensure that the risk management approach adopted is appropriate to the organization and to the obstacles that may affect the achievement of its objectives (Standards New Zealand, 2009).

1.2.2 Risk identification

After the context has been established, the risk management process begins with risk identification. Risk identification requires initial identification of hazard, which typically involves reviewing literature and completing geologic investigations to characterise the previous spatial and temporal occurrences of hazards in the area (Kaye, 2008). Once hazards have been characterised, all of the exposed elements and their potential vulnerabilities should to be identified. Risk identification is required to identify all the issues that need further investigation in the risk analysis stage (Crozier and Glade, 2006).

For this thesis, risk identification involves identifying potential tephra fall hazards within Auckland and characterising how they can impact on Auckland's buildings. This involves an assessment of the magnitude and the spatial distribution of tephra from past AVF eruptions combined with a review of how tephra fall has impacted buildings in previous eruptions from around the world.

1.2.3 Risk analysis and evaluation

Risk analysis develops an understanding of how hazards interact with exposed elements based on their vulnerability (e.g. Figure 1). Combining these three components through geospatial modelling forms the basis of risk assessments (King and Bell, 2009). Risk assessments may use deterministic or probabilistic models or a combination of both. Deterministic, scenario based assessments use theoretical eruption scenarios, which are backed up by data from previous eruptions to estimate the impacts of volcanic hazards on exposed elements. These assessments can only focus on one scenario at a time for which they give definite 'yes it will occur/no it won't occur' type answers as opposed to quantifying the likelihood of the risks from the range

of possible scenarios (Haneberg, 2000). The latter can be achieved by moving towards probabilistic risk assessments.

Probabilistic risk assessments are used to model a range of scenarios and are capable of calculating the overall probability of a hazard occurring with its associated damage for a specific location. These assessments are better at modelling complex interactive hazards over a range of magnitudes and they require less subjective input. To quantify the likely impact caused by hazards, fragility functions can be used to characterize vulnerability in probabilistic risk assessments. Fragility functions relate hazard intensity to the expected impact severity experienced by a specific element of interest. For example, several tephra fall fragility functions for buildings relate tephra fall loading (kPa) to the probability of roof collapse for specific building types. Fragility functions provide the crucial calculation link between hazard and vulnerability in a quantitative, non-subjective manner, making them powerful risk assessment tools.

1.2.4 Risk evaluation

Risk evaluation is the final stage of risk assessment. It involves consideration of different risks so they can be compared and ranked. This helps to determine what actions should be taken for risk reduction. In the context of tephra fall impacts to buildings risk evaluation should ideally aim to answer the following questions:

- What are the insurance and repair costs associated with tephra impacts to Auckland's buildings?
- What loss of functionality will buildings experience?
- How long will building repairs last?
- What strengthening or new building guidelines could be made to reduce impacts?

These are important questions which are difficult to answer with any certainty. However, the assessment of vulnerability conducted in this thesis can help to reduce uncertainty in risk assessments and provides direction for risk mitigation measures.

1.2.5 Risk treatment

Risk treatment is the final stage of the risk management process. It takes advantage of the knowledge gained during risk assessment (identification; analysis; evaluation) to decide how best to reduce the hazard and/or the exposure and vulnerability that comprise risk. Volcanic hazards are powerful naturally occurring phenomena which are not easily managed by human activities, often making it impossible or very difficult to reduce the hazard. This means reducing the vulnerability of exposed elements or reducing their overall exposure may be more effective. These reductions can be achieved through the implementation of various, scientifically tested mitigation techniques, into society. Building exposure can be reduced through risk conscious land use planning but when it is not practicable to reduce exposure (as is the case in Auckland city), reductions in vulnerability can be achieved through strengthening of vulnerable system elements. A second way to reduce society's vulnerability is through intensive volcanic surveillance, which can provide warnings prior to impending eruptions. This increases the time available for emergency managers to conduct evacuations, reducing exposure of people to volcanic hazards (Donovan et al., 2012). Lastly, through communicating with at risk groups about the hazards and risks they may face during an eruption, these groups can take steps to understand, accept and reduce their personal risk to volcanic hazards (Paton et al., 2008).

1.3 Background of Auckland volcanic hazards

Auckland is unique in being a metropolitan area located on top of an active volcanic field. The AVF has produced at least 54 volcanoes over the last 250,000 years with most of these being relatively small and monogenetic in nature (Kereszturi et al., 2013). This means that each volcano is expected to only erupt once, with magmatic feeder systems being too small to stay open over long periods between eruptions so each episode of volcanism will break out at its own, distinct site. Although all previous eruptions have been constrained within the ~360 km^2 elliptical area that comprises the AVF (Figure 4), past volcanism does not appear to follow any spatio-temporal patterns (Lindsay et al., 2010). This means there is a large uncertainty associated with predicting the vent location or the timing of future eruptions. Another source of uncertainty in assessing the AVF's volcanic risk is associated with predicting eruption

magnitude. Eruptive volumes from most of the past eruptions have been relatively small but they are also highly variable. In total, the field has produced over 1.7 km^3 of eruptive deposits (dense rock equivalent), of which nearly half was all produced in the most recent eruption which formed Mt Rangitoto ~0.6 Ka (Kereszturi et al., 2013).

Despite magma from all the AVF's eruptions being in a narrow compositional range, past eruptions in the AVF display a wide variety of eruption styles (Allen and Smith, 1994). These styles range from phreatomagmatic, forming tuff rings and maars, to Hawaiian and Strombolian which produce cones and lava flows (Houghton et al., 1996). Eruption styles control the type and severity hazards produced. Identified potential hazards of an AVF eruption include: explosions, earthquakes, base surges, cone growth, lava flows and tephra fall.

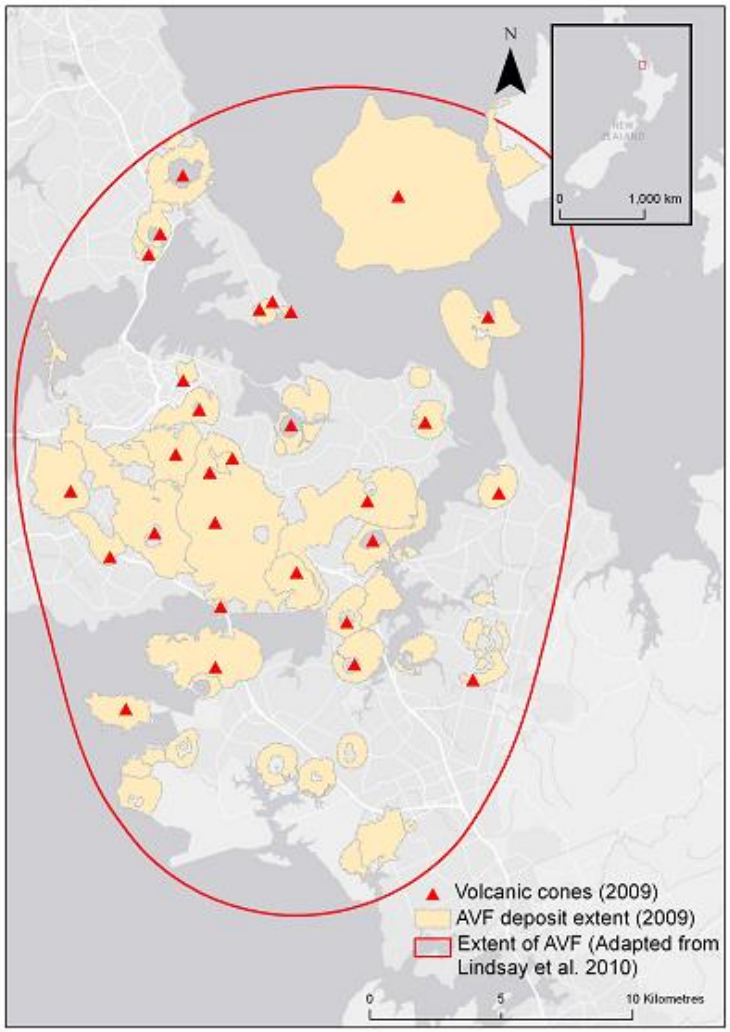

Figure 4: Extent of the Auckland Volcanic Field. From Hayes 2014, adapted from Lindsay et al. 2010.

Any buildings or infrastructure in the area of cone building are expected to be completely destroyed and hazards like lava flows typically destroy or bury anything they come into contact with (Houghton et al., 2006; Wilson et al., 2014). By comparison, tephra fall hazards are less destructive but typically much more widespread. Thus, depending on the style of eruption, tephra fall hazards present a significant risk to the Auckland building stock. Aspects of AVF tephra fall and ballistic hazards are outlined below but for more detailed review tephra fall and ballistic dispersal patterns in relation to their hazard, refer to Appendix A.

Although large thickness tephra falls are possible within Auckland, lighter falls between 1-10 mm occur more frequently and are not expected to cause structural damage to buildings (Magill and Blong, 2005; Magill et al., 2006a). Lake cores taken within Auckland have identified 70 distal tephra fall deposits ranging from 0.5-630 mm (Green et al., 2014). From probabilistic modelling the most likely source of tephra fall in Auckland is not from the AVF but from Mt Taranaki, with most thicknesses between 1-10 mm and a mean thickness of 1.7 mm across Auckland (Magill et al., 2006b; Hurst and Smith, 2010). Though relatively less likely to occur, large thickness tephra falls up to a maximum of 150 mm have been modelled for an AVF eruption (Magill et al., 2006b).

In previous AVF eruptions, ballistics have been produced from both ‘wet’ and ‘dry’ eruptions (Allen and Smith, 1994). Wet, phreatomagmatic eruptions occur when magma intrudes water and/wet sediment. They are more explosive than dry eruptions and based on the presence of significant aquifers, relatively high present day sea level and water-saturated Miocene sedimentary rock throughout Auckland, there is a high probability that a future AVF eruption will begin with a phreatomagmatic phase (Sandri et al., 2012). Based on studies of eruption deposits, ballistics are expected to be restricted within a 1-3 km radius of the vent during phreatomagmatic eruptions (Allen and Smith, 1994). During less explosive, ‘dry’ Strombolian or Hawaiian eruptions ballistics are expected to have a shorter range. This has been captured in the range of ballistic particles from two ballistic hazard models developed for a Strombolian and a Vulcanian scale phreatic eruption in Auckland (Chapter 4). The models have been developed using the Tsunematsu ballistic trajectory model (Tsunematsu et al., 2014)

and parameterised using studies of AVF ballistic deposits and analogous eruptions from more intensely studied volcanoes. Although several studies have investigated the probabilistic tephra fall risk to Auckland (e.g. Magill et al., 2006b; Hurst and Smith, 2010), they do not rank the risk from ballistics as very highly due to their relatively limited dispersal. Also there have been no probabilistic risk models specifically for ballistic impacts perhaps due to ballistics being regarded as a highly destructive hazard which will destroy any buildings they come into contact with (Magill and Blong, 2005).

Volcanic fields such as the AVF typically remain active for around 1 million years, meaning it is expected the AVF has many eruptions still to come and with a current trend of increased activity and higher volume volcanism during the last 40 Ka (Kereszturi et al., 2013). Despite this trend, AVF eruptions are still categorised as relatively low magnitude and low frequency events with probabilistic hazard models suggesting that an eruption occurs approximately once every 1,200 years (Hurst and Smith, 2010). This means Auckland has a higher likelihood of being impacted by tephra falls from distal volcanism than from an AVF eruption. However, due to the heavily populated and developed environment directly above the field, highly destructive proximal volcanic hazards from a local AVF eruptions have the potential to bear higher consequence.

The magma source beneath Auckland is at least 30 kilometres deep (Horspool et al., 2006). Based on magma ascent rates from suitable analogue eruptions, a warning time of 1-2 weeks between the onset of monitored seismicity and magma outbreak at the surface is expected (Blake et al., 2006). However, the report by Blake et al. (2006) also modelled the magma ascent rates through dikes and found that 0.3 m wide dikes could transport magma at up to 6 m/s giving a lead in times of less than 5 hours. If this scenario was to occur, evacuations are unlikely to be properly coordinated and people may be required to shelter-in-place inside suitable buildings. The longer 1-2 week warning time will hopefully give emergency planners time to identify and evacuate the zone surrounding the expected vent location to minimise loss of life. Building damage cannot be prevented in the same manner so it is important for researchers to provide a clearer picture of the impacts that can be expected to Auckland's building stock following an eruption as this can aid in pre-event disaster recovery planning. A large source of uncertainty in any such risk assessment is the current lack of understanding

surrounding how vulnerable different types of buildings and their critical building elements are to tephra fall hazards.

1.4 Aims and objectives

The main aim of this research is to quantify the vulnerability of a variety of building types to tephra fall hazards, helping to make volcanic risk assessments more accurate. This aim is aligned with the primary aim of volcanologists being to “use and improve the science for public safety and welfare” (Newhall et al., 1999).

The objectives of this research are:

1. To develop a framework that guides the derivation of tephra fall and ballistic fragility functions for buildings.

2. To improve understanding of building vulnerability to tephra hazard by deriving new tephra fall and ballistic fragility functions for New Zealand buildings using data from review of previous impacts research, experimental and field based studies.

3. To use the new fragility functions in assessing tephra impacts to Auckland’s buildings by undertaking a deterministic impact assessment using a credible AVF eruption scenario.

1.5 Thesis structure

To achieve these objectives, the main body of the thesis has a structure that aligns with the risk/impact assessment concept outlined in Figure 5.

- Chapter 1 has introduced the thesis and its scope and it has established the context of tephra hazards in Auckland.
- Chapter 2 presents a framework for deriving tephra fall and ballistic fragility functions for buildings. This framework:
    - Reviews previous instances of tephra fall and ballistic impacts to buildings.

- Identifies the key aspects of hazard and vulnerability which influence the impacts associated with each hazard.
- Critically reviews the previously developed tephra fall and ballistic fragility and vulnerability functions for buildings.
- Identifies different sources of data required to produce functions, provides a function derivation methodology and then follows the methodology to derive new functions for tephra fall and ballistic impacts buildings.

- Chapter 3 presents the results and analysis of experiments used to derive new ballistic fragility functions for New Zealand buildings. Experimental design has been informed by analysis of the most common building types in Auckland and by findings from recent ballistic impact assessment trips to two Japanese volcanoes. The experiments involved destructive materials testing on various building claddings using an air cannon which ejects rocks to simulate ballistic hazard.
- Finally Chapter 4 utilises the fragility functions developed in Chapters 2 and 3 to undertake a deterministic impact assessment for tephra fall and ballistic hazard impacts to Auckland's building stock.

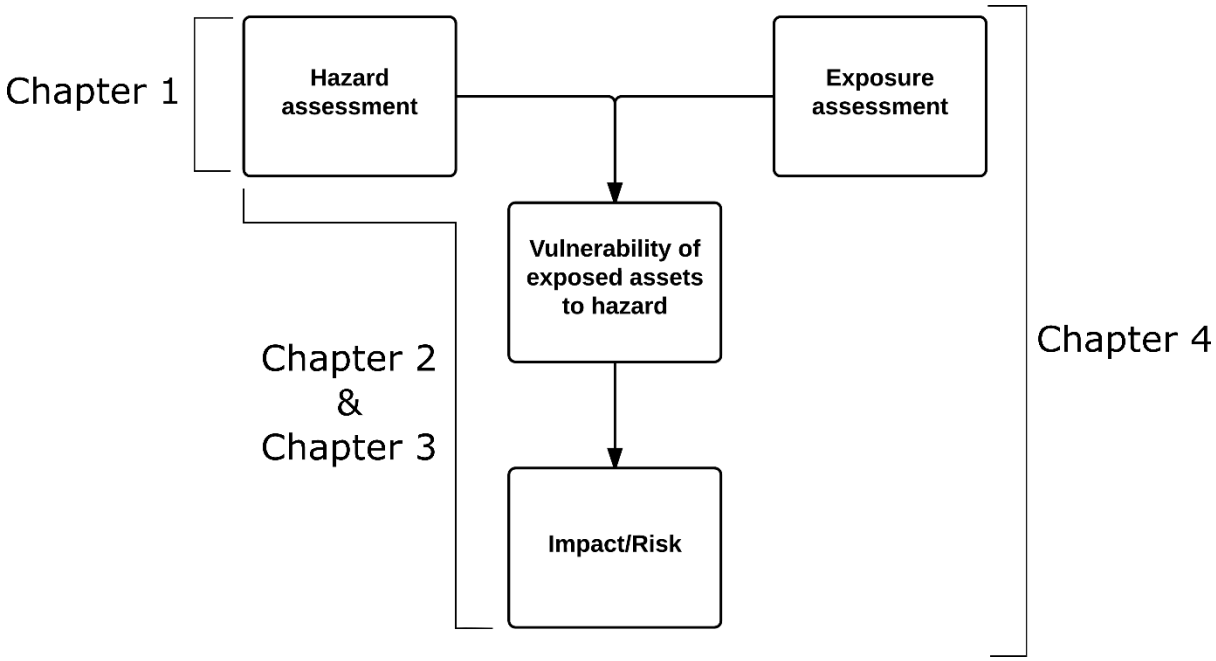

Figure 5: Chapter alignment with the impact/risk assessment concept.

Chapter 2 Framework for the Development of Tephra-building Fragility Functions

2.1 Introduction

Effective volcanic risk management requires an understanding of the vulnerability of assets exposed to volcanic hazards. Although there are a range of different methods that can be used to assess vulnerability, this thesis focusses on quantifying vulnerability through the development of fragility functions for use in a quantitative risk assessment. The quantitative assessment of vulnerability of buildings to natural hazards such as tsunami, earthquake, flooding and hurricane is typically determined through the development of fragility and/or vulnerability functions (see section 1.2.3) (Rossetto et al., 2014; Maqsood et al., 2015; Tarbotton et al., 2015). For tephra fall hazards there have been relatively few fragility and vulnerability functions developed and they are often only applicable to the local building stock they were developed for, thereby limiting their use in impact assessments. Previously developed functions have largely focussed on structural damage and roof collapse associated with heavy tephra loads. Available functions rarely consider other aspects of tephra-building impacts such as damage to non-structural building components from light tephra falls or perforations caused by ballistic impacts. This chapter reviews previous instances of tephra impacts to buildings, critically reviews the currently available tephra-building fragility functions and provides a framework for developing new functions. The purpose of this review is to identify gaps in current knowledge of building vulnerability to tephra hazards and provide direction to the development of new fragility functions for New Zealand buildings.

This chapter's structure follows that of the framework's which is outlined in Figure 6. The first section provides an overview of fragility and vulnerability functions, their dependant and independent variables, and the main sources of data used to develop functions for buildings impacted by tephra hazards. The next section reviews the impact data available from previous instances of tephra impacts to buildings and identifies the key aspects of tephra fall and ballistic hazards which enable them to cause impacts to buildings. Then, a method for function fitting that requires only a

limited number of data points is outlined. The documentation stage of function development is then outlined. Documentation provides transparency so end users may understand how reliable the functions are and how best to implement them or update them as more data becomes available (Rossetto et al., 2014; Wilson et al. in review). The framework presented in Figure 6 provides a systematic approach to developing fragility functions. It is based upon similar frameworks used in vulnerability assessments for many natural hazards including tsunami (e.g. Tarbotton et al., 2015), earthquake (Rossetto et al., 2014), hurricane (e.g. Barbato et al. 2013) and volcanic (e.g. Wilson et al.in review). The final stage of function development is the incorporation of functions into risk assessments or risk assessment software (e.g. RiskScape(King and Bell, 2009) or HAZUS-MH (FEMA, 2003)). Implementing these fragility functions into RiskScape will enable a more accurate assessment of tephra impacts to buildings in New Zealand.

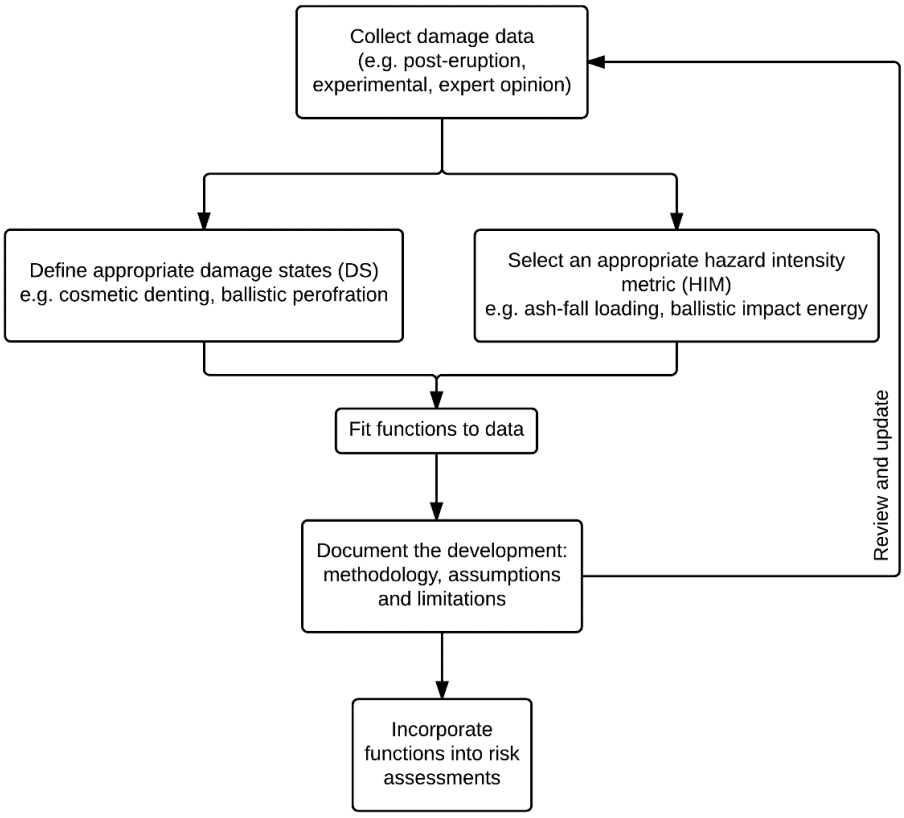

Figure 6: Framework for the development of tephra-building fragility functions. After Wilson (2015)

2.2 Introduction to fragility and vulnerability functions

Fragility and vulnerability functions are commonly used in risk assessments to translate an assessed level of hazard to an estimated level of impact (damage and disruption) for a given asset of interest. Fragility functions and vulnerability differ in the way they represent impacts (Figure 7). Vulnerability functions correlate hazard intensity to an asset's expected mean damage or functionality loss where the overall impact to a structure is represented in one of two ways. Either 1) as an index (e.g. damage ratio – cost to repair : cost to replace) or 2) as a percentage relative to total impact (e.g. 80% damaged) (Tarbotton et al., 2015). Fragility functions express the conditional probability that a pre-defined level of impact will be reached or exceeded for a given hazard intensity (measured using an appropriate hazard intensity metric (HIM)) (Rossetto et al., 2014; Tarbotton et al., 2015).

Whether fragility of vulnerability functions are developed is dependent on the nature of available impact data and objective of the risk assessments in which they are to be used. In the context of this thesis, these functions are used to predict likely building damage and associated reconstruction costs caused by tephra hazards produced in future AVF eruptions. These predictions can be used to inform pre-event recovery planning (e.g. demolition waste management decisions (Hayes, 2014)). They can also inform risk mitigation actions such as building strengthening and identifying which buildings are the most appropriate for people to shelter-in-place (Jenkins et al., 2014).

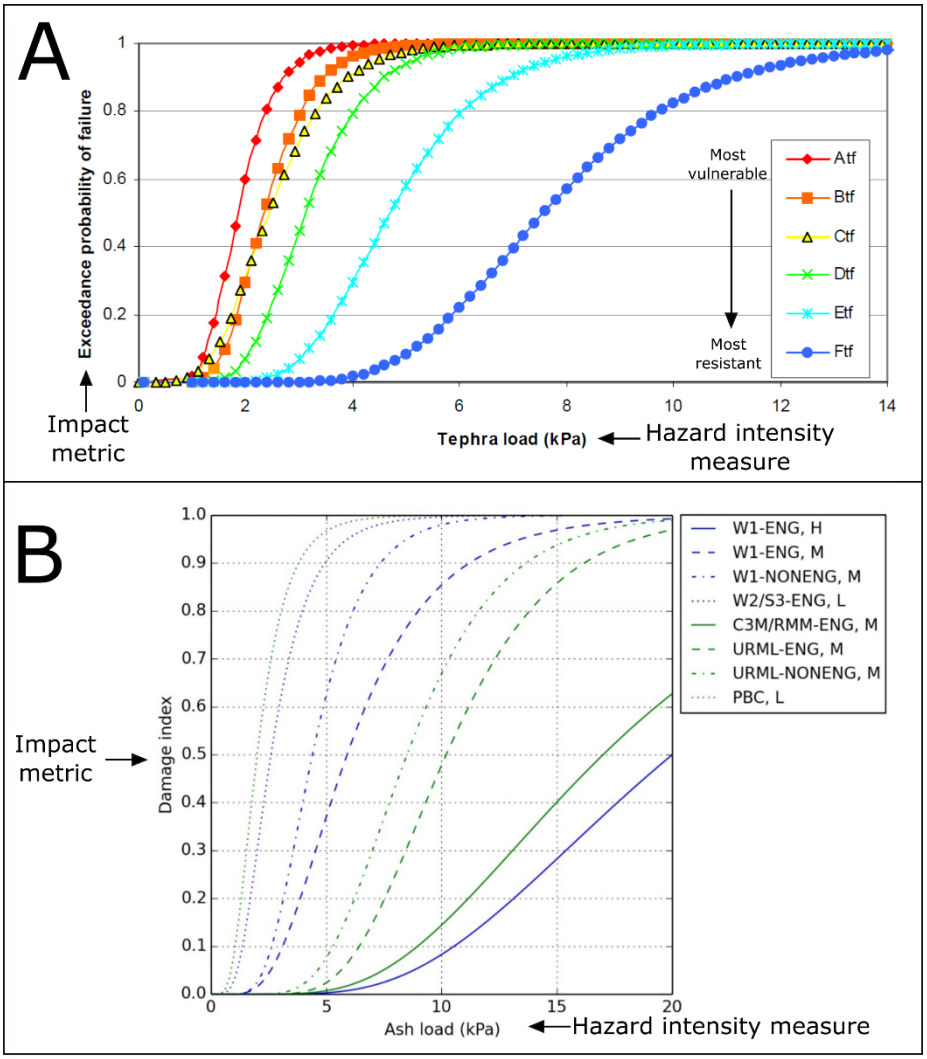

Figure 7: Illustration of tephra fall-building fragility and vulnerability functions. A) Roof collapse fragility functions for different roof typologies from Jenkins and Spence (2009). B) Tephra loading vulnerability functions from the United Nations Global Assessment of Risk 2015, (Maqsood et al., 2015). Hazard intensity measures and impact metrics and are outlined in the following sections 2.2.2 and 2.2.3 respectively.

2.2.1 Damage data

The data which is required to derive fragility functions is termed here as damage data. Damage data is quantitative and relates building damage to hazard intensity. Data such as this can be classified into three types: empirical; expert elicitation and analytical (Schultz et al., 2010). The advantages and disadvantages of each type are summarised in Table 1:.

Table 1: Advantages and disadvantages associated with using different types of damage data to develop fragility and vulnerability functions. Modified from Schultz et al. (2010) and Wilson (2015).

Data type	Advantages	Disadvantages	Examples
Empirical: Post-eruption impact assessment	Can observe impacts to the entire building system, true representation of hazard	Data often limited, Region/site specific construction types, difficult to measure hazard intensity	Spence et al, 1999; Blong, 2003
Empirical: Controlled experiments	Repeatable experiments, detailed measurement of hazard intensity, control on asset type impacted	Costs (time and resources), Difficulties in simulating hazard and asset in laboratory environment	Oze et al, 2014; Hampton et al, 2015
Analytical	Easily repeatable once models are developed, models can be altered and extrapolated to new building types	Models based on simplifications and assumptions, requires empirical data for validation	Pomonis et al, 1999; Zuccaro et al, 2008
Expert elicitation	Can rely on judgement to refine other functions, not limited by lack of data	Differing levels of expertise, differing or contradictory opinions, requires empirical data for validation	Maqsood et al, 2015;

2.2.1.1Empirical data

Empirical data includes measurable observations of damage at different hazard intensities either from previous volcanic eruptions (post-eruption impact data) or controlled laboratory experiments. Post-eruption impact data has the advantage of providing a true representation of the diverse range of impacts that volcanic hazards cause to real buildings. However because impacts are rarely directly measured for safety reasons and because eruptions are infrequent events, data are often scarce or of variable quality and the impacts may only be applicable to the building typologies in the impacted region (Douglas, 2007; Jenkins et al., 2014; Wilson et al., 2015).

To date no functions have been produced purely from data gained during post-eruption impact assessments. This is likely because no impact assessments have been undertaken with the main goal being to specifically produce fragility or vulnerability functions and also because post-eruption impact assessments follow a reactive research model which rarely allows for in depth analysis into why or how observed impacts occurred (Wilson et al., 2012).

Due to these issues, experimental studies that simulate tephra impacts in a controlled laboratory environment work well in conjunction with post-eruption impact studies.

They complement post-eruption impact research by allowing for repeatable experiments and an in depth analysis of impacts to various building components at a range of hazard intensities. The main challenges of experimental studies include their generally high cost (in terms of resources and time) and the difficulties of accurately replicating complex natural hazards and their impacts to real buildings in a laboratory

2.2.1.2Analytical data

Analytical data can be produced using statistical or numerical models that calculate building vulnerability at different hazard intensities (Rossetto and Elnashai, 2003; Li and Hao, 2014). This approach requires the development of models that accurately represent buildings and their vulnerability. However, any modelled results should ideally be verified against results from experimental or post-eruption impact studies (Maqsood et al., 2015). Pomonis et al (1999)and Zuccaro et al (2008) used numerical modelling (based on experimental strength testing of timber and R.C structures respectively) to determine vulnerability of Azorean and Neapolitan buildings subjected to tephra fall.

2.2.1.3Expert elicitation data

When analytical or empirical data are not available or scarce, expert elicitation can be used to generate data for vulnerability assessments (Zuccaro et al., 2008; Rossetto et al., 2014; Maqsood et al., 2015). Advantages of the elicitation process include its ability to draw on expert judgement and logic to refine previously developed functions or to develop new functions with limited data by combining data from different sources (Wilson, 2015). Disadvantages such as the differing levels of expertise, contradicting opinions and subjectivity can be overcome using a range of averaging or weighted averaging methods (Aspinall and Cooke, 2013).

2.2.2 Hazard intensity measures (HIMs)

A hazard intensity meaure (HIM) is used to quantify the intensity of a hazard and is the independent variable for both vulnerability and fragility functions. Tephra fall and ballistic hazards have a number of different measurable properties which can be used to express intensity and different properties are responsible for different mechanisms of building damage. This means that although no single HIM can capture all of the impactful attributes for either of these hazards, some measures correlate with damage

more strongly than others (Wilson et al., 2014). Therefore, the selection of a suitable HIM is an important step in fragility or vulnerability function development. In addition to the HIM's ability to describe the range of possible building damage, ideally they should also be easily measurable in the field or in the laboratory, be easily incorporated into existing hazard models and have also been recorded in existing impact databases. For tephra fall the most common HIMs are thickness or mass loading and for ballistics the most common HIMs are impact energy and impact density per unit area (Jenkins et al., 2014).

2.2.3 Impact metrics (IMs)

For functions in this framework, impact metrics (IMs) are used to assess impact intensity either for individual buildings or for individual ballistic strikes to buildings. Impact metrics are the dependent variable for both types of function and are commonly bounded between 0 and 1. As described above the representation of impact metrics differs for vulnerability and fragility functions. For vulnerability functions, the IM will typically be either an index (e.g. damage ratio – cost to repair : cost to replace) or a percentage relative to total impact (e.g. 80% damaged)).

For fragility functions the IM is the probability that a building will be impacted to (or exceed) a specified level of impact. Successive levels of impact are expressed semi-qualitatively using descriptions of building damage state (DS) or impact state (IS). Ideally for each type of asset a suite of fragility functions are developed with one function for each DS/IS. Given that DSs and ISs are sequential, (i.e. if DS2 has occurred this implies that DS1 has occurred), then the probability of being equal to a specific DS can be calculated from the difference between consecutive DSs at a given hazard intensity (See Figure 8 for an example).

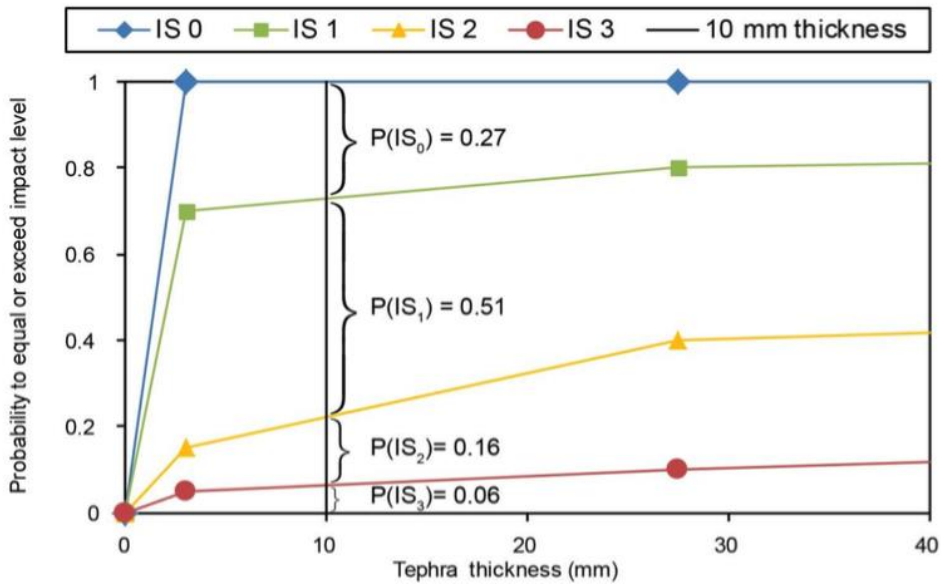

Figure 8: Illustration of the probability of occurrence calculation for each impact state at 10 mm tephra thickness. Functions are for impacts to electricity transmission sites. Figure from Wilson (2015).

2.3 Previous instances of tephra fall and ballistic impacts to buildings

In previous tephra risk assessment studies, the incorporation of quantitative impact data and vulnerability assessments are often not well established, especially in comparison to earthquake risk assessments (Douglas, 2007). Effective risk assessment requires consideration of hazard, exposure and vulnerability but compared to the sophistication of probabilistic tephra fall hazard models (e.g. Bonadonna et al., 2005; Hurst and Smith, 2010) and ballistic hazard models (e.g. Tsunematsu et al., 2014), tephra vulnerability models are lagging. As a result few, if any fragility functions have been developed for certain aspects of tephra impacts. To improve the state of vulnerability assessments, studies that investigate tephra impacts need to provide quantitative data and present it in a way that datasets from multiple studies may be combined and potentially be developed into fragility or vulnerability functions. Although there is limited quantitative empirical data available from previous instances of tephra impacts to buildings, qualitative evidence can be used to gain an understanding of the range of key vulnerability indicators for buildings and aspects of the hazard that enable them to cause impacts. The following sections outline previous instances of both tephra hazards and the key aspects of hazard and vulnerability that influence their impacts.

2.3.1 Tephra fall impacts to buildings

As tephra fall can be a widespread hazard, deposited with varying thicknesses in different areas (See Appendix A), it has the potential to impact large numbers of buildings in a variety of different ways. Impacts can be separated broadly into structural and non-structural damage. Structural damage is primarily dependent on tephra fall load (kPa) and the impacted building's load bearing capacity. Non-structural damage can affect a large number of building components and a number of factors control the damage mechanisms. A more detailed examination of factors influencing non-structural impacts is presented in section 2.3.1.3.

Several eruptions that have caused tephra fall impacts to buildings are outlined in (Table 2). The most studied tephra fall induced damage to buildings is the collapse of roofs under thick (> 100 mm) falls, and so these tend to dominate known accounts of tephra impacts to buildings (e.g. Spence et al., 1996; Pomonis et al., 1999; Blong, 2003; Zuccaro et al., 2008; Jenkins and Spence, 2009).

Table 2: Examples of tephra fall impacts to buildings ordered by increasing thickness.

Eruption	Uncompacted tephra thickness (mm)	Impacts/damage	Reference
Ruapehu, 1995 - 1996	<5 mm	Thousands of houses exposed to < 5 mm of tephra. Insurance claims for 213 houses for damage to roofs, gutters and drains	Trebilco, 1997
PCC, 2011	<10 mm	Widespread ongoing ash ingress into buildings following wind remobilisation	Wilson et al., 2013
PCC, 2011	15-17 mm	16 houses suffered roof collapse and 40 were braced to prevent collapse 54 km from the vent	Wilson et al., 2013
Usu, 2000	10-20	Ash ingress through ballistic perforations to >100 buildings	Takarada et al., 2002
Mount St Helens, 1980	Not reported (~10 -20)	Damage to gutters, down spouts, interior floors etc.	Dillman and Roberts, 1982
Tambora, 1815	95	Roofs collapsed	Anon, 1816

Soufriere 1902	75-125	Roofs collapsed	Anderson and Flett, 1903
Mount Pinatubo, 1991	200 mm (wet)	51 buildings surveyed: 15 had no damage, 3 had light damage and 33 were collapsed or severely damaged	Spence et al., 1996
Soufriere 1902	460	Houses collapsed	Anderson and Flett, 1903
Tavurvur and Vulcan, 1994	100-950	Cosmetic damage, corrosion of sheet metal roofs through to collapse across 173 buildings	Blong, 2003
Eldjfell, 1973	<100	Collapse of flat roofs on strong buildings	Booth, 1979
Eldjfell, 1973	2000-4000	Complete burial of buildings	Booth, 1979

2.3.1.1 Factors influencing structural tephra fall impacts to buildings

By reviewing previous instances of tephra fall impacts to buildings, several of the factors influencing structural tephra fall impacts to buildings have been identified. These include the building's cladding type and cladding support systems, roof span and pitch, the tephra deposit's load, and environmental conditions (particularly rainfall) before during and after tephra is deposited on a building (Hampton et al., 2015; Maqsood et al., 2015; Wilson et al., 2015a).

Structural impacts include roof sagging and roof, wall or building collapse caused by excessive tephra loading typically onto the building's roof. Therefore, the two primary factors controlling the extent of structural damage to a building are its superimposed tephra load and the building's capacity to bear this load (Figure 9).

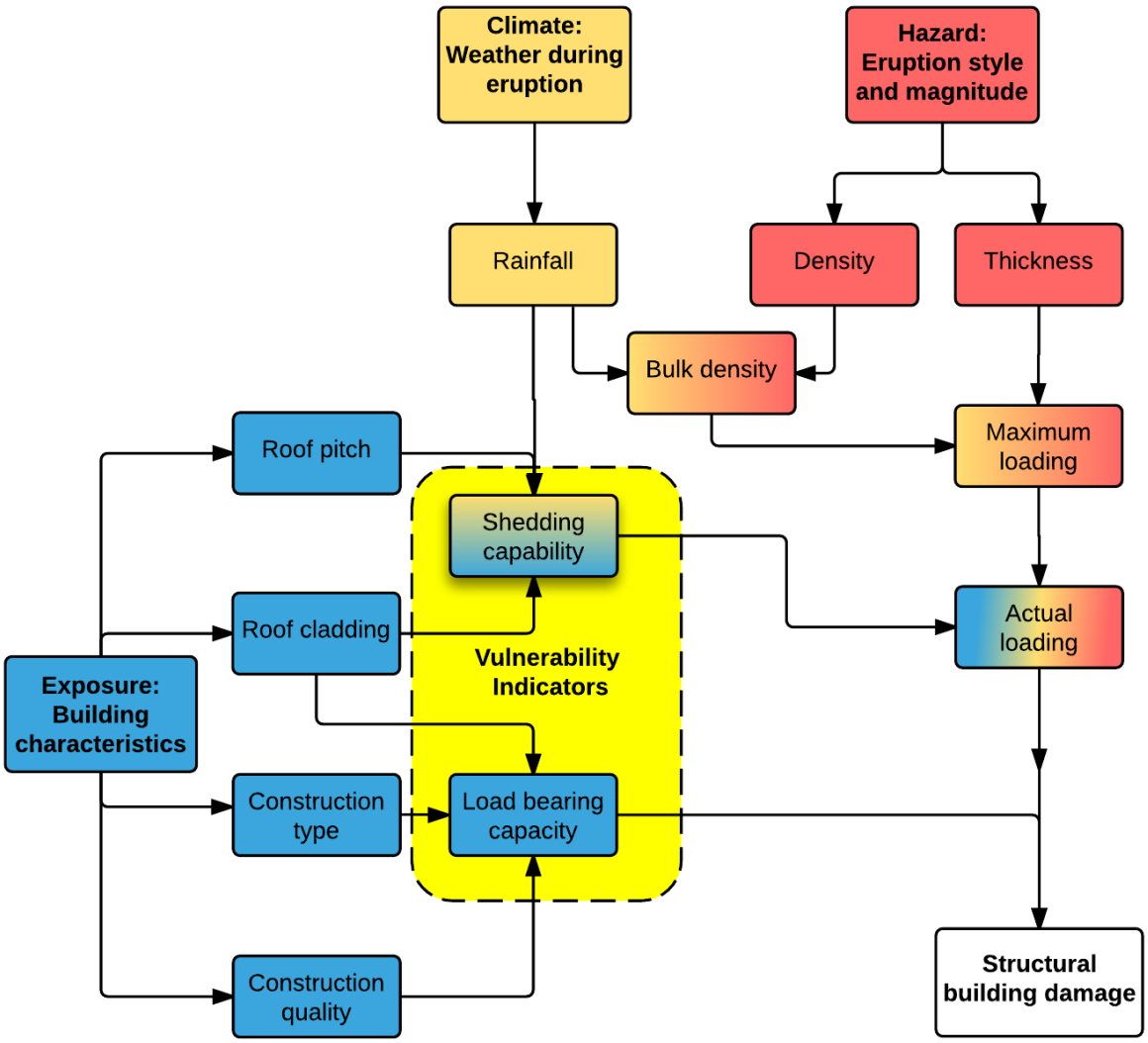

Figure 9: Factors controlling the extent of tephra fall induced structural building damage. Processes with colour gradients signify the process is controlled by a combination of factors including tephra hazard (red), exposure (blue) and/or climate (orange).

Tephra loading is measured from the thickness and bulk density of a roof's tephra deposit (See equation in section 4.2.4.1). A deposit's bulk density will vary between different eruptions or for changing conditions of the same eruption, such as a transition in eruption style or if a dry tephra deposit becomes saturated with rainwater (Macedonio and Costa, 2012). Many factors control deposit thickness but generally, thickness decreases with distance from the eruptive vent. If 100% of tephra settling on a roof remains accumulated there, then its actual loading and maximum loading are the same (Figure 9). In most cases however, a percentage of the tephra deposit will

be shed (Pomonis et al., 1999; Hampton et al., 2015). Four mechanisms for tephra shedding include:

1) Tephra sliding under gravity,
2) Wind remobilisation,
3) Washing by rain or
4) Manual removal.

Hampton et al (2015) conducted experiments investigating the effect of roof pitch on tephra's ability to slide from corrugated iron roofs and found that at pitches of 35° or higher, significant amounts of dry tephra would slide from clean, dry roofs. Blong (1981) identified wind remobilisation as a potential means for a tephra load to become unevenly distributed across roofs but didn't point out the possibility that wind could also remove tephra from the roof all together. In terms of wind speed thresholds for remobilisation, wind tunnel testing of loose dry tephra from the 1980 Mt St Helens eruption became suspended at speeds ranging from 6-12 km/h depending on tephra surface smoothness (Fowler and Lopushinsky, 1986). However, if fine tephra becomes wet it may form a firm surface, stabilising itself against wind speeds <69 km/h (Wilson et al., 2011). Rainfall has the potential to either decrease or increase loading. Loading can increase by up to 100% when tephra becomes saturated with water (Macedonio and Costa, 2012), but conversely, loads may decrease if sustained rainfall is able to wash tephra from roofs (Hampton et al., 2015). In an eruption, if buildings being impacted by tephra are outside of evacuation zones and tephra accumulation rates are not exceedingly high, building owners may be able to periodically remove tephra from roofs manually as it falls, preventing excessive loads from accumulating. However, cleaning tephra from roofs presents new problems such as people placing themselves at risk of falls from height (Blong, 1984) or because the removal process can at times cause additional damage (e.g. from ladders being braced against roof gutters (Dillman and Roberts, 1982) or from people standing on roofs and increasing the live load during removal (Blong, 1984)).

Once the residual tephra loading on a building's roof has been established, the other primary factor influencing structural damage severity is the building's load bearing capacity. A roof will collapse when tephra load exceeds either the strength of the roof cladding or the cladding's supporting structure or both (Jenkins et al., 2014). Following

the 1991 eruption of Mount Pinatubo, Jenkins et al. (1996) conducted surveys on 51 buildings impacted by tephra fall and found the most significant indicator of structural building damage to be the roof's supporting structure. Of the 12 buildings they surveyed with roof spans of over 5 metres, 75% were severely damaged compared to 16% for short-span roofs. For three different roof designs identified for timber framed buildings in the Azores Pomonis et al. (1999) used a combination of strength tests, elasticity tests and numerical modelling to calculate expected roof failure loads and found that the strongest roofs were those using the thickest framing members spaced the least distance apart. Flat roofs are also generally more susceptible to loading damage than pitched roofs which transfer loads more efficiently down into their walls (Booth, 1979; Pomonis et al., 1999).

The number of storeys a building has also affects its overall vulnerability to tephra fall impacts (Marti et al., 2008; Maqsood et al., 2015). If for example a multi-storey building experiences roof collapse this may only cause serious damage to the uppermost storey of the building. This is because catastrophic failure of subsequent floors is assumed to be unlikely due to floors having already been designed to bear loads which are heavier than that of the roof's. Also in cases of extreme tephra falls such as the 1973 Eldjfell eruption, multi-storey buildings are less vulnerable to complete burial (Booth, 1979).

Finally the age and by association, the condition of the building plays a role in load bearing capacity by effecting the building's overall strength (Jenkins et al., 2014).Newer or cleaner metal roofs are also more likely have a smooth surface to facilitate tephra shedding (Hampton et al., 2015).

2.3.1.2 Impacts to Non-Structural Building components

From the examples of tephra fall impacts in Table 2, there appears to be a pattern of studies prior to the 1980 eruption of Mount St Helens focusing on severe structural building damage which typically did not occur for tephra thicknesses <100 mm. Non-structural damage on the other hand can occur for tephra thicknesses as low as 1-2 mm (Johnston, 1997). This means that for any given eruption, non-structural damage has the potential to be significantly more widespread than structural damage. In this case the issue of tephra fall impacts shifts from one of life safety and large repair costs for a select group of heavily impacted buildings into an issue of cumulative damage to

the overall building stock. This could present problems to a wide range of groups from the community level through to insurers and the construction industry (e.g. Canterbury earthquake sequence 2010-2011, Doherty, 2011). Several post-eruption impact studies have investigated the impact of light tephra falls to non-structural building components and experimental studies provide further insight into the vulnerability of some of these components.

Following the 1980 Mount St Helens eruption, Dillman and Roberts (1982) used data gathered from 900 households in eastern Washington State to report on the damage caused to various parts of their property. Nearly half of the respondants (48%) reported no housing-related damage at all but for those who did, the majority of reported damage was for gutters, roof coatings and downspouts. In the same eruption, about 10 mm (~0.1 kPa loading) of tephra fell on the city of Yakima and insurance payments averaged between $300-$400 and 90% or more of the cost was attributed to the labour and cleaning (Dillman and Roberts, 1982). During the clean up process, roofs were damaged by snow shovels and by having to support the live loads of cleaners which were in many cases, over 100 times heavier than the tephra load itself (Blong, 1984). This serves as an example of light tephra fall's capacity to produce almost negligible direct physical damage to buildings whilst still incurring significant costs.

2.3.1.2.1 *Impacts to roof gutters*

Hampton et al. (2015) summarised known historical impacts to roofs and gutters from 6 eruptions and also conducted experiments into roof gutter damage caused by tephra loading under wet and dry conditions. The review found that in several cases removing tephra from gutters had prevented blockages and damage but that occasionally, more damage was done during the clean-up process than during the eruption itself. The experiments found that gutters may be completely filled with dry tephra without failure but that wet tephra loads >1.0 and >1.5 kPa caused gutter deformation and failure respectively. In terms of tephra loading under different roof pitches and weather conditions, dry tephra accumulates on dry roofs at pitches up to 35°, above this pitch tephra begins to shed off the roof into gutters and to the ground. Tephra fall can adhere to wet roofs, allowing it to accumulate at higher pitches. These experiments provide a useful quantitative examination of roof gutter vulnerability under different tephra fall and roof pitch scenarios. However, they were conducted only using one type of roof

cladding (corrugated metal), shedding tephra into PVC gutters of a specific design. Also due to the large quantities of tephra required to carry out these experiments, “pseudo ash” particles (milled from basaltic lavas) were used as opposed to real tephra. The pseudo ash particles used in these experiments did have realistic grainsize distributions but they also had a relatively low surface roughness and a more tabulate morphology compared to real tephra which could decrease the pseudo ash’s angle of repose and therefore increase deposit’s tendency to shed.

2.3.1.2.2 *Impacts to HVAC units*

Another set of critical building components which are vulnerable to tephra impacts are heating, ventilation and air-conditioning (HVAC) systems. HVAC systems are a critical component to any building that requires temperature control to function (e.g. telecommunication exchanges and cell sites, medicine stores in hospitals, storage facilities that hold perishable food, etc.) (Wilson et al., 2012). Disruption to HVAC systems has occurred from tephra falls as light as 1-2 mm, either by air-intake blockage, or by precautionary shut-downs to avoid blockages (Johnston, 1997). To better understand tephra fall impacts to HVAC systems, laboratory experiments were carried out by Barnard (2009). The experimental results introducing tephra to HVAC systems semi-continuously over 15 hours suggested that if air conditioners are monitored and regularly maintained following an eruption, they are likely to remain viable during light tephra falls (<20 mm). The study also found that modern units which are designed to reduce noise with lower internal air flow speeds, were more vulnerable than older style units with higher internal air flow speeds.

2.3.1.2.3 *Impacts to metal roofs*

Corrosion of metal roof materials by acidic tephra leachates can potentially weaken roofs and shorten their lifespan in volcanically active areas. Several studies have attributed metal corrosion to volcanic tephra from Sakurijima (Deguchi, 1990), Rabaul (Blong, 2003) and Mt Ruapehu (Johnston, 1997). However these assessments were observational and lacking quantitative data. Oze et al. (2014) presented results of weathering chamber experiments in which different roof metals were subjected to tephra leachates for 30 days to investigate possible corrosion damage. The tests could

not identify significant corrosion to any of the roofing metal samples and suggest that corrosion is a more complex, long term, dynamic process that couldn't easily be reproduced in these experiments.

2.3.1.2.4 *Impacts to building interiors*

Fine ash can penetrate buildings causing a health hazard and damage to contents (Wilson et al., 2011; Wilson et al., 2013). Even in well-constructed buildings, fine ash can enter through small gaps in windows, doors, walls or through the roof to contaminate exposed surfaces. Ash particles suspended inside buildings can be breathed in with common impacts to human health including irritation of the eyes, skin and respiratory tract. Ash ingress can remain an issue years after eruptions have ceased with the possibility for additional episodes of contamination to occur when ash deposits become remobilised by wind (Wilson et al., 2011).

2.3.1.3 Factors influencing non-structural tephra fall impacts to buildings

Compared to structural impacts, there are a wider range of tephra fall induced non-structural impacts that can occur, mostly due to the number of different building elements which are susceptible to impacts. With such a large number of factors influencing impacts and the lack of large empirical or analytical impact datasets, it becomes challenging to analyse the relationships between hazard and vulnerability that contribute to impact. However there are a different set of relevant tephra properties and vulnerability indicators with a recognised influence to different types of impacts outlined in Table 3 below.

Table 3: Relevant tephra properties and vulnerability indicators. Each property has been assigned a unique letter or symbol: thickness, T; grainsize distribution Φ; airborne volcanic tephra concentration, C; particle density, ρ; presence, P; surface composition, SC; abrasiveness, A. The importance of each property in terms of its influence on impacts is indicated using an 'X' for a key property or an 'o' for possible influence. After Wilson et al (2015).

Impact description	Relevant tephra properties							Relevant vulnerability characteristics	Reference
	T	Φ	C	ρ	P	SC	A		
Roof gutters and drains blocked	X	X					X	Roof catchment area, pitch, gutter diameter and strength	Hampton et al, 2014
Metal roof claddings corroded	o	X				X		Metal type, coating and condition	Johnston, 1997; Oze et al, 2014
Building interiors contaminated	X	X	X			o	X	Building ventilation, construction quality and entry protocol	Wilson et al, 2011; Wilson et al, 2015
Painted surfaces stained or leached	X		o			X		Age/freshness of paint	Dillman and Roberts, 1982; Blong, 1984
HVAC systems: filters blocked, abrasion damage, decline in functionality	X	X	X	o	o	X	o	Internal air flow speed, air intake location	Johnston, 1997; Barnard, 2009
Water tanks blocked or contaminated	X					X		Source of water, open air or covered	Stewart et al, 2006; Wardman et al, 2012

2.3.2 Ballistic impacts to buildings

There have been relatively few quantitative studies investigating ballistic impacts to buildings and in contrast to tephra fall no ballistic-building fragility functions have been published to date. However some studies provide useful observations on ballistic damage to buildings (Table 4). Nearly all of the studies identified in this table provide a distance that ballistics have travelled from their source and state what type of damage occurred at that distance. Several of these studies provide further details such as measurements of the ballistic's diameter or weight and stating what type of building(s) or building material(s) have been damaged. Nairn (1975) for example provides a detailed description of ballistic damage to Mt Ruapehu's Glacial Hut which was apparently mostly caused by "one large block which formed a 2 m wide impact

crater near the hut, broke into pieces and bounced upward through the hut walls leaving holes up to 0.3 metres across". These accounts provide useful insights into what damage has occurred in the past but they do not provide enough information about the hazard or the type of material impacted to quantify its vulnerability retrospectively.

Table 4: A selection of observations on ballistic damage to buildings.

Eruption	Damage type	Damage description	Reference
Soufriere, 1902	Light - no damage	Bombs up to 900 grams dented galvanised iron roofs but left shingle roofs undamaged	Anderson and Flett 1903
Upper Te Maari, 2012	Moderate damage: Cladding perforation	Ketetahi Hut perforated from roof to floor in several locations	Fitzgerald et al., 2014
Soufriere, 1976		Metal roofs perforated without complete building collapse	Blong, 1984
Ruapehu, 1975	Severe damage: Roof and wall cladding perforation	The Glacier Hut, 1200 m from Ruapehu's Crater Lake was hit 35 times with some block fragments burning holes in the floor	Nairn, 1975
Mt Usu, 2000		>50 residential, commercial and municipal buildings damaged beyond repair by ballistic perforations up to 600 metres from multiple vents	Fitzgerald et al., in prep.
Mt Ontake, 1979 and 2014		Timber roofed mountain lodges perforated by blocks up to 1 km from vent	Maeda et al., 2015; Fitzgerald et al., in prep.
Stromboli, 1912	Complete building collapse	Ballistics weighing up to 30 tonnes destroyed several buildings 3 km from the vent	Rittman, 1962
Mt Lassen, 1914-1915		The timber framed lookout at Lassen Peak was destroyed by successive ballistic impacts 400 metres from the crater	Hill, 1970
Pacaya, 2010	Buildings completely burnt	5 buildings burnt following perforation of sheet metal roofs by blocks up to 3.5 km from vent during rainfall, concrete roofs destroyed by 0.5 m diameter blocks 1 km from vent	Wardman et al. 2012
Sakura-jima, 1914		Buildings from 4 separate villages ignited by bombs falling up to 6 km from vent	Omori, 1916b
Eldjfell, 1973		Ignition following perforation of roofs and unprotected windows by bombs	Booth, 1973
Asama, 1783		52 out of 162 houses completely burnt following perforation by red hot pumice blocks 11 km from vent	Aramaki, 1957

The first significant attempt to quantify building vulnerability to ballistic impacts comes from Blong (1981). In this pioneering study the author collated work from previous cyclone and impact engineering studies to calculate the minimum impact energies required to perforate a range of common building claddings with a cubical block

striking perpendicular to the plane of the cladding (Figure 10). More recent hurricane vulnerability studies investigating windborne debris impacts to buildings have come up with similar impact energy thresholds for the perforation of metal hurricane shutters, despite these tests using timber 2×4's and roof tiles as their missiles instead of lithic blocks (Fernandez et al., 2010; Alphonso and Barbato, 2014).

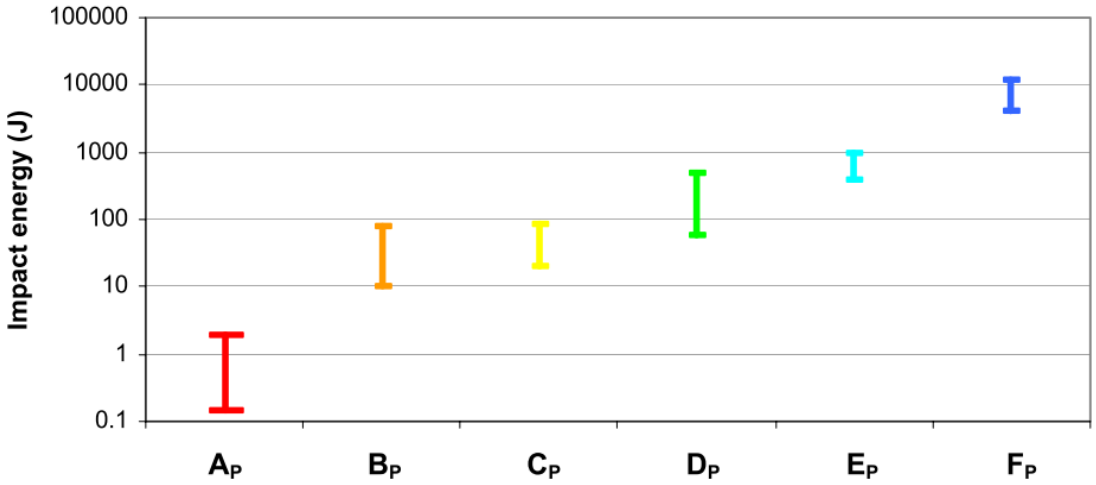

Figure 10: Minimum impact energies required for perforation of different roof cladding materials. After Blong (1981). Material types and thicknesses outlined in Table 5 below. Graph from Spence et al. (2011).

Table 5: List of building materials tested. Note that the original Dp (timber boards) has been broken down into Dp1 and Dp2 (hardboard and plywood respectively).

Building material	Thickness (mm)	Minimum perforation energy (J)
Ap: Glass sheet	2.5 - 4	0.15 - 1.25
Bp: Tile	10 - 40	10 – 90
Cp: Fibre reinforced concrete sheet	4.5 - 9.5	20 -85
Dp1: Hardboard	9.5	60 – 90
Dp2: Plywood	4.5 - 12	90 – 500
Ep: Steel Sheet	0.42 - 0.7	150 - 1000
Fp: Reinforced concrete slab	50 - 125	4000 -11000

Blong's (1981) perforation threshold calculations have been used in more recent publications (e.g. Blong, 1984; Jenkins and Spence, 2009; Jenkins et al., 2014) but they make no significant advancements on the initial study. Jenkins et al. (2014) referred to the work and stated that perforation may occur for impacts below the minimum value and that some roofs may remain intact following impacts above the maximum value but the ranges indicate where most of the damage may be expected

for a typical roofing stock. Jenkins and Spence (2009) note the calculations should be treated with caution as they rely on data collated from numerous studies which used different testing conditions and building materials. Other knowledge gaps surrounding this work include the effect of impact obliquity away from perpendicular, the effect of strikes to cladding which is directly supported by framing and the damage associated with impacts by partially molten, visco-elastic bombs compared to the relatively harder, denser blocks which are currently considered. These knowledge gaps are investigated using post-eruption ballistic impact assessments and ballistic cannon experiments (Chapter 3).

2.3.2.1 Important factors influencing ballistic impacts to buildings

Assessing building vulnerability to ballistic hazards requires an initial identification of the factors which influence ballistic impacts to buildings. The development of fragility and vulnerability functions in particular requires the selection of an appropriate hazard intensity metric (HIM). The following flowchart identifies two possible HIM's for ballistic fragility or vulnerability functions and important aspects of building exposure and vulnerability that influence the hazard's overall damage to buildings (Figure 11). One way to quantify the total ballistic damage to a single building is to model the damage from each individual impact, then sum all of the impacts.

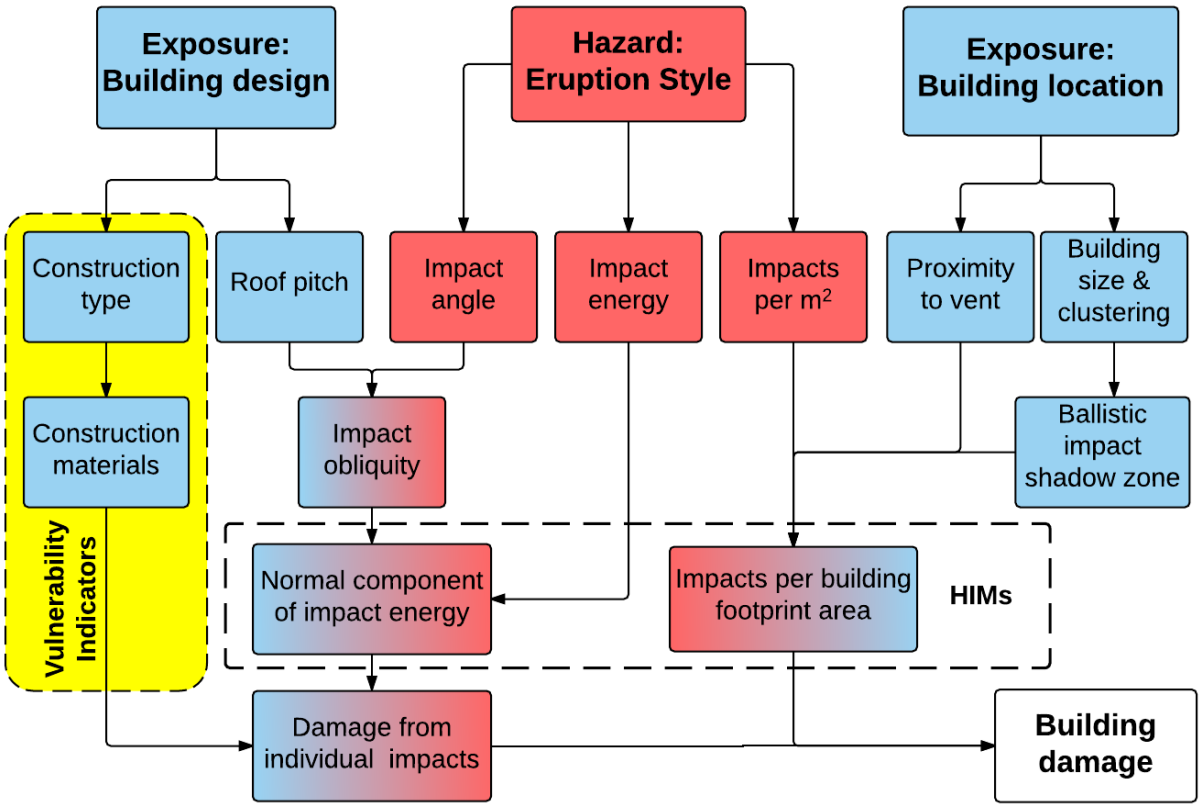

Figure 11: Factors influencing ballistic impacts to buildings. Factors have been identified from review of literature (Chapter 2), post-eruption impact assessments and cannon experiments (Chapter 3). Boxes with colour gradients signify the outcome is controlled by a combination of hazard (red) and exposure (blue) factors. Two potential HIM's have been identified.

2.3.2.1.1 *Damage from individual impacts*

The amount of damage caused by an individual ballistic impact increases significantly if the ballistic is able to perforate the building envelope (see Table 4). This is likely due to a perforating ballistic being able to continue on its trajectory to cause further damage inside the building and because any perforation created increases the building's exposure to rain, wind and other volcanic hazards (Herbin and Barbato, 2012; Fitzgerald et al. in prep). In turn, the single most important factor influencing ballistic perforation potential is the ballistic's impact energy (rather than the building's construction materials). This is because most construction materials (other than RC) have perforation thresholds of less than 1000 joules. By comparison, the impact energy estimations for most ballistics (>20 cm diameter that attain terminal velocity whilst falling) are typically over an order of magnitude higher (Blong, 1981; Fitzgerald et al., 2014; Tsunematsu et al., 2014). However, as the ballistic models that calculate

impact energies have been calibrated predominantly using ballistic craters (e.g. Fitzgerald et al., 2014), the models may be biased towards high energy impacts that leave craters whilst neglecting to model smaller ballistics that do not. Video footage of the 2014 Mt Ontake eruption shows hundreds of relatively small (<10 cm in diameter) ballistic blocks impacting, bouncing and shattering on the ground but leaving no noticeable crater (NipponNewsNet, 2014). Ballistics of this size will have lower impact energies that may not be capable of perforating certain building claddings. Therefore at the lower range of ballistic impact energies, cladding strength becomes an important factor influencing overall building damage.

Oblique WBD impact experiments conducted by McDonald (1990) and Masters et al. (2010) were less likely to cause perforation than perpendicular impacts of the same energy. Obliquity is calculated from the difference between a projectile's trajectory and a line perpendicular to the face of target. For ballistic impacts obliquity is a function of impact angle and the pitch of the cladding it is striking (Figure 12). The reduction in perforation probabilities associated with the full range of obliquities is a knowledge gap that must be quantified as a part of more accurate ballistic-building impact assessments (see section 3.3.2.2.1).

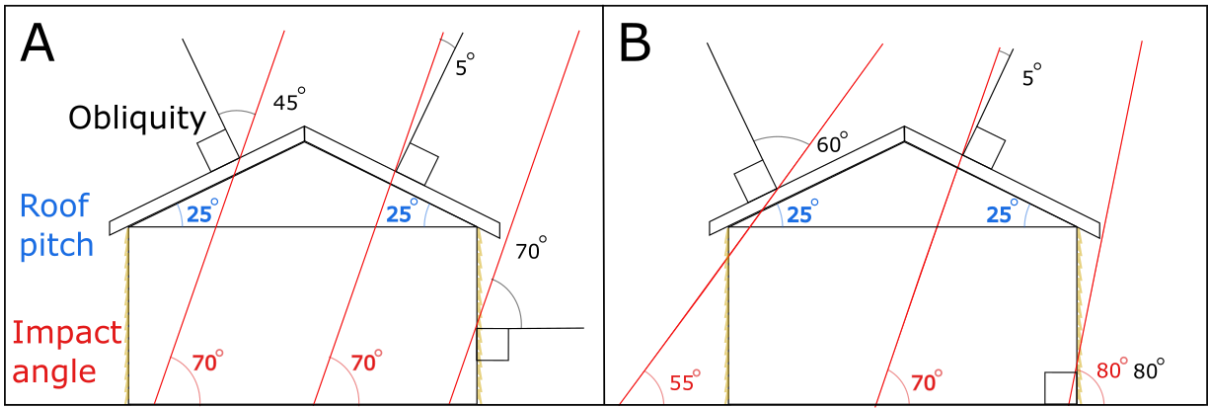

Figure 12: A) Obliquities for ballistic strikes of the same, 70° impact angle but different cladding pitches and B) obliquities for a range of impact angles and cladding pitches. Note that for impacts to vertical walls, obliquity is equal to impact angle.

Another factor to consider is the added perforation resistance buildings possess when impacts strike cladding at locations supported by framing. Impacts of this type will require higher impact energies to perforate the building envelope as ballistics must pass through additional layers of material which are potentially stronger than the cladding itself. The vulnerability of buildings to this type of impact has yet to be

incorporated into modelling to produce more accurate risk or impact assessments. Should framing be impacted and still fail to resist perforation, the ruptured framing member will contribute to additional total building damage and the structure is likely to have a lower load bearing capacity making the building more vulnerable to tephra fall loading. Additionally from studies of building vulnerability to hurricane hazards when a building envelope becomes perforated by windborne debris, the structure is subjected to a much higher risk of damage due to increased internal wind pressure (Herbin and Barbato, 2012). This same phenomena could be applicable to pyroclastic density currents acting on ballistic perforations but this is an aspect of multi-hazard impacts that has yet to be investigated.

Another aspect of ballistic impacts to buildings that Blong's (1984) thresholds do not consider are the differences between juvenile bombs and lithic blocks. The two types of ballistics have different properties influencing their potential impacts to buildings. Bombs ejected during Strombolian or Hawaiian style eruptions typically have slower ejection velocities than blocks ejected during more explosive eruptions (e.g. 25 – 65 m/s mean ejection velocity of bombs from Yasur Volcano, Vanuatu (Gaudin et al., 2014) compared to 200 m/s modelled ejection velocity of blocks from Upper Te Maari (Fitzgerald et al., 2014)). Bombs experience fluidal deformation during flight and often form a distinctive, 'cow patt' shape on impact (Cas and Wright, 2012). Also hardness of projectiles has been found to have a measurable effect on their ability to perforate layers of metal, concrete and soil targets (Kar, 1979; Børvik et al., 2004) thus semi-molten bombs which can deform on impact may be less likely to perforate building envelopes than harder, solid blocks. Bombs typically also have lower densities than cooled, solidified blocks, further reducing their perforation capabilities (e.g. 1810 kg/m^3 average density of 53 bombs from Stromboli (Gurioli et al., 2013) compared to 2400 and 2100kg/m^3 for the two main block lithologies ejected in the 2014 Te Maari Eruption (Breard et al., 2014)). However, the high temperatures that incandescent bombs possess when they are ejected (ranging up to ~1100°C (Blong, 1981; Vanderkluysen et al., 2012)) mean that bombs have the potential (and have been observed) to trigger fires inside buildings, sometimes leading to their complete destruction (Booth, 1979; Wardman et al., 2012; Blake et al., 2015). Blocks on the other hand are much cooler and therefore less likely to start fires (Vanderkluysen et al., 2012)

High temperature, ballistics penetrating through roofs and windows caused fires inside buildings during the 1973 Eldjfell eruption. Sheets of metal were fixed over the windows of walls facing towards the vent in attempt to reduce building damage (Booth, 1979). Holes were burnt in the floor of Mt Ruapehu's Glacier Hut by fragments of a ballistic which shattered directly in front of the hut during the 1975 eruption (Nairn, 1975) and Blong (1984) stated that complete building destruction appears to occur more often from bombs starting fires rather than from repeated block impacts that do not start fires. Forest fires have also been initiated by ballistics on multiple occasions meaning ballistics do not necessarily need to directly impact buildings in order to start fires capable of destroying them (Zobin et al., 2002; Alatorre-Ibargüengoitia et al., 2012).

If a ballistic does perforate the building envelope, making accurate damage estimates becomes more complicated as there are additional factors to consider besides impact energy, obliquity and the cladding's impact resistance. New factors to consider include: the number of internal walls and floors that could be impacted; the contents value of the building; the likelihood that electrical, plumbing or gas lines may be destroyed or the likelihood that a hot ballistic could set fire to the house. Due to the complexities and unknowns involved in calculating ballistic damage caused to building interiors, estimates will rely heavily on assumptions.

A final factor to consider during damage estimates is the time taken to repair a building. When a perforation is made in the building envelope the building may start to take on damage from accelerated water (Herbin and Barbato, 2012) and ash infiltration, especially when the perforation is to the roof.

2.3.2.1.2 *Impacts per building footprint area*

Once a method for estimating the damage from individual impacts has been established, the total damage can be estimated from the sum of these impacts relative to the size of the building. Buildings can absorb a relatively high density of impacts without completely collapsing (Figure 13), but based on repair costs there is likely to be a threshold beyond which repair becomes uneconomical regardless of whether the building has fully collapsed or not. Unless multiple impacts are close together (<1 m apart) each impact is assumed to cause damage independent of neighbouring impacts.

Figure 13: High ballistic impact densities to a timber clad apartment block ~600 m from one of the vents formed during the 2000 eruption of Mt Usu. Photo credit to Professor Hiromu Okada.

2.4 Previously developed tephra-building fragility and vulnerability functions

This section compares the currently available group of tephra-building fragility and vulnerability functions and the impacts they model against the range of possible tephra impacts identified in the previous section (Section 2.3.). This forms a gap analysis which can be used to direct the future development of functions. For ballistic impacts to buildings there are currently no published fragility functions. For tephra fall impacts to buildings, functions focus on a limited range of impacts to a building types which are specific to Neapolitan building types (Pomonis et al., 1999; Zuccaro et al., 2008; Jenkins and Spence, 2009; Jenkins et al., 2014) which reduces their relevance to New Zealand building stocks and their applicability to AVF risk assessments.

All the studies that have produced tephra-building fragility or vulnerability functions to date have followed methods which require the use of analytical, experimental or expert judgement elicitation data (Table 6). Post-eruption impact assessments do not usually the specific aim to develop fragility functions as this requires a large number of restrictive requirements to be met. Firstly, a population of buildings (ideally >30 (Rossetto et al., 2014)) of a particular building typology must be impacted so that

different buildings of the same typology provide examples of the range of potential damage that can occur under varying hazard intensities. This situation is relatively unlikely to occur meaning if fragility functions are to be derived from impact assessments, the data gained across multiple campaigns needs to be recorded in such a way that it can be easily combined and 'harmonised' (Rossetto et al., 2014).

Blong's (2003) survey of 173 buildings impacted by the 1994 eruptions of Mt Tavurvur and Mt Vulcan in Rabaul, Papua New Guinea represents the closest attempt to produce fragility or vulnerability functions using a post eruption impact assessment. The study plotted tephra loading against damage indices (using a five point damage scale from zero representing no damage through to five for collapse beyond economic repair) for 98 timber framed buildings with metal deck roofs (Figure 14). The author has not fit a curve to the data, perhaps due to a lack of impacted buildings, especially for the three lowest damage indices with <15 buildings each.

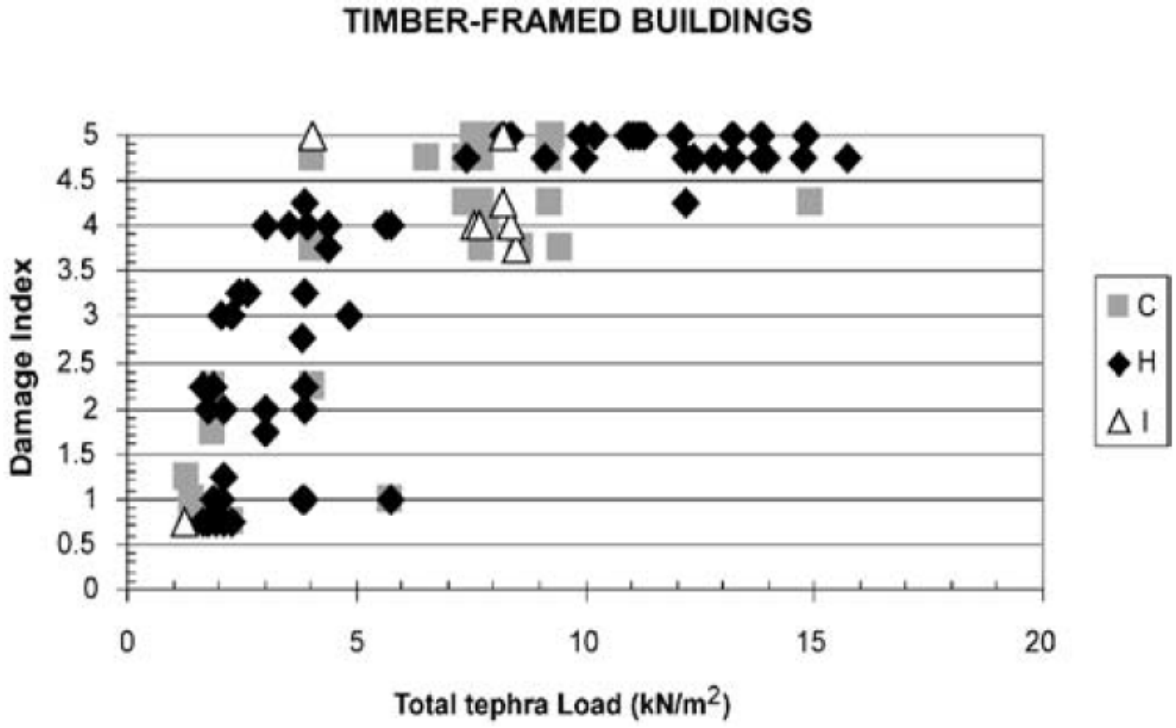

Figure 14: Damage indices plotted against tephra loads for 98 timber framed buildings surveyed in Rabaul, 1994. C, H and I stand for commercial, residential (houses) and industrial buildings respectively. Figure from Blong (2003)

Table 6: Studies and reports that have produced fragility or vulnerability functions using analytical, experimental or expert elicitation data

Study area	Data source	Number of functions	Building types	Reference
Asia-Pacific	Expert elicitation	32	All building types recognised in the GAR 15 "Global Building Schema"	(Maqsood et al. 2015)
European MIA-VITA Volcanoes	Expert elicitation	6	5 major residential roof types and long-span non-residential roofs	(Jenkins and Spence, 2009)
Vesuvius, Italy	Expert elicitation	4	Weak (Old sheet roof), Medium weak, Medium Strong and Strong (Reinforced concrete)	(Spence et al., 2005a)
Sao Miguel, Azores	Analytical and experimental	3	Timber framed buildings of three types based on member dimensions and spacing	(Pomonis et al., 1999)

Roof collapse thresholds are the focus of the studies in Table 6. This is likely to have been driven by concerns for the life safety of building occupants during eruptions (Wilson, 2015). Three of the five functions have been developed for European (specifically Neapolitan) building types, reflecting their origin from the EXPLORIS and MIA-VITA projects which aimed to provide better risk assessment and mitigation to populations surrounding several European volcanoes(Spence et al., 2005b; Zuccaro et al., 2008; Jenkins and Spence, 2009).

In the United Nations Global Assessment of Risk report 2015 (GAR15), Maqsood et al. (2015) produced vulnerability functions for tephra impacts to a wider range of building types within a global building schema. The vulnerability functions they produced relate a roof's superimposed tephra load to an expected, mean damage ratio. Their damage ratio falls between 0 and 1 for the total cost to repair building damage divided by the total cost of the building's replacement. This work resulted in the development of vulnerability curves for 31 different building types. With the wider range of building types considered by this report, several types can be considered more applicable to Auckland's buildings than those developed in the previously mentioned, European vulnerability studies.

For ballistics, there are currently no functions of either type available to date. There is less information for ballistic impacts to buildings than there is for tephra fall for a

number of possible reasons. Perhaps the most important being that tephra fall is a more widespread hazard than ballistics meaning far fewer buildings have been impacted by ballistics. This results in having fewer buildings to survey for vulnerability assessments and ballistic impacts being perceived as less important to study than tephra fall impacts. A further deterrent to researchers developing ballistic fragility function is that the HIMs used for ballistics (impact energy and density for example) are more complicated to measure than the main HIM used for tephra fall functions, which is loading (kPa). The variables required to calculate tephra loading are tephra thickness and density. These variables are more rapidly calculated during a post eruption survey than the variables required to calculate a ballistic's impact energy. This requires measurement of a ballistic's mass and impact velocity. For these measurements to be taken and then correlated with damage, the individual ballistic that has caused building damage first needs to be located. This in itself can prove challenging as ballistics striking with high impact energies are prone to burial, shattering or bouncing. If a ballistic is located and linked back to the damage it caused, the next step is to calculate the block's final velocity which requires modelling of its trajectory. These unavoidable complexities associated with measuring ballistic impact energies in the field support the notion that empirical vulnerability data for ballistic-building impacts is more easily obtained through controlled laboratory experiments. However, before conducting laboratory experiments, it is worth noting that it is possible to develop new fragility functions from the review of previous ballistic-building vulnerability studies (see section 2.5.).Few accounts of ballistic impacts to buildings provide sufficient detail to measure hazard intensity or identify what specific types of building or cladding have been impacted (Table 4). For this reason the perforation thresholds from Blong (1981) represent the most complete source of data for ballistic-building impacts that could be used to derive fragility functions. Jenkins and Spence (2009) stated that due to limited available data they were unable to derive fragility functions for ballistic impacts and instead suggested applying binary cladding failure probabilities at either 0 or 1.

2.5 Developing new ballistic-building fragility functions from review of literature

A more sophisticated approach to derive ballistic perforation fragility functions from a dataset with only two end points, is to find the two impact energies (constants on the HIM, x-axis) where the probability of perforation transitions from 0% to < 0% and from > 100% to 100%. This locates the maximum and minimum perforation thresholds from Blong (1981)'s study. If we assume the mid-point between the maximum and the minimum has a 50% chance of perforation, this allows a third point to be plotted onto the graph. Fitting a curve to these three points with a cumulative distribution gives a fragility function with a typical sigmoidal shape often used in seismic fragility functions (Baker, 2014)(Figure 15). The resulting fragility function implies that there is a 0% chance of a cladding being perforated by a ballistic whose impact energy is below the minimum energy required for perforation as stated in Blong (1981). It also implies that there is a 100% chance of perforation for any impact over the maximum perforation threshold value.

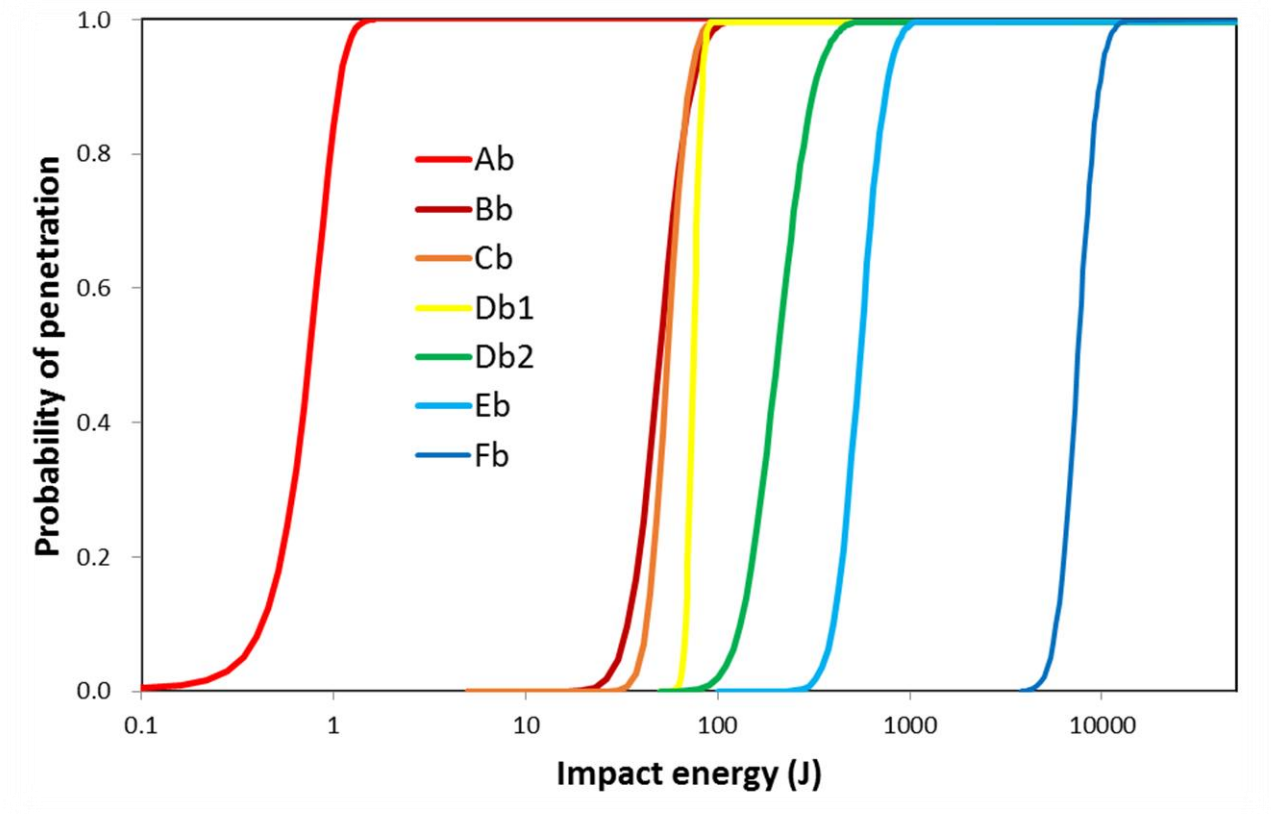

Figure 15: Perforation fragility functions for ballistic blocks striking perpendicular to the plane of various roof claddings. Refer to Table 7 for cladding types and function values.

The ballistic perforation fragility curves are defined using a lognormal cumulative distribution function, which is commonly applied in seismic building fragility studies (Baker, 2014):

$$P(p|IM = x) = \Phi \frac{\ln\left(\frac{x}{\theta}\right)}{\beta}$$

Where the probability of a roof cladding material being perforated (p) is dependent on a ballistic's impact energy (*IM*) which is measured in x joules, Φ is the standard log normal cumulative distribution function (CDF), θ is the median of the fragility function (the IM level with 50% probability of perforation) and β is the standard deviation of lnIM. The functions in Figure 15 can be reproduced using the θ and β values listed in Table 7.

Building material	**Median (θ)**	**Standard deviation (β)**
Ab: Glass sheet	0.75	0.25
Bb: Tile	50	0.3
Cb: Fibre reinforced concrete sheet	55	0.2
Db1: Hardboard	75	0.078
Db2: Plywood	295	0.35
Eb: Steel Sheet	550	0.25
Fb: Reinforced concrete slab	7500	0.2

Table 7: A list of the median and standard deviation parameters for reproducing fragility functions.

2.5.1 Documentation of limitations and applicability

These functions have been derived using simplistic function fitting techniques on a limited dataset from Blong (1981) which in turn gathered its data by collating work from a range of cyclone engineering studies, each using different testing procedures and materials built to different building codes. Furthermore, the perforation impact energy thresholds given by Blong come predominantly from cyclone vulnerability experiments which used roof tiles, steel pipes and wooden 2x4's as their missiles. Ballistic blocks have different properties than these missiles and would perhaps produce different perforation thresholds.

For these reasons it is important to apply confidence intervals to these functions to account for their considerable uncertainty. Jenkins and Spence (2009) suggest

applying uncertainty bounds of ± 20% of the ballistics impact energy. The methodology used to derive these functions is simplistic but in the absence of more detailed, quantitative data, this method has been adopted to derive, the first (known) ballistic-building fragility functions. It is important to validate these curves using empirical data, either from laboratory experiments or post-eruption impact assessments (Chapter 3).

2.6 Summary and research gaps

A critical aspect of volcanic risk assessment is the quantification of probable impacts to society. Despite the large costs associated with building repairs during the recovery phase of eruptions and potential for loss of life from tephra induced roof collapse or ballistic impacts there is limited, useful quantitative vulnerability research on the impacts of tephra hazards to buildings. The framework presented in this chapter has provided a systematic approach for the development of new tephra-building fragility functions so that the vulnerability component of risk and impact assessments may be enhanced.

From the reviews in this chapter, suitable HIMs and building vulnerability indicators have been identified for both tephra fall and ballistic impacts to buildings. The reviews have also been used to develop new ballistic fragility functions and identify tephra fall vulnerability functions that could be used to assess Auckland's tephra risk. However, several questions that require further investigation include:

- How vulnerable are non-structural building components to impacts from light tephra fall hazards?
- How vulnerable are buildings to impacts from ballistic hazards? (Chapter 3)
- How do ballistic hazards interact with or potentially exacerbated the damage to buildings caused by tephra fall and other volcanic hazards? (Section 4.5)

The following chapter investigates building vulnerability to ballistic hazards presenting insights gained from two post-eruption tephra-building impact assessment trips and incorporates the knowledge gained into the development of new ballistic fragility functions derived using ballistic cannon experiments. Chapter 5 then provides an example of the usefulness of these functions in a deterministic impact scenario for the AVF.

Chapter 3 Ballistic Cannon Experimentation

3.1 Introduction

Although ample anecdotal evidence from past eruptions and a group of impact engineering studies provide some understanding of building vulnerability to ballistic impacts, a systematic examination has not been conducted to date. This chapter presents results from ballistic impact experiments to three building claddings commonly used in New Zealand construction (sheet metal, weatherboards and reinforced concrete slabs). A suite of fragility functions has been derived for each cladding to determine the relationship between ballistic hazard intensity and the probability of a given level of damage occurring. The experimental design has been informed by building surveys conducted during two recent post-eruption ballistic impact assessment trips to Mt Usu and Mt Ontake, Japan. This chapter contributes to one of the key thesis objectives to quantify building vulnerability to ballistic hazards and it addresses the risk analysis stage of the risk management framework.

The chapter first presents the findings of the impact assessment trips. The trips identified new factors that influence building damage severity (in addition to those identified in Chapter 2) and common damage mechanisms for different building claddings. Data from the impact assessment trips was used to develop its own suite of fragility functions and to inform the experimental design of ballistic cannon testing (outlined in section 3.3.2). In addition to the development of fragility functions, experiments have also provided information on the velocity of concrete fragments ejected during impact with implications for occupant life safety.

3.2 Post-eruption ballistic-building impact assessment

Post-eruption impact assessments are a source of empirical data on the impacts of volcanic hazards to society (Wilson et al., in review). The focus of previous tephra impact assessment trips has been to gain an understanding of tephra fall impacts to individual system components and the more complex impacts associated with overall system functionality and system interdependencies (Wilson et al., 2012). The two impact assessment trips described below were taken by our research group with one of the specific objectives being to collect data for the development of ballistic-building fragility functions. Data was collected using building surveys on a small number of

buildings impacted by ballistics and tephra fall. Aside from the surveys providing quantitative, empirical damage data they also allowed us to gain qualitative insights of the typical damage patterns that occur when ballistics and tephra fall impact buildings. Qualitative insights such as these can be used to inform assumptions made during impact assessment modelling and they can be used to identify which buildings and even the areas within them, are most suitable for sheltering in during an eruption.

3.2.1 Ballistic-building impact assessment for the 2000 eruption of Mount Usu

In July 2015, a group of eight buildings impacted by ballistics during the 2000 eruption of Mt Usu were surveyed to assess the vulnerability of two separate building types to ballistic damage. Building damage from ballistics in this eruption was primarily controlled by building proximity to vent rather than building cladding type. This suggests impact density (impacts per unit area) may be a more appropriate HIM than impact energy. However, there was one area where the importance of cladding type was illustrated by two reinforced concrete buildings which sustained far less ballistic damage than two adjacent timber and metal clad buildings despite all four being relatively close together and subjected to similar impact densities (Figure 20).

It's important to note that ballistics were not the most destructive hazard for four of the eight buildings surveyed. Two buildings were damaged by severe ground deformation making it difficult to determine how much damage was caused by ballistics and a further two buildings were impacted on their ground floors by a mudflow, leaving ballistic impacts to the roofs and walls still preserved.

From observations and measurements taken in the field previous ballistic hazard studies have shown it is possible to model individual ballistic trajectories and estimate their impact energy (Alatorre-Ibargüengoitia et al., 2012; Alatorre-Ibargüengoitia et al., 2016). In these surveys impact energy is then compared to the damage caused so that data can be plotted onto existing ballistic fragility functions to test their accuracy or it can be used to develop new functions. Qualitative insights into building damage were also obtained during these surveys. The diameter of perforations in metal roof cladding were found to be roughly equal to the diameter of the ballistic causing them. The same is true for the exterior face of concrete slabs. The backface of concrete slabs however displayed a typical high-velocity impact response of back-face scabbing (shattering with fragments being propelled into the building) (Beppu et al., 2008; Peng

et al., 2015). Further insights included the observation that for buildings with pitched roofs, the sides sloping away from the vent received notably less damage and the same was observed for walls facing away from the vent. This suggests that if people were to be caught inside a building during an eruption the safest place to shelter would be on the end of the building on the farthest side from the erupting vent and under any available robust furniture or bed mattresses. This protective action places as many layers of the building envelope as possible, in between a person and the erupting vent.

3.2.1.1Summary of the 2000 eruption of Mount Usu

Mount Usu, located in southern Hokkaido, is one of the most active volcanoes in Japan having had nine major eruptions since 1663 (Takarada, 2003). The most recent eruption began on 31 March 2000 following four days of precursory seismicity and ground deformation. Similar eruption precursors had occurred in the three most recent eruptions, allowing scientists to alert local governments on 29 March and make the first successful prediction of a volcanic eruption in Japan. An evacuation of over 10,000 local residents was completed the day before the eruption (Takarada, 2003). As a result of the evacuations, no lives were lost in the eruption. However, the close proximity of the Toyako Township to the vents resulted in extensive building damage.

Over 50 new craters opened up during the eruption in two distinct areas. The largest eruptions occurred from first craters which opened up on the western flank of Mt Usu on 31 March (Takarada et al., 2002). Volcanic plumes reached 500 m a.s.l. before collapsing to form base surges along Highway 230. Relatively small amounts of tephra were deposited to the northeast with 100 cm being deposited 90 metres from the vent thinning to 2.5 cm at 1 km from the vent. The first ballistic blocks were ejected in the opposite direction to tephra falls in a west- northwest directed swath. The ballistic field extended just over 1 km from the initial vents, with blocks up to 65 cm in diameter landing beyond the highway to the neighbouring Date city (Takarada and Hasaka, 2000). New eruption craters formed with a NW trend towards the main Toyako Township and damage by ballistic blocks continued until June 2000. Despite a large number of buildings being impacted by ash and ballistics, ground deformation and hot mudflows were responsible for the most severe damage in this eruption.

3.2.1.2Building damage surveys

Eight buildings impacted by ballistic blocks during the 2000 eruption that have been preserved within the Usu Caldera Geo-Park were surveyed. Three of these buildings were made of reinforced concrete and five were timber framed buildings with a sheet metal roofs and fibre reinforced concrete sheet wall cladding. During surveys, data on these two groups of buildings and their performance under varying ballistic impact intensities was obtained. Ballistic hazard data collected in the field (including: block size and weight, distance travelled, impact angle etc.) allows for the trajectory of individual ballistics to be modelled so that their impact energy can be estimated and compared to the building damage caused. Although damage data was gathered for both of these groups of buildings there was only a sufficient number of impacts recorded to develop fragility functions for the metal roof clad, timber framed buildings. However, in addition to fragility function development, important qualitative insights into building vulnerability and sheltering capacity have also been made.

3.2.1.2.1*Damage surveys on timber framed buildings with sheet metal roofing*

Ballistic damage caused to timber framed buildings with sheet metal roofing was of particular interest during this study as this is the most common building typology for Auckland's residential buildings (Magill et al., 2006a). This building typology was found to be significantly more vulnerable than buildings with reinforced concrete slab roofing. Across the surveys we observed several damage patterns with important implications for building vulnerability and ballistic hazards.

The main type of ballistics observed in these surveys were relatively high density andesite blocks and although there were no ballistic bombs of unsolidifed magma ejected during this eruption, there were several buildings impacted by 'mudbombs'. Mudbombs had a lower density than the blocks but could still cause considerable damage to buildings (Figure 17B).

Buildings were found to preserve important information that can be used during ballistic hazard mapping such as impact angles, impact densities and size distributions. Information on the diameter of ballistics was recorded by roof perforation diameter as these were found to have very similar size and shape to the ballistics that formed them (Figure 16).

Figure 16: Building damage illustrating the relationship between block diameter and perforation diameter for metal roof cladding.

Impact angles can also be measured in cases where multiple layers of the building envelope are perforated. The trajectory taken between successive perforations gives the impact angle of the block that caused damage. This technique was used during surveys to identify which vent from a group of possible candidates produced the damage causing ballistics for particular buildings (Figure 17).

Figure 17: Building damage illustrating how buildings preserve impact trajectories of ballistics. A) Trajectory measured from alignment of perforations, scratches or mud streaks (red lines) and measuring the impact angle. This technique was used to identify the single vent which ejected ballistics causing this damage from a group of four possible candidates. B) Mudbomb impact with

fragments of timber framing embedded in the wall (orange circle). Photo credit to Professor Hiromu Okada.

All buildings surveyed showed a pattern of having received significantly less damage on the walls and roof slopes facing away from the erupting vent (Figure 18). The walls furthest from the erupting vent have at least one additional layer of the building envelope to reduce a ballistic's speed and impact energy. There's also the possibility that a ballistic will shatter into smaller fragments during its impact to the first layer of the envelope. This produced a shadowing effect with reduced damage to the walls furthest from the erupting vent. Roofs sloping away from the vent also received less damage (Figure 18C & 3D), not due to shadowing but more likely due to the increased impact obliquity as the slope of the roof was more closely aligned to the trajectory of incoming ballistics. The influence of impact obliquity on perforation potential is especially important considering that if a high obliquity impact does result in perforation, the ballistic takes a longer trajectory through the wall potentially causing more damage to framing than a perforation from a perpendicular strike (Figure 19).

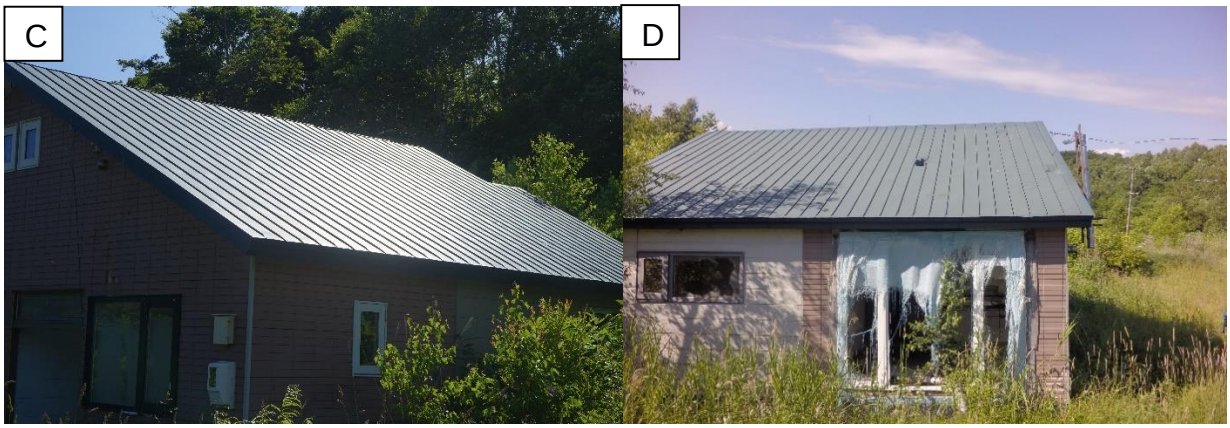

Figure 18: Two buildings which illustrate reduced damage to walls and roofs facing away from the vent. A) The west facing wall of Toyako Kindergarten which received significantly less damage than B) the east facing wall closest to its erupting vent. C) The north facing slope of a metal roof in Kompiriyama which received three minor dents compared to the south slope D) which received one perforation and several large dents.

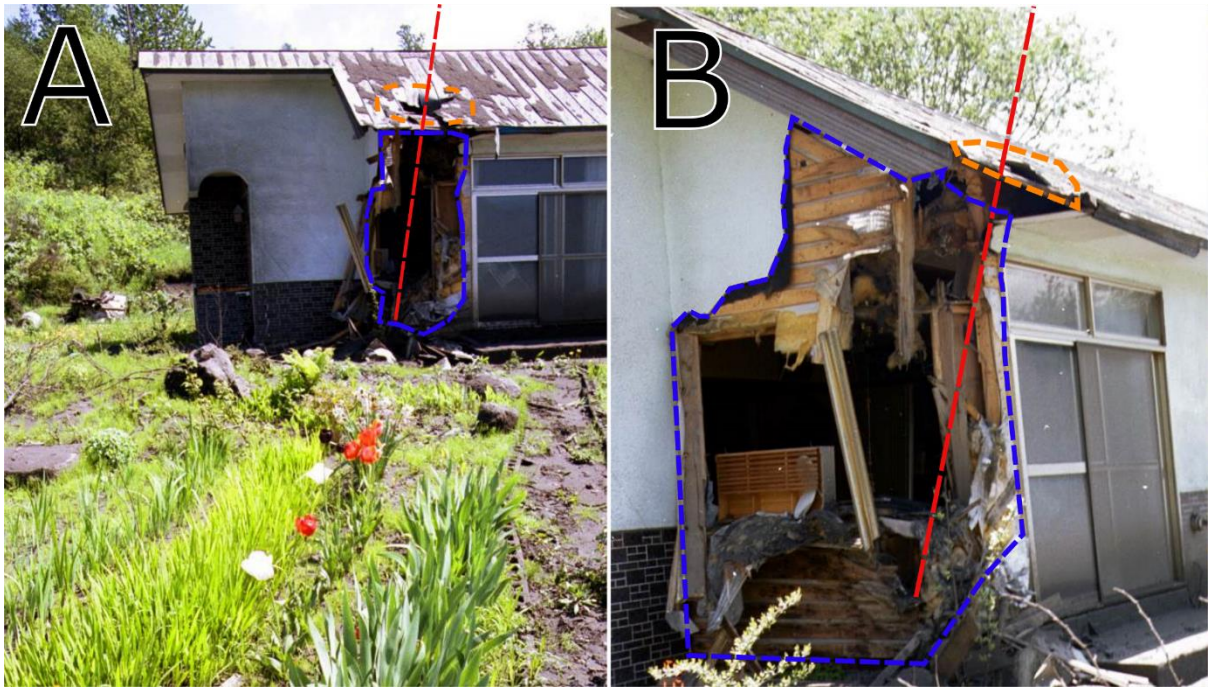

Figure 19: An illustration of the effect of impact obliquity on building damage from a ballistic impact (trajectory in red) from the 2000 eruption of Mt Usu. A) Moderate roof damage from a low obliquity ballistic perforation (orange) transitioning into B) a high obliquity impact causing relatively severe damage to the wall (blue). Photo credit to Professor Hiromu Okada.

3.2.1.2.2*Damage surveys on buildings with reinforced concrete roofs*

Buildings with reinforced concrete made up three of the eight damage surveys. Reinforced concrete clearly offered buildings higher ballistic impact resistances than sheet metal cladding. This was particularly evident for mudbomb impacts to concrete

(Figure 20). The large variability of slab thickness, concrete composition and spacing of reinforcement across the three buildings surveyed made it impractical to produce a single suite of fragility functions. Despite this lack of quantitative vulnerability information, qualitative insights have still been made with implications for life safety and building repair costs.

In all three buildings there was evidence of back-face scabbing (Stephenson et al., 1978) where ballistic impacts had shattered the concrete and sent fragments flying into buildings. The impact sites had large masses of concrete sheared out in a conical shear shape typical of projectile impacts (Yankelevsky, 1997). Scabbing had ejected fragments over a wide area increasing damage to the building interior and increasing the potentially lethal zone had anyone been sheltering inside the building.

Figure 20: Performance of different roof claddings in impacted by predominantly by ‘mudbombs’ in Toyako. Timber cladding performed the worst (orange) followed by metal (blue) and concrete (black). Two perforations to the concrete apartment examined during surveys are circled. Photo credit to Professor Hiromu Okada.

The presence and spacing of reinforcing bars was found to strongly influence the sizes of ballistics that could perforate into a building and contradicted the assumption that larger blocks were more likely to perforate the building envelope (Figure 21). It was found that if a ballistic was too large to fit between reinforcement bars then it was less likely to perforate the concrete. At the Yasuragi No Le municipal bathhouse, the largest ballistic to impact did not perforate the building despite having an impact energy an order of magnitude higher than the threshold for ballistic perforation suggested by Blong (1981) . Instead the ballistic was suspended by the reinforcement bars, spaced 20 cm apart so that the ~60×40 cm sized block could not pass between them (Figure 21B). This phenomenon reduces the probability of a large ballistic puncturing successive layers of reinforced concrete however there is still potential for the increased volume of shrapnel produced by large blocks to cause significant building damage.

Figure 21: Illustration of ballistic impacts from the 2000 eruption of Mt Usu causing concrete slab perforation without complete ballistic perforation due to reinforcing bars. A) Impact at Toyako Kindergarten, ~600 m from vent, 15 cm spacing between bars. B) Impact to Toyako's municipal bathhouse ~550 m from vent, 20 cm spacing between bars.

The surveys of concrete buildings also found evidence of increased ash ingress through ballistic perforations. At the Sakuragaoka apartment complex, ballistic impacts caused perforations to the concrete roof above two rooms on the top floor of the building. An estimated 20 mm of tephra fell in this area during the 2000 eruption (Takarada, 2003), yet now there is a 30 cm thick deposit of wet tephra inside unit 505, in which a tree has grown over the past 15 years. The ash layer is thickest in the room where its ceiling was perforated by two impacts, it then thins to around 10 cm thick in

the adjacent room with no significant volumes of ash being found beyond the entrance to unit 505.

3.2.2 Ballistic-building impact assessment for the 2014 eruption of Mount Ontake

The sudden phreatic eruption at the summit of Mt Ontake in 2014 took 63 lives (Murase et al., 2016). At the time of our visit there were still 6 people missing and we were unable to conduct an impact assessment near the summit. Instead we gathered data from semi-structured interviews with local scientists from Nagoya University and from video footage and photos taken before, during and after the eruption. In the last 40 years Mt Ontake has had four phreatic eruptions (Maeda et al., 2015), two of which have resulted in building damage caused by ballistics . Video footage taken during the eruption suggests that many of the ballistic blocks impacting near the summit were relatively small (<10 cm in diameter) and that relatively few of the ballistics impacting buildings were able to perforate the building envelope (NipponNewsNet, 2014). The fact that none of the people sheltered inside buildings were killed and at least one hiker was able to successfully avoid injury by holding their pack over their head suggests buildings can offer effective shelter from some ballistic impacts and that building occupants should seek to put as many layers of the building envelope or furniture and bags etc. in-between themselves and incoming ballistics in order to increase their safety.

3.2.2.1 Impacts to mountain huts

The mountain lodge area is has eight timber structures with metal clad roofs, roughly 600 metres from the vent. Their roof cladding is weighted with boulders 30-40 cm in diameter to prevent roof detachment in high winds. During the eruption, the structures were impacted by surge, tephra fall and ballistics. Damage from tephra fall appears to be limited to contamination with loads not being high enough to cause structural damage. Ballistic damage included perforations through roofs, walls and floors. Tephra fall and ballistics appear to have influenced each other's impacts (Figure 22B). Ballistic perforations have become points for increased tephra contamination into buildings and tephra deposits in conjunction with the boulders placed on the roofs prior to the eruption appear to have provided an armouring effect to buildings, increasing

their resistance to ballistic damage. The armouring effect is inferred from ballistics ~15 cm diameter, being unable to perforate the timber roof cladding and instead being resisted to form small impact craters in the tephra. Ballistics of this size, impacting 600 metres from their vent possess impact energies in excess of 4000 joules, about four times higher than the energy sheet metal cladding is capable of resisting (Blong, 1981; Herbin and Barbato, 2012).

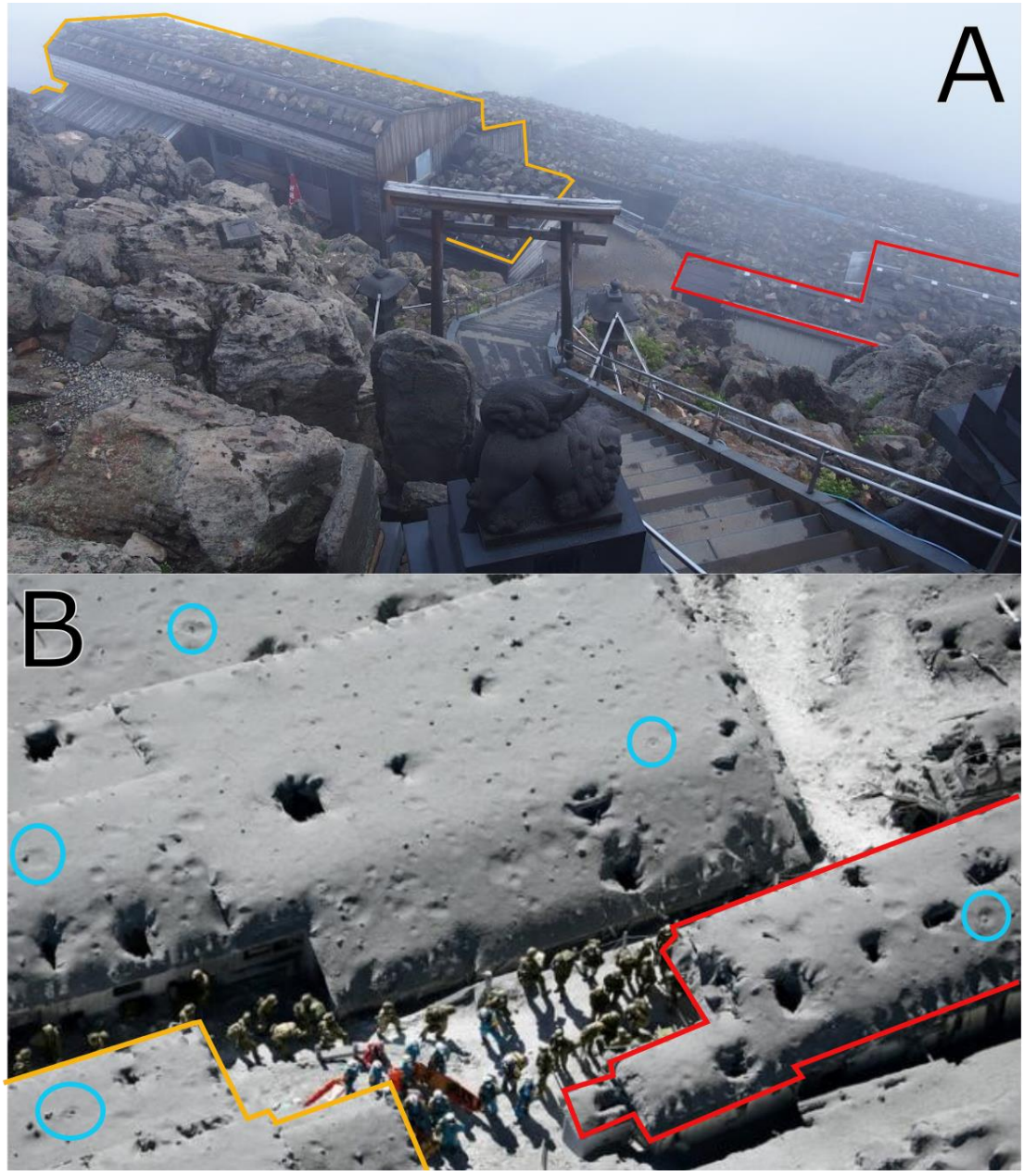

Figure 22: Mountain huts near the peak of Mt Ontake. Buildings outlined for comparison (red and orange). A) 30-40 cm diameter boulders visible on roofs before the eruption. B) Huts with ballistic perforations covered in tephra fall. Some small ballistics have remained near their impact craters in the tephra (blue circles). Photo A) from, Wikimedia Commons (Alpsdake, 2014) and photo B) from Kyodo News (Wang, 2014).

Despite individual ballistics perforating entirely through buildings in places, no deaths occurred inside buildings (Fitzgerald et al. in prep). From Figure 22B and video footage from inside the hut during the eruption, it is clear that a large number of ballistics impacted the huts, yet the relatively low number of perforations suggests the majority of these impacts did not cause perforation (NipponNewsNet, 2014). These impacts are likely to have been from small ballistics whose mass (and therefore impact energy) was too low to perforate the building envelope, allowing the huts to successfully shelter their occupants. Ballistic cannon experiments have been conducted to quantify the impact resistance of cladding materials to relatively low energy ballistic impacts such as these (section 3.3).

3.2.3 Fragility functions for timber framed buildings with sheet metal roofing

The following fragility functions provide the conditional probability of a specific level of damage being caused to a sheet metal roof depending on the impact energy of a ballistic. A ballistic's impact energy is defined as its kinetic energy at the moment it impacts. Therefore impact energy can be calculated using the equation for kinetic energy.

$$Impact\ energy\ = \frac{1}{2}\ mass\ \times\ velocity^{\,2}$$

Where impact energy is measured in joules, mass is measured in kilograms and velocity in metres per second. Accurate impact energy calculations are difficult to make from surveys as the mass and velocity of individual ballistic impacts is not able to be directly measured in the field and therefore requires modelling. In rare cases where ballistics have been recovered and matched to their impact point, their mass can be measured. When ballistics that have caused damage cannot be recovered, mass calculations first require their mass be estimated based on their size (from perforation/dent diameter) and the assumption that their density is similar to that of other ballistics found in the vicinity. Calculating the final velocity of a ballistic at the moment it strikes a building requires modelling and further assumptions. Modelling was completed using the "Eject!" ballistic model (Mastin, 2001) which requires 11 input parameters to output a ballistic trajectory with horizontal travel distance and final velocity calculated. Values for several input parameters could not be measured using

building surveys alone meaning assumptions have been used to assign values where necessary (Table 8). Assumptions are a significant source of uncertainty to any resulting impact energy estimates and this must be acknowledged with the use of uncertainty bounds on fragility functions. Once the first ten input parameters have been assigned a value, the last parameter (initial velocity of ejection) is adjusted until the block's horizontal travel distance matches the map distance the block must have travelled between the block's vent and the point where it impacted. A similar method for estimating ejection velocity based on field mapping of ballistics has been used in other studies (Alatorre-Ibargüengoitia et al., 2012; Alatorre-Ibargüengoitia et al., 2016). Once the ballistic's trajectory has been modelled, the final velocity associated with this trajectory is used in the above equation to calculate impact energy.

Table 8: Eject! input parameters that required assumptions to allow parameterisation.

Input parameter	**Assumed value**	**Assumption rationale**
Block diameter	Equal to diameter of cladding perforate/area damaged	Relationship observed during surveys
Block shape	Cubes (blocks) or spheres (mud balls)	Angular blocks of country rock observed during surveys of six buildings. Two buildings were predominantly impacted by well-rounded pyroclastic "mud balls"
Block density	2200 kg/m^3 blocks or 1800 kg/m^3 mud balls	Typical andesite lava density (Breard et al., 2014) with lower density for "mud balls"
Drag coefficient	1.0	Consistent with experimental and numerical studies (Alatorre-Ibargüengoitia and Delgado-Granados, 2006; De'Michieli Vitturi et al., 2010)
Ejection angle	Less than or equal to the impact angles measured during surveys	Ballistics follow near parabolic trajectories where it is possible for the impact angle to be higher than the ejection angle (due to air drag) but it is very unlikely that the ejection angle be higher than the impact angle

Once impact energies have been calculated, they are compared to their damage caused. The damages caused by individual ballistic impacts were categorised into one of four damage states (DS). The damage state descriptions are based on sheet metal failure mechanisms of increasing severity commonly observed during surveys Table 9.

Table 9: Damage state descriptions for ballistic impacts to buildings with sheet metal cladding.

Sheet metal cladding	
Damage state	**Damage description**
DS 0	Cosmetic damage: scratches as evidence of impact
DS 1	Cosmetic damage: denting
DS 2	Moderate damage: tearing
DS 3	Severe damage: ballistic perforation

Impact energies were calculated for a total of 26 individual ballistic impacts to buildings with sheet metal roofing. Due to a limited data set, fragility functions have been produced using the simplistic binning methodology outlined in Porter (2007). The data on impact energies and their associated damage states is summarised into a fragility function bin plot (Figure 23). Damage data has been ordered by increasing impact energy and grouped into three bins so that each contains a similar number of data points. The probability of a given damage state being reached or exceeded is calculated for each bin by counting the number of data that are equal to or greater than the damage state of interest (see Table 10 for an example). The probability is applied to the median value in the bin range. Using three bins provides fragility functions made up of three straight line segments (Figure 24).

Table 10: Calculations for damage state exceedance probabilities for the 500 – 1500 joule impact energy bin.

Impact energy (j)	Damage state (DS)	Exceedance probability calculation
504	1 (denting)	$P(ds \geq 0) = \frac{8}{8} = 1$
504	1	
566	2 (tearing)	$P(ds \geq 1) = \frac{8}{8} = 1$
566	2	
1347	2	$P(ds \geq 2) = \frac{6}{8} = .75$
1347	2	
1347	2	$P(ds \geq 3) = \frac{1}{8} = .125$
566	3 (perforation)	

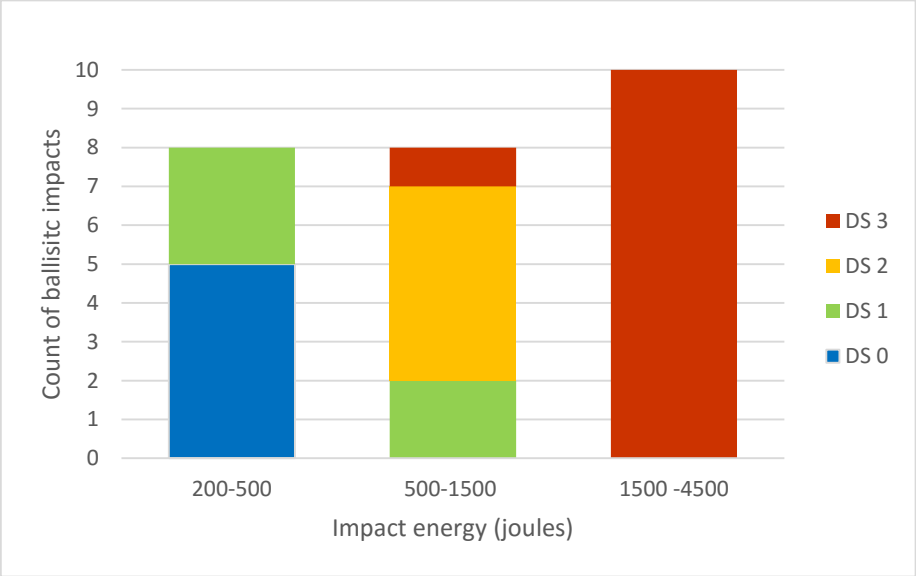

Figure 23: Bin plot of damage data from 26 ballistic impacts to sheet metal roofs.

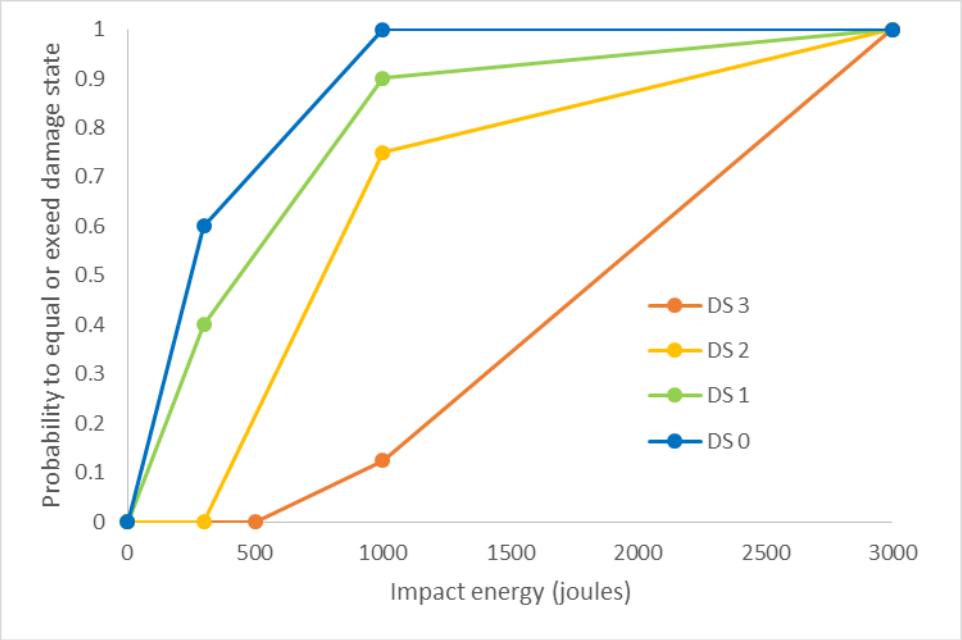

Figure 24: Fragility functions produced using damage data presented in Figure 23.

Despite these fragility functions having large uncertainties they can still be used to quantify building vulnerability to ballistic hazards. Perforation can occur at any impact energy higher than 500 joules and in this survey all ballistics of >10 cm in diameter exceeded this meaning all but the smallest ballistic particles are capable of puncturing metal roofs. With this in mind some of the impacts >1000 J did not cause perforation meaning the sheet metal may have a higher impact resistance than previous research suggests (e.g. Blong, 1981; Alphonso and Barbato, 2014). In these surveys 5 impacts with energies estimated at over 1400 joules resulted in DS 2 tearing without DS 3 perforation. This response is attributed to variable impact obliquities and the additional resistance offered by timber framing beneath certain sections of cladding. Research into the vulnerability of sheet metal roofs with timber framing is important as this roof typology is the most common within the Auckland building stock.

3.2.3.1 Limitations of fragility functions derived from impact assessments

The biggest limitation of these fragility functions is that they have been derived from a small dataset of 26 impacts to a population of five buildings with impact energy calculations relying on numerous assumptions. As a comparison with seismic fragility functions, Rossetto et al (2014) suggest function derivation requires a minimum of 30 buildings of a given class and recommends >100 buildings.

Although impact obliquity is known to have an effect on target damage (Johnson et al., 1982; Chen et al., 2006), the obliquity of each impact is not possible to measure during surveys and thus damage from impacts of varying obliquities have been aggregated into one suite of fragility functions. During these relatively rapid surveys there is also likely to be a bias towards perforations being recorded compared to less severe DS 1 and DS 0 impacts which are more difficult to notice.

Another limitation of these damage state functions is that they provide predictions of when very specific types of damage may occur to cladding. They do not give a wider indication of the overall impact to the building, i.e. on whether or not it may be habitable or structurally sound. Fragility functions also do not provide an indication of the likely cost to repair damage. These are important areas of future research for ballistic impacts to buildings. To overcome issues associated with impact energy and obliquity calculations from post-eruption building surveys, fragility functions can be developed from experimental studies.

3.3 Ballistic cannon experiments

3.3.1 Previous experimental studies

This study builds on the preliminary research of Blong (1981) and the functions produced from experimental data may be used to assess the accuracy of Blong's perforation threshold estimates. More recent experimental studies from the fields of impact engineering and hurricane-building vulnerability have informed the experimental design and parameters (e.g. McDonald, 1990; Fernandez et al., 2010; Masters et al., 2010; Alphonso and Barbato, 2014; Chen and Hao, 2015).

Windborne debris (WBD) impacts to metal hurricane shutters have been experimentally investigated by Fernandez et al. (2010) and Alphonso and Barbato (2014). Alphonso and Barbato (2014) conducted 48 impact tests using 2×4 lumber missiles to produce fragility functions defining the relationship between kinetic energy and the probability of shutter failure. Their preliminary experiments found that a missile's kinetic energy is a suitable hazard intensity measure to use in functions. Kinetic energy correlated more strongly with observed damage than other possible HIM's such as missile velocity or missile length. The maximum threshold that shutters

were found to be capable of resisting puncture was 1150 joules. Fernandez et al. (2010) completed a similar study investigating tile impacts to metal shutters. They conducted 180 tile impact tests and 60 2×4 tests using lumber missiles of the same weight and velocity to compare performance as a function of debris type. The shutters performed to their certification standard under normal 2×4 tests with 4.1 kg (9 lb) missiles launched at 15.25 m/s (50 fps) but the equivalent kinetic energy for the tile tests produced significantly more total shutter deformation. Fernandez et al. (2010) also investigated the effect of tile's impact orientation. Tiles were launched to produce both edge and flat impacts and in all but three of the 180 tile tests, the edge impacts produced greater total deformation, demonstrating the effect of impact surface area on damage. All tests in both studies used 90° impact angles and produced curves for impact locations not directly supported by framing.

WBD impact experiments to a range structural insulated wall and concrete masonry wall configurations were carried out by Chen and Hao (2015) and McDonald (1990) respectively. Chen and Hao (2015) conducted 2×4 timber impact tests to 14 wall panels. They found walls with ductile skin materials had a higher penetration resistance capacity than walls with brittle rigid skin materials such as fibre cement, even if the brittle materials possessed higher compressive strengths. McDonald (1990) launched 15 lb, 2×4 timber missiles at 11 concrete masonry wall specimens of various configurations. The study found that reinforced masonry cells could resist timber missile puncture by causing missiles to splinter when impact velocity was over 100 mph. Unreinforced cells were perforated by missiles travelling over 65 mph unless the panel was tilted to produce a 45° oblique impact angle. In these cases the missile tended to bounce off the panel without causing damage. Masters et al. (2010) also found that oblique impact angles produced less damage than perpendicular impacts with the same kinetic energy during tests on glass sheets impacted by roof shingles.

Projectile impacts to reinforced concrete targets have been extensively studied for both military and civil applications over the last century (e.g. Yankelevsky, 1997; Chen et al., 2004; Warren et al., 2004; Li and Hao, 2014; Imran Latif et al., 2015). Stephenson et al. (1978) and Haldar and Miller (1982) used rocket propelled sleds to launch 12 inch steel pipes at reinforced concrete panels to investigate the effect of concrete thickness, impact angle and impact location on observed damage. Their

studies identified common impact responses for RC and these have been adopted for use as damage states in the development of RC slab fragility functions. One common impact response with significant implications for property damage and life safety is the high velocity ejection of fragments from the back-face of panels when they are impacted by projectiles (Li and Hao, 2014; Imran Latif et al., 2015).

These experimental studies use projectiles, targets and impact velocities that are not highly applicable to ballistic impacts to buildings. Many of the impact engineering studies reviewed are concerned with the military applications of high velocity (>400 m/s) impacts by bullets, rods or metal pellets into targets specifically designed to resist damage such as thick steel plates or high strength reinforced concrete (e.g. Bryan, 1962; Chen et al., 2004; Peng et al., 2015). Hurricane vulnerability studies provide a closer simulation of ballistic impacts to buildings as both are concerned with the same type of target, namely building claddings and because the impact velocities of WBD and relatively slow ballistics are comparable (i.e. 30-50 m/s) (Stephenson et al., 1978; Fernandez et al., 2010; Alphonso and Barbato, 2014). However none of the studies reviewed used projectiles that adequately simulate ballistic block or bomb impacts.

3.3.2 Methods

These experiments subjected sheet metal, weatherboard and reinforced concrete panels to impacts from volcanic blocks. Blocks weighing 3.5 – 10 kg were launched at up to 37 m/s using the University of Canterbury's ballistic cannon. Panel damage and block velocity were recorded using two GoPro cameras. Impact energies from 90 - 3500 J were calculated and compared to the damage caused by individual tests to construct fragility function suites for each cladding type tested. Claddings were fixed to timber framing in such a way that structures would fit beneath the cannon apparatus whilst adhering to New Zealand building standards as closely as practicable. The cannon was constructed to launch blocks with controlled accuracy and speed for consistency between tests.

3.3.2.1 Air cannon apparatus

The air cannon apparatus is comprised of 4 major components; the pneumatic ram which propels blocks into free flight towards targets, the air compressor and barrel which supply the pressure force to the ram, the trigger which releases the ram allowing built up air pressure to accelerate it forward and the tripod system which absorbs the cannon's recoil during firing (Figure 25).

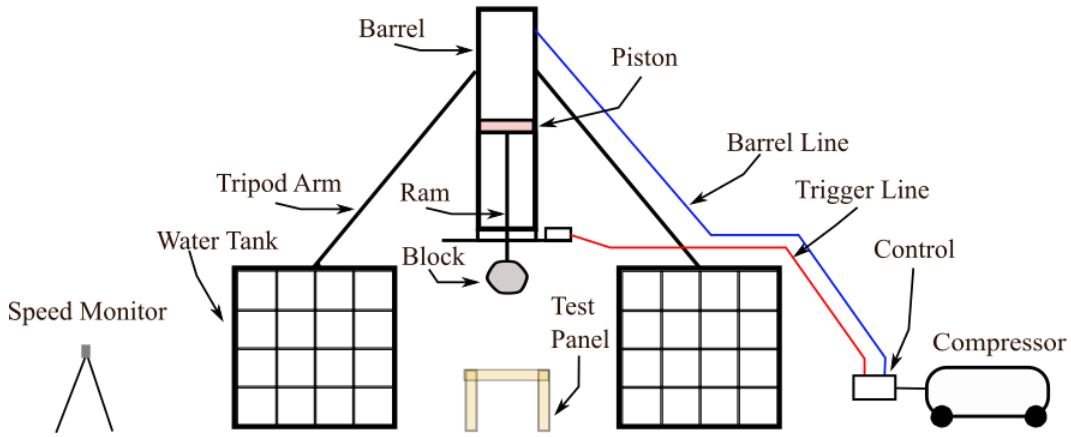

Figure 25: Testing apparatus schematic. Not to scale.

The pneumatic ram fits within the barrel and harnesses the pressure built up behind it. It consists of a firing rod and plastic piston with a rubber ring around the perimeter. The ring forms a seal between the piston and the barrel's inner wall. The rod provides a) the location point for loading blocks onto the cannon and b) a lock that allows pressure to be built up inside the barrel prior to firing.

The barrel is a 1200 mm length of 208 mm diameter drilling pipe. Internally, the barrel is divided into an upper air cylinder where pressure is built up and a lower actuating cylinder where the ram can accelerate forward (Figure 25). The ram's forward motion is arrested as the piston collides with the end of the actuating cylinder. This propels the block from the rod sending it into free flight towards the target below.

The ram and barrel are held in the air by a tripod which is attached to a set of 1000 litre water tanks (Figure 25). The tripod system reduces recoil during firing but also constrains the height and dimensions of test structures as they must fit under the cannon within a test space of around 1 m^3. The tripod also holds the barrel in the air so that a greater flight distance can be achieved by projectiles allowing for more accurate velocity measurements from video recordings.

3.3.2.2 Impact energy measurements

As outlined in the equation from section 3.2.3, a ballistic's impact energy is dependent upon its mass and final velocity. To measure impact energy the mass of each block was recorded prior to testing and the velocity of blocks during individual experiments was measured using videos from two GoPro cameras filming at their highest frame rate of 240 frames per second. To measure the velocity of a block, the number of frames taken by cameras during a block's flight were counted then compared to flight distance. Frame counting began from when the block first started moving to when it first touched the test structure. This distance was then measured and divided by the flight time to calculate velocity.

3.3.2.2.1 *Impact energy measurements for oblique impacts*

For oblique impacts, impact energy was initially measured using the same method as for perpendicular impacts described above. However, studies of high velocity impacts to concrete, metal and soil targets in the field of impact engineering have shown oblique impacts typically cause less damage than perpendicular impacts of the same energy (Bruce, 1962; Bryan, 1962; Kar, 1979; McDonald, 1990; Chen et al., 2004; Masters et al., 2010). There were not enough materials available to produce fragility functions at several specific impact obliquities. Instead, impacts with obliquities ranging 20-70° were carried out for all three types of cladding and the normal component of impact energy was resolved for each test so that data from different testing conditions could be aggregated. To calculate the normal component of impact energy, first the normal component of velocity must be calculated. The equation used by Bryan (1962) and Bruce (1962) to calculate the normal component of impact velocity is set out below.

$$Normal\ component\ of\ velocity\ (V_n) = \ Original\ velocity\ (V_o) \times Cos\theta$$

Where θ is impact obliquity, defined in Chapter 2 as the angle between a missile's incoming trajectory and a line perpendicular to the face of a target. This reduced velocity was then used in place of the original velocity to calculate the normal component of impact energy so that damage from oblique impacts could be used to create fragility functions consistent with perpendicular impacts.

3.3.2.3 Block projectiles

Volcanic rocks from the Taupo Volcanic Zone (TVZ) and Halswell Quarry in Christchurch weighing between 3.5 and 10.0 kg were used as the projectiles in this testing (Figure 26). The TVZ rocks were andesite with an average density of 2569 kg/m^3, similar to that of the most commonly ejected ballistic block lithology from the 2012 eruption of Upper Te Maari (Breard et al., 2014; Fitzgerald et al., 2014). Aluminium mandrels (Figure 26B) were fitted to each block to allow for intimate contact between the block and the ram, giving more controlled flight paths and preventing the ram from shattering blocks. To further decrease the likelihood of blocks shattering, only relatively dense blocks were used. For the metal and weatherboard tests, this meant the same block could be used for nearly all of the shots, decreasing the number of variables responsible for observed impacts. These blocks were examined for chips after each test to ensure block weight remained constant. Using blocks of the same weight throughout a set of experiments also gave a near linear relationship between the barrel's air pressure and the block's velocity, allowing for better control on impact energies during tests.

The same exact block could not be used for all shots fired at the reinforced concrete slabs as most blocks were damaged beyond use after only one shot. To reduce variability in the experiments 11 of the 16 different blocks used, were all the same rock unit, Stoddart Basalt from Halswell Quarry in Christchurch. TVZ andesite blocks were used as the remaining five projectiles in these tests. To investigate the effect of rock strength on projectile impacts, strength and density tests were carried out on the basalt blocks and on andesite blocks from Mt Ruapehu, similar to the ones used in testing. The basalt blocks were tested by laboratory technicians from the University of Canterbury's Department of Geological Sciences and tests on andesite from Mt Ruapehu were conducted by a fourth year University of Canterbury engineering geology student (Cook, 2015). The basalt blocks were denser and stronger than the andesite blocks (Table 11).

Table 11: Summary of strength and density tests carried out on both projectile types. Cook's test methods were in accordance with Ulusay and Hudson (2007).

Test	Stoddart Basalt		TVZ andesite	
	Average value	Number of tests	Average value	Number of tests
Bulk density (kg/m^3)	3027	16	2569	5
Unconfined compressive strength (Mpa)	187	25	98	5
Point load strength (Mpa)	7.15	35	Not tested	0

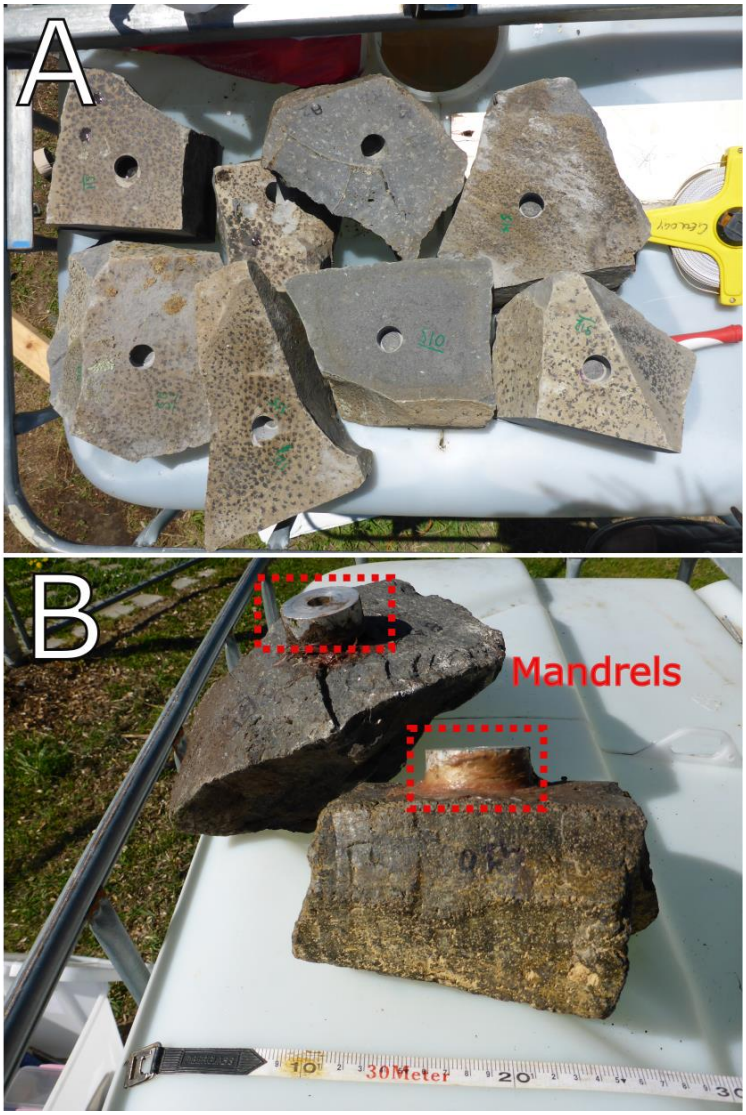

Figure 26: Volcanic rocks used as projectiles during testing. A) Stoddart Basalt from Halswell quarry used in the concrete tests. B) TVZ andesite blocks used in the sheet metal, timber framing and weatherboard tests.

3.3.2.4 Cladding materials tested

Three different types of cladding materials were tested to produce suites of fragility curves that quantify the cladding's vulnerability to ballistic impacts. Large quantities of sheet metal and rimu bevel-back weatherboards were donated for testing by the Pumphouse Salvage Yard in Christchurch and reinforced concrete slabs were prepared by Stahlton Precast. Sheet metal and weatherboards were chosen for testing as these comprise the two most commonly used roof and wall claddings in the Auckland building stock respectively. The cladding panels were subjected to impacts of various angles and framing configurations to capture the range of impacts that claddings could be subjected to during an eruption.

3.3.2.4.1 *Sheet metal tests*

The sheet metal impact tests consisted of 50 shots fired at steel and aluminium sheet metal panels under varying conditions. The same 3.5 kg andesite block was used during all tests and it sustained no significant mass loss throughout testing. Twenty shots were used to develop fragility functions for impacts where ballistics a) have impact trajectories perpendicular to the plane of the sheet and b) impact the metal at a location where it spans between framing members (Figure 27). This impact scenario was chosen to test the accuracy of Blong's (1981) study.

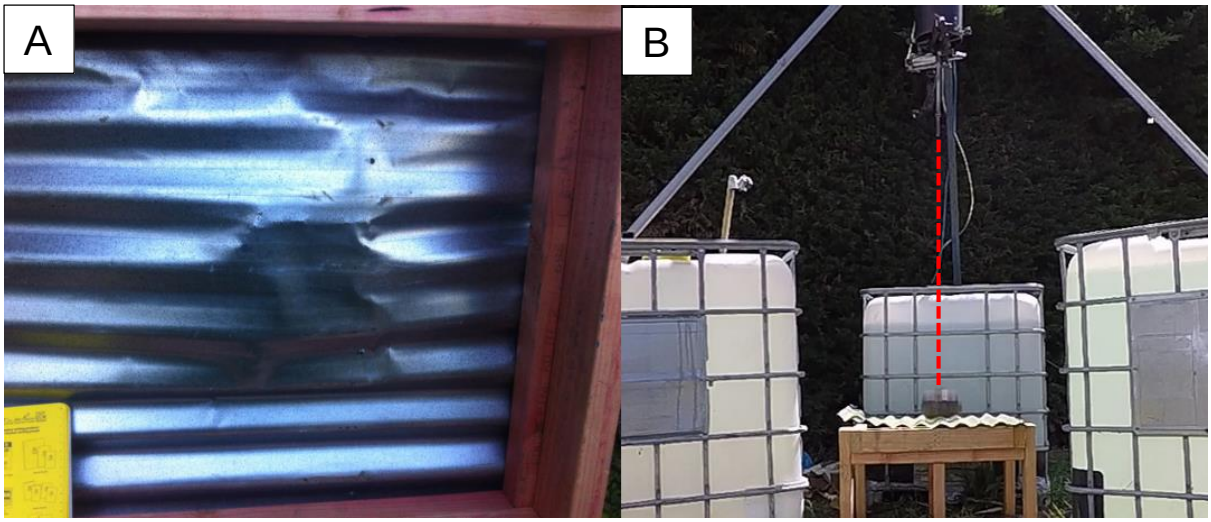

Figure 27: Perpendicular cladding strike tests. A) The cladding has been impacted where it spans between framing members. B) Snapshot from Test 29 illustrating cladding orientation perpendicular to the block's trajectory (red line).

Sheet cladding materials are expected to be highly vulnerable to impacts of this type as ballistics can puncture the building envelope without having to rupture framing

members and because perpendicular impacts absorb maximum impact energy compared to oblique impacts which have the potential to deflect impacts. To capture the increased resilience cladding has for oblique impacts and impacts to framing, additional tests were conducted.

3.3.2.4.1.1 Perpendicular cladding strike experiments

These experiments were used to produce fragility functions from 20 shots fired at corrugated steel roof cladding panels 0.52 mm thick. The panels were fixed to a timber frame according to the New Zealand Building Code (Department of Building and Housing 2011). The frame itself was built to comply with NZS:3604 for timber framed buildings as closely as practicable. It was made using H1.2 treated timber with the maximum member spacing for a high wind zone roof, of 90 and 60 cm spacings between the centres of purlins and rafters respectively. The test structures could not fully comply with building standards for several reasons. Limited space beneath the cannon apparatus was the main constraint on building more accurate model structures. Other discrepancies such as having to fix sheet metal over two purlins as opposed to the requisite three and the fact that all salvaged metal had slight defects are assumed to have little effect on impact resistance. Defects included all salvaged sheets already having screw holes from their original fixing and some having isolated areas of rust damage at their unpainted edges.

3.3.2.4.1.2 Perpendicular timber framing strike experiments

These experiments consisted of 14 shots using the same 3.5 kg block projectile and basic frame design as previous experiments. The only difference to the frame was the addition of a third ‘rafter’ down the centre which projectiles would be targeted at. The same H1.2 treated timber was used and vertical support studs were installed under the rafter – purlin joints in accordance with NZS 3604 (Figure 28A).

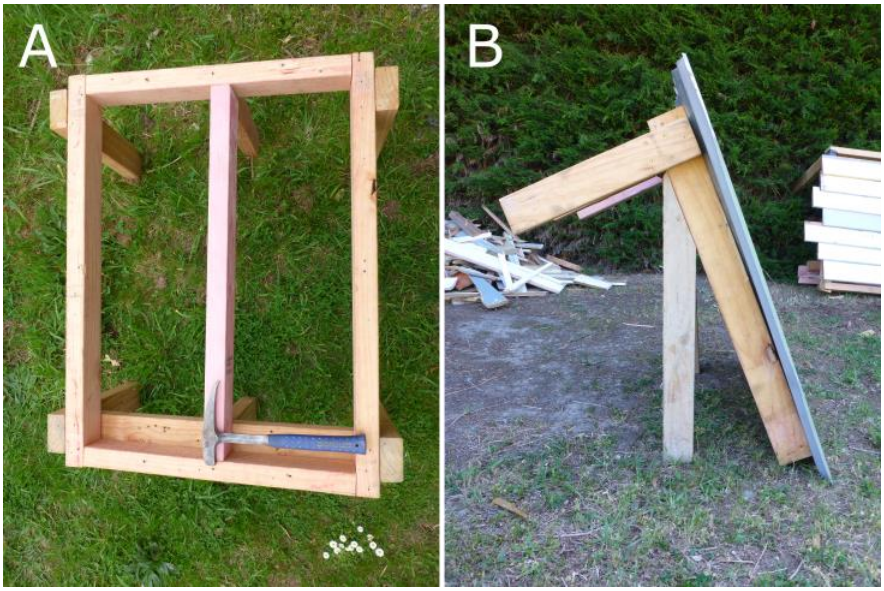

Figure 28: Framing set ups for A) perpendicular timber framing strike experiments and B) inclined cladding strike experiments.

3.3.2.4.1.3 Inclined cladding strike experiments

These experiments consisted of 16 shots with obliquities of 20-70°. The same 3.5 kg block and frame configuration was used as in the initial perpendicular tests with the exception of the frame's leg lengths being changed to produce different impact obliquities (Figure 28B). Another key difference between these tests and the perpendicular ones was the type of metal used. All but one of the steel sheet panels were damaged preventing re-use during the two previous types of tests. The other five panels used in this final round of tests were all made of 0.6mm aluminium sheets which despite being slightly thicker, were significantly lighter and more malleable than the steel sheets. Therefore, the impact resistance of these sheets is expected to be lower than that of the steel sheets and the two tests are not easily comparable. However these tests still provide information on whether or not high obliquity impacts cause less damage than lower obliquity impacts of the same energy. This information can allow for more accurate modelling of damage caused by oblique strikes in ballistic risk and impact assessments.

3.3.2.4.2 *Weatherboard tests*

These tests used rimu and pine bevel-back weatherboards fixed to a frame of similar design to that used for the inclined sheet metal tests (Figure 29). This allowed weatherboard test panels to be impacted by ballistics striking with high obliquities between 75 -60°. This was done to simulate impacts to vertical walls which commonly

experience higher obliquities than roofs. The initial 75° obliquity was chosen based on my use of a hazard model with a mean ballistic impact angle of 75° for ballistics landing between 0.5 and 2 km from vent (hazard model presented in Chapter 4).

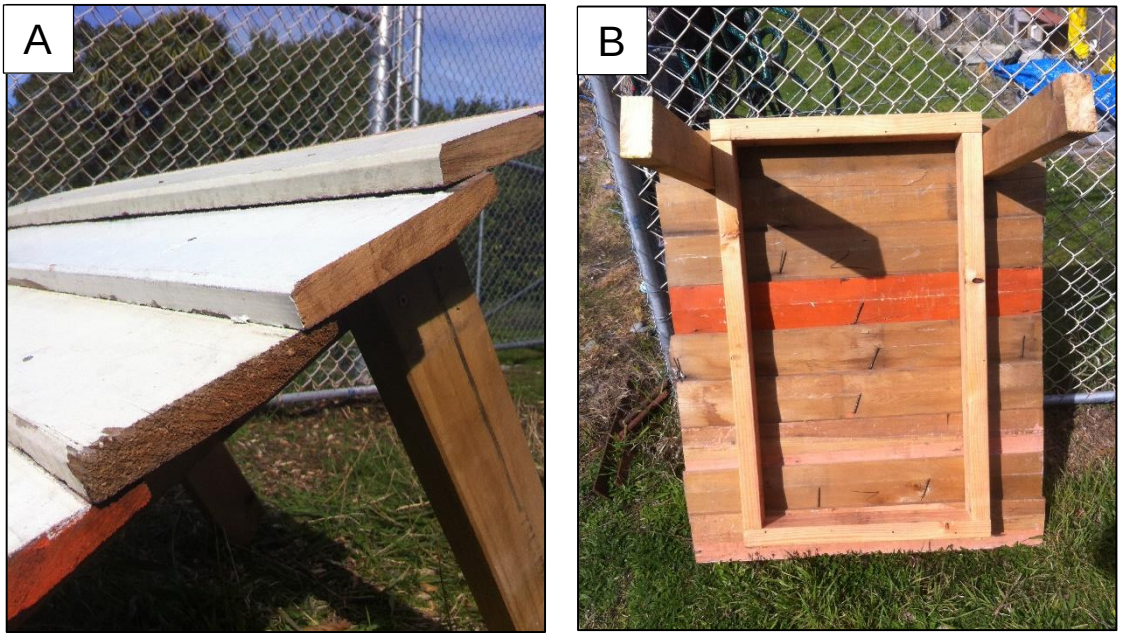

Figure 29: Weatherboard test panel design: A) use of salvaged bevel-back weatherboards B) original nails still attached and leg length varied to simulate steep wall pitch.

The weatherboards were fixed to the frame using 75×3.5 mm flat head annular nails fixed 10 mm above the top of the previous board. Regulation rose head nails specified for use in the New Zealand Building Code (E2: External moisture) were not used in these tests but this deviation from code was assumed to have little effect on the structural strength of the nail connection. The weatherboards were generally of good condition aside from their original nails still being attached (Figure 29). Rimu weatherboards were commonly used in New Zealand construction pre 1970 with Pinus radiata being more commonly used since then (Elkink, 2011).

3.3.2.4.3 *Reinforced concrete slab tests*

These tests consisted of 27 shots fired at 19 separate RC slabs, designed to fit the New Zealand specifications for roof slabs (NZS:3101, 2006). To investigate the effect of concrete strength on impact response, half of the slabs were cured to have an unconfined compressive strength of 25 mPa and the other half were cured to 35 mPa. Unconfined compressive strength tests carried out on 24 standard concrete cylinders and surprisingly the 25 MPa samples were stronger than the 35 MPa samples.

Records of the compressive strength testing can be found in Appendix B2. Aside from the strength difference, all other specifications were kept the same (Table 12).

Length and width (mm)	1000x1000
Thickness (mm)	75
Reinforcement bar diameter (mm)	10
Two-way reinforcement bar spacing (mm)	200
Slab weight (kg)	~190
Unconfined compressive strength target (mPa)	25 and 35
Average unconfined compressive strength from testing (mPa)	36 and 35

Table 12: RC slab specifications and strength test results.

The testing regime planned for tests to be carried out on 24 separate slabs with 12 slabs placed for perpendicular impacts and 12 for oblique impacts. However, due to the repeated firing of the cannon at its maximum air pressure, the piston of the cannon was eventually destroyed, preventing it from maintaining pressure. As a result, further testing could not be carried out in time for this thesis. To develop one suite of fragility functions from these two sets of experiments (normal and oblique impacts), the normal component of impact energy was resolved using the equation above in section 3.3.2.2.1.

3.3.2.4.4 *Data recorded from impact tests*

Multiple variables were recorded for each test including the weight and speed of the projectile, its impact location and the post impact condition of the cladding. The post-impact condition (e.g. nails bent, screws snapped, length of tears in sheet metal, scratches, cracks *etc.*) was recorded using photos taken before and after impact. For photos of the tests, refer to Appendix B1. For each test the damage could be classified into one of four damage states. A different set of specific damage state descriptions were applied to each building material based on its unique failure mechanisms (Table 13). However the same general amount of damage can be attributed to each damage state across all the building materials with Damage State 0 equating to either no visible damage or slight cosmetic damage, Damage State 1 for cosmetic damage, Damage State 2 for moderate damage without ballistic perforation and Damage State 3 for perforation of the material.

Table 13: Damage state descriptions for ballistic impacts to sheet metal, timber framing, weatherboards or reinforced concrete slabs.

Sheet metal cladding

Damage state	Damage description
DS 0	No damage – cosmetic scratches
DS 1	Cosmetic denting
DS 2	Tearing (at impact site or around connections)
DS 3	Ballistic perforation

Timber framing (clad in sheet metal)

Damage state	Damage description
DS 0	No visible damage
DS 1	Denting to framing
DS 2	Cracking, splitting or loss of nail connections
DS 3	Ballistic perforation

Reinforced concrete slabs

Damage State	Damage description
DS 0	No damage - cosmetic front-face damage
DS 1	Front-face cratering and/or back-face cracking
DS 2	Back-face scabbing
DS 3	Perforation (ballistic perforation did not occur)

Bevel-back weatherboards

Damage State	Damage description
DS 0	No damage – cosmetic denting
DS 1	Boards cracked but still in contact
DS 2	Boards cracked apart
DS 3	Ballistic perforation

For the concrete tests, additional damage data was recorded to assess the threat that ejected concrete fragments pose to building occupants and property when they are ejected from the back-face of the slab following impacts. Peng et al (2015) estimate that rear shear fragments have ejection velocities equal to $\sim 20\%$ of the residual velocity of the projectile. Residual velocity is the velocity of a projectile after it has lost kinetic energy by perforating a target (Kar, 1979). For ballistic impacts to RC panels, severe backface scabbing can occur even though the ballistic itself is often too large to perforate in-between reinforcing bars (Figure 21). This complicates the Kar, (1979)

model for residual velocity calculations and associated fragment ejection velocity estimates, making this aspect of ballistic impacts a source of uncertainty for risk assessments. In these experiments we aim to establish a relationship between the velocity of ballistics and the velocity of fragments they eject. This relationship can be used to estimate fragment velocities from higher velocity ballistic impacts, giving insights on expected interior damage costs and occupant safety in reinforced concrete buildings.

3.3.3 Results

Processed damage data for all three cladding types are presented in a series of bin plots. These plots have been used to derive fragility functions using the same methodology outlined above in section 3.2.3. Raw damage data for the three cladding types are provided in Appendices B3.

3.3.3.1Sheet metal tests

3.3.3.1.1*Perpendicular cladding strike experiments*

For the perpendicular cladding strike experiments, the 20 data points were put into a bin plot but could not be divided equally between the four bins (Figure 30). This was due to multiple data points with the same impact energy value which could not be split into separate bins.

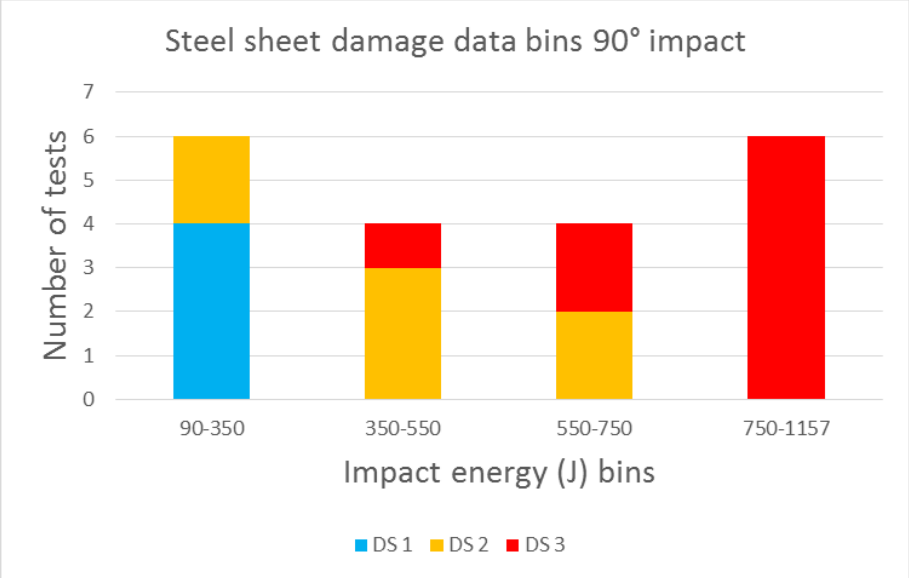

Figure 30: Bin plot of damage data for individual ballistic strikes perpendicular to the plane of corrugated sheet metal at a location where the cladding spans between framing members.

Figure 31 shows three fragility functions with one function for each damage state recognised in Table 13. Unlike the 'standard' functions used in seismic building fragility studies which are a cumulative log normal (Baker, 2014; Rossetto et al., 2014), each of these functions is made up of linear segments which connect adjacent data points. Functions made up of linear segments have been developed in several past vulnerability studies (e.g. Herbin and Barbato, 2012; Wilson, 2015). The functions show that higher impact energies correlate with increased likelihood of higher damage states occurring.

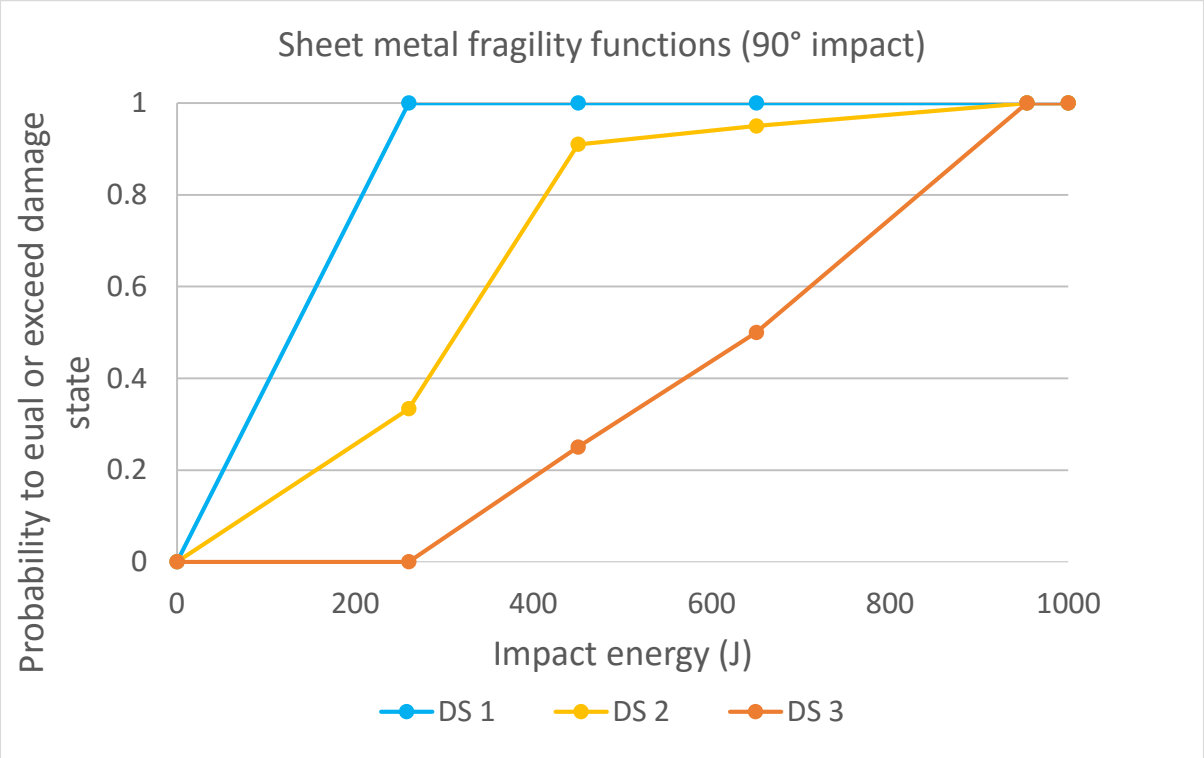

Figure 31: Fragility functions for individual ballistic strikes perpendicular to the plane of corrugated sheet metal at a location where the cladding spans between framing members.

3.3.3.1.2*Perpendicular timber framing strike experiments*

The framing strike experiments were also processed into a bin plot for the development of fragility functions (Figure 32). The functions show that cladding which is supported by framing has a higher impact resistance than cladding that spans between framing (Figure 33). Comparison of their DS3 fragility functions shows the impact energy required to perforate timber supported cladding is around double the energy required to perforate cladding alone.

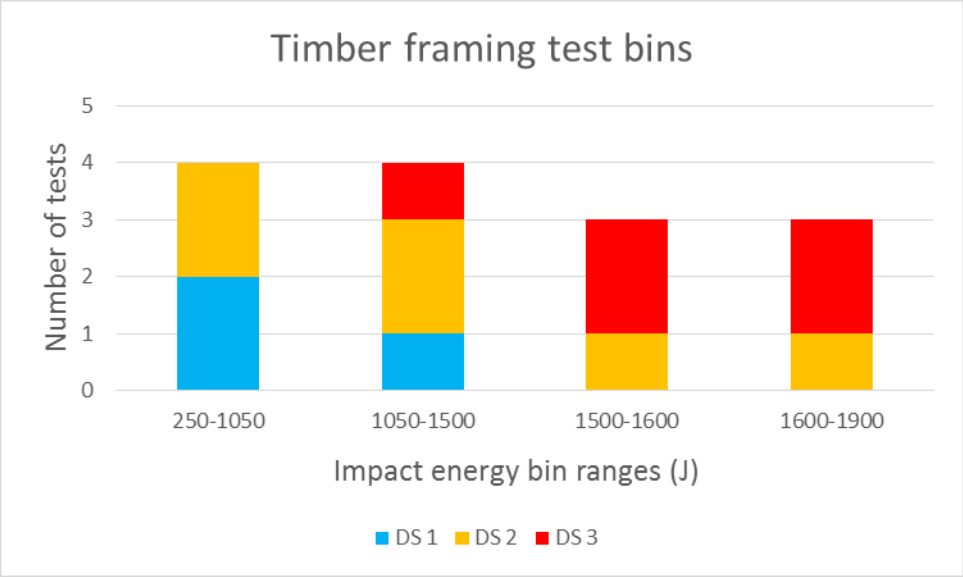

Figure 32: Bin plot for individual ballistic strikes perpendicular to the plane of corrugated sheet metal at a location where the cladding was directly supported by framing members.

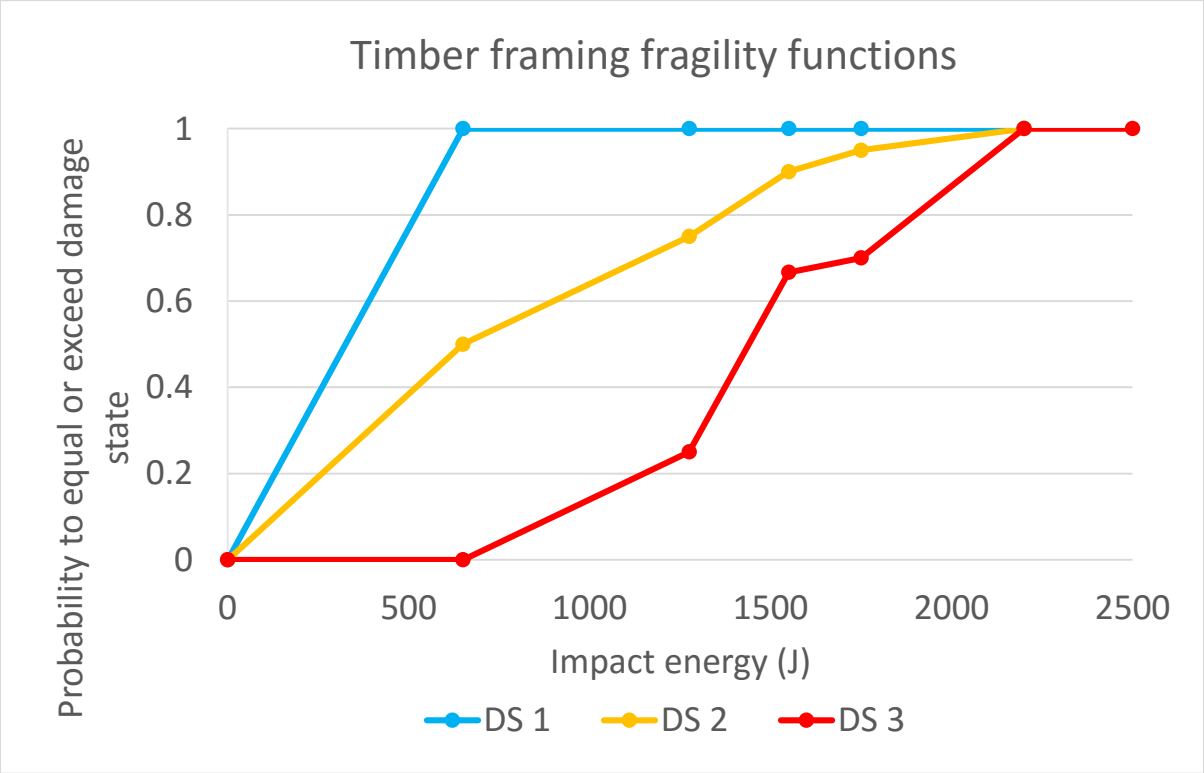

Figure 33: Fragility functions for individual ballistic strikes perpendicular to the plane of corrugated sheet metal at a location where the cladding is directly supported by framing members.

3.3.3.1.3*Inclined cladding strike experiments*

These experiments investigated the damage produced from different impact obliquities compared to the damage from perpendicular attack angles. A total of 16

shots were taken at four different obliquities from 40-70° and damage was categorised into the same three damage states as in previous sheet metal tests (Figure 34). Comparing raw data from the inclined and perpendicular impact tests, claddings are more resistant to DS1 and DS2 damage at higher impact obliquities than they are for perpendicular impacts of the same energy (Figure 35). However, two of the inclined tests (50 and 51) resulted in DS3 despite impact energy being below the minimum DS3 threshold for perpendicular impacts. These low impact energies are likely to have resulted in DS3 damage because the sheet metal panel used in these tests was made of the weaker, lighter aluminium compared to the steel used in the perpendicular tests. Also the second impact location influenced by the first impact location further weakening the panel (Figure 36D).

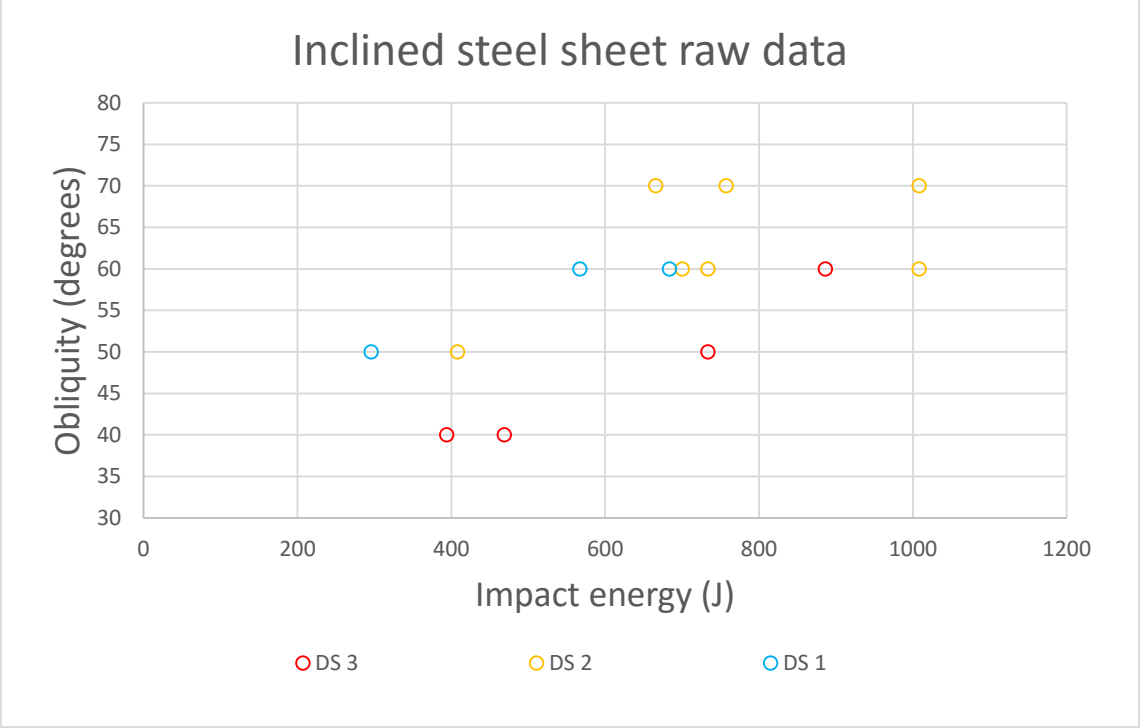

Figure 34: Raw data from oblique impacts to sheet metal.

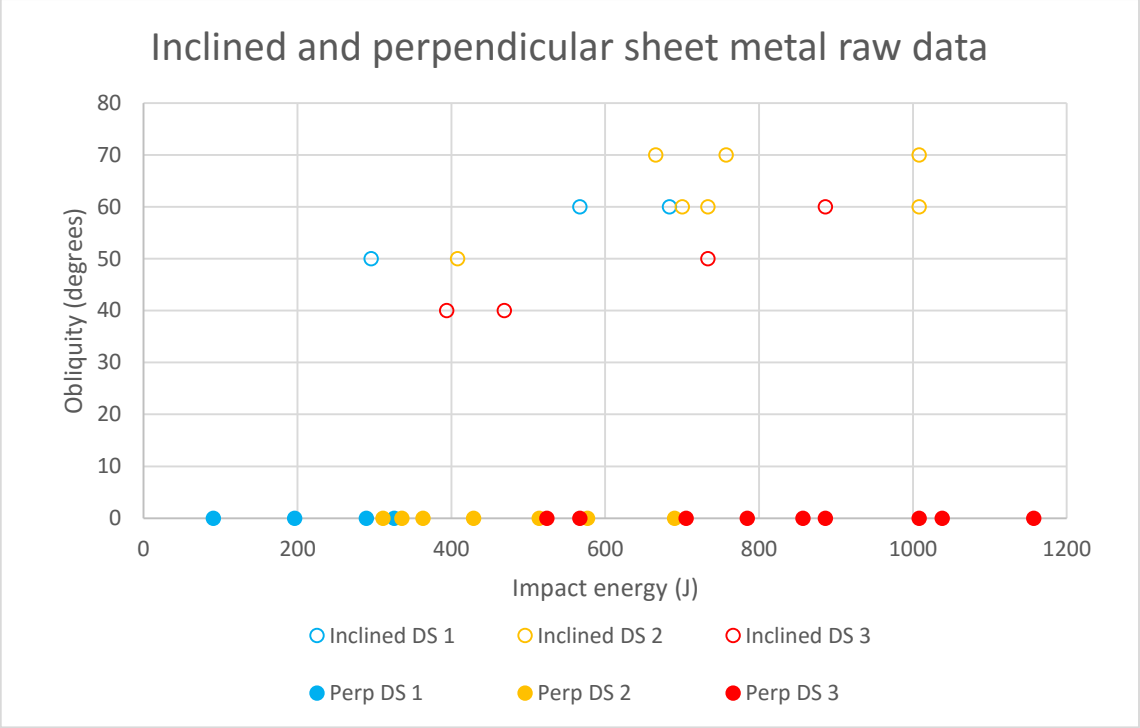

Figure 35: Raw data from both oblique and perpendicular impacts to sheet metal.

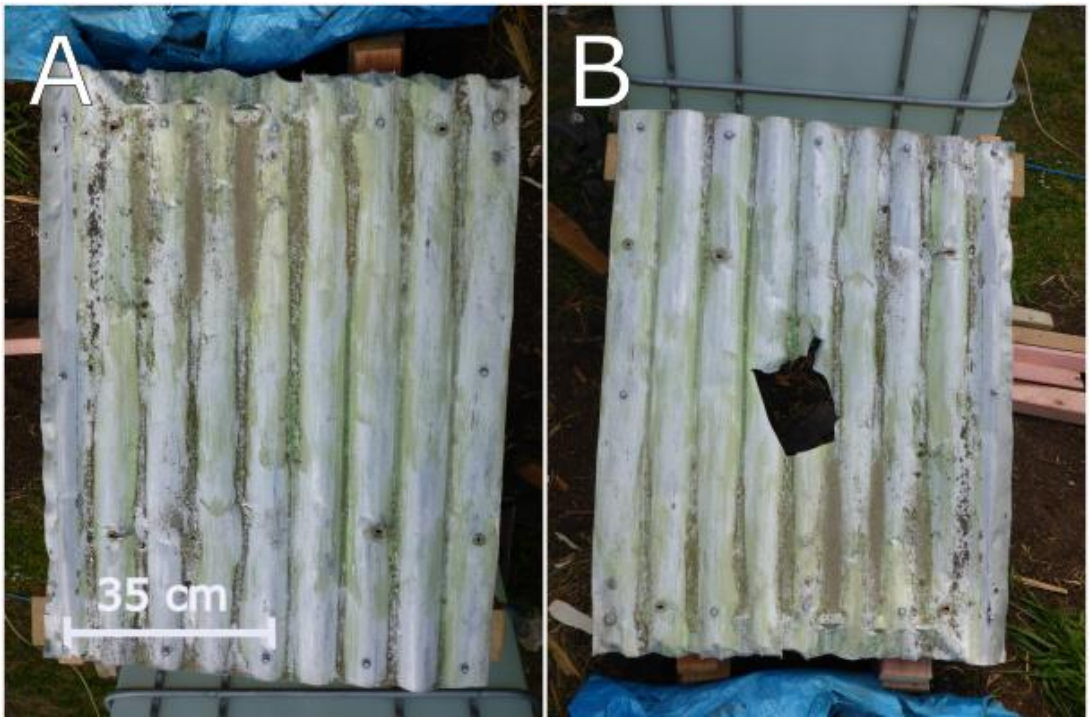

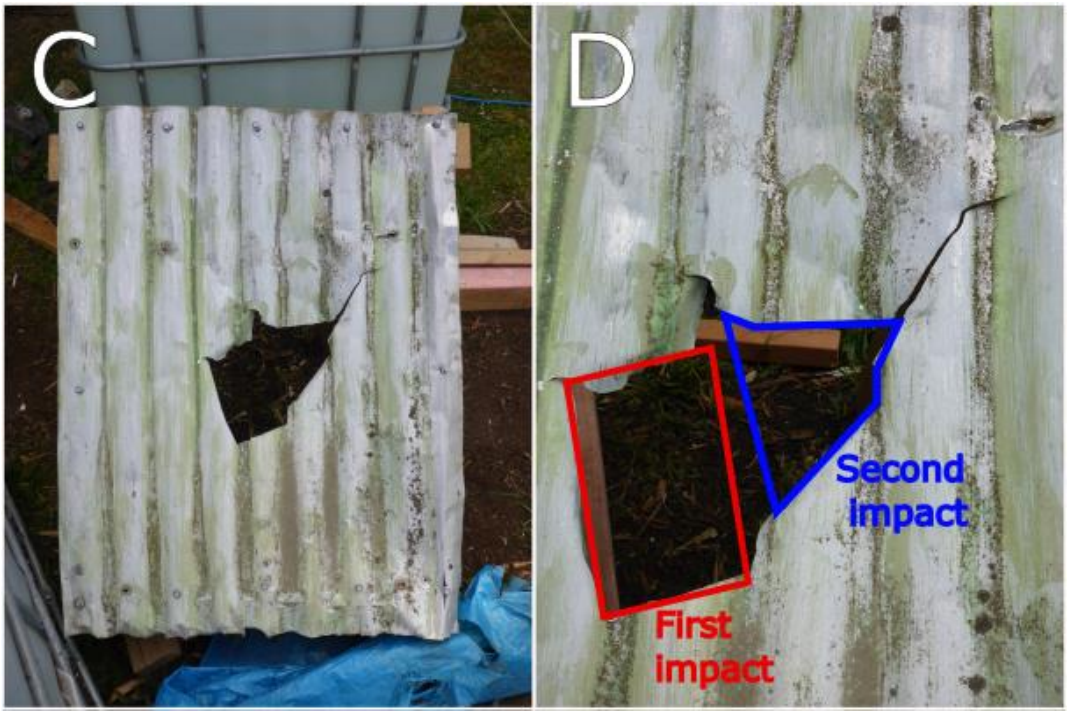

Figure 36: Relatively weak aluminium sheet metal used in tests 50 and 51. A) pre-test condition, B) post-test 50 condition 468 J impact energy , C) post-test 51 condition 393 J impact energy, D) close up on perforation site.

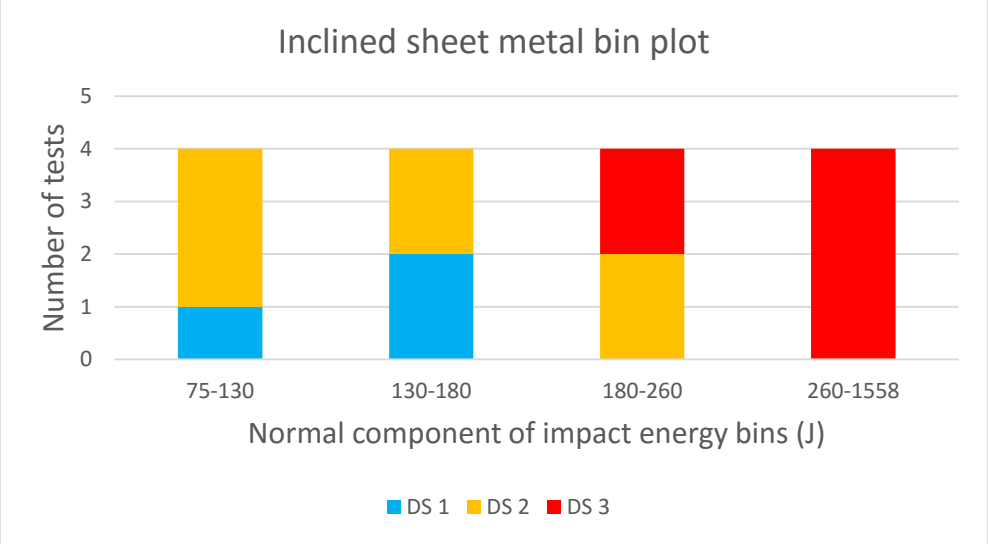

Figure 37: Bin plot for individual ballistic strikes oblique to the plane of corrugated sheet metal at a location where the cladding spanned between framing members.

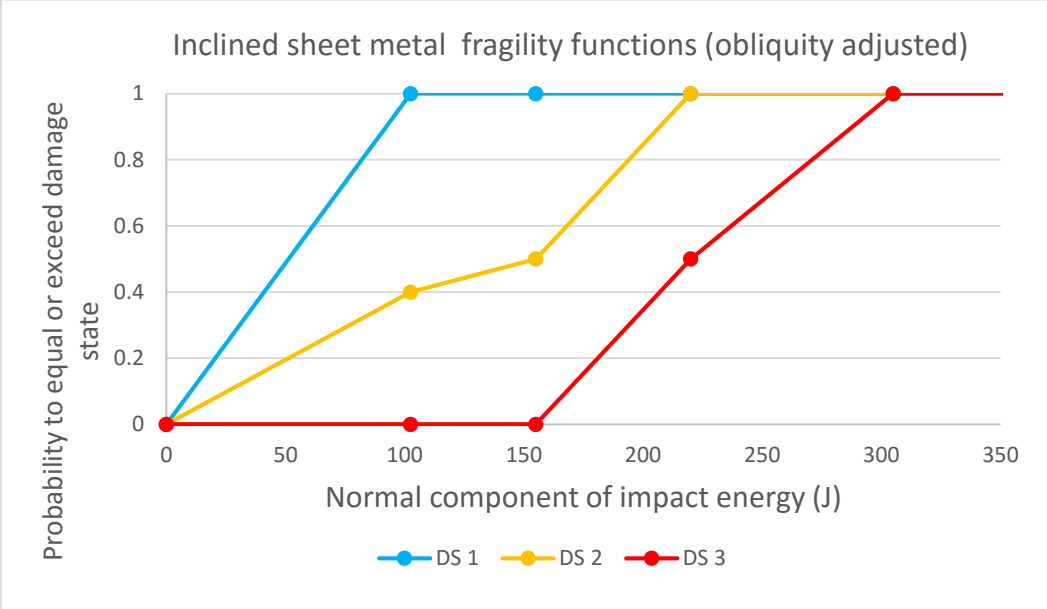

Figure 38: Fragility functions for individual ballistic strikes oblique to the plane of corrugated sheet metal at a location where the cladding spans between framing members.

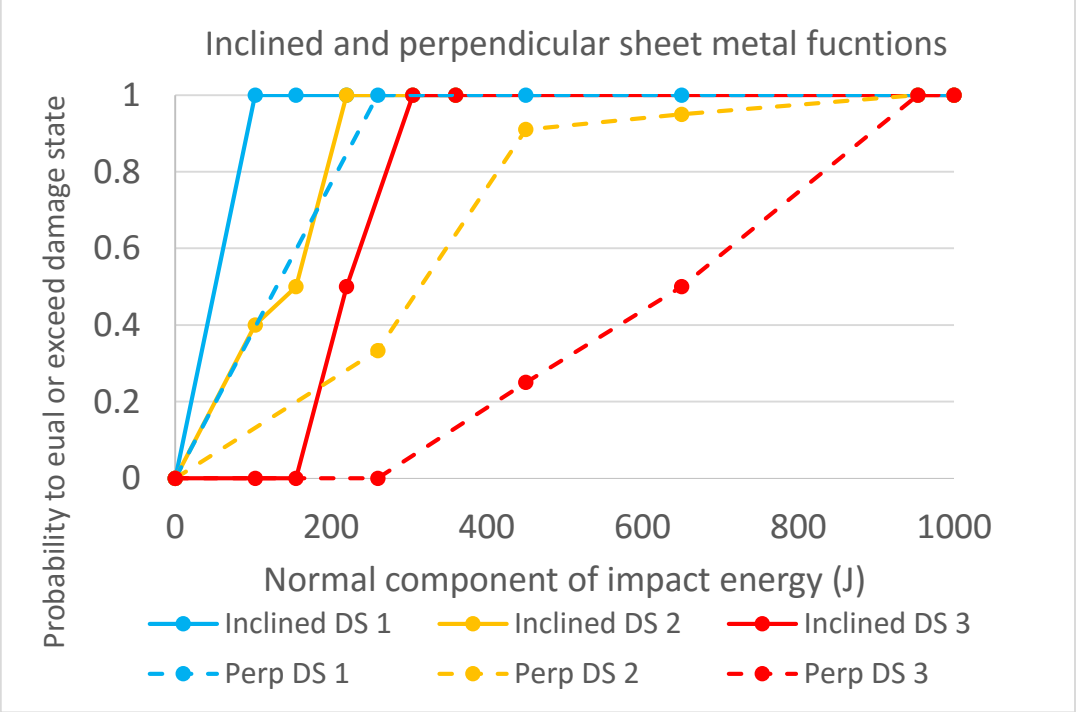

Figure 39: Fragility functions from both oblique and perpendicular impacts to sheet metal.

When the fragility functions from the two sets of tests are compared, inclined impacts (using the normal component of impact energy as their HIM) appear to be significantly more vulnerable (Figure 39). The impact condition of panels after oblique impacts, with long scratches preceding perforations, suggests a high component of shear stress is responsible for the damage (Figure 40). This shear component is disregarded during calculation of the normal component of impact energy. This means perforation potential from oblique ballistic impacts cannot be accurately measured using the same method as in high velocity impact engineering studies. This is an important area of future ballistic impacts research.

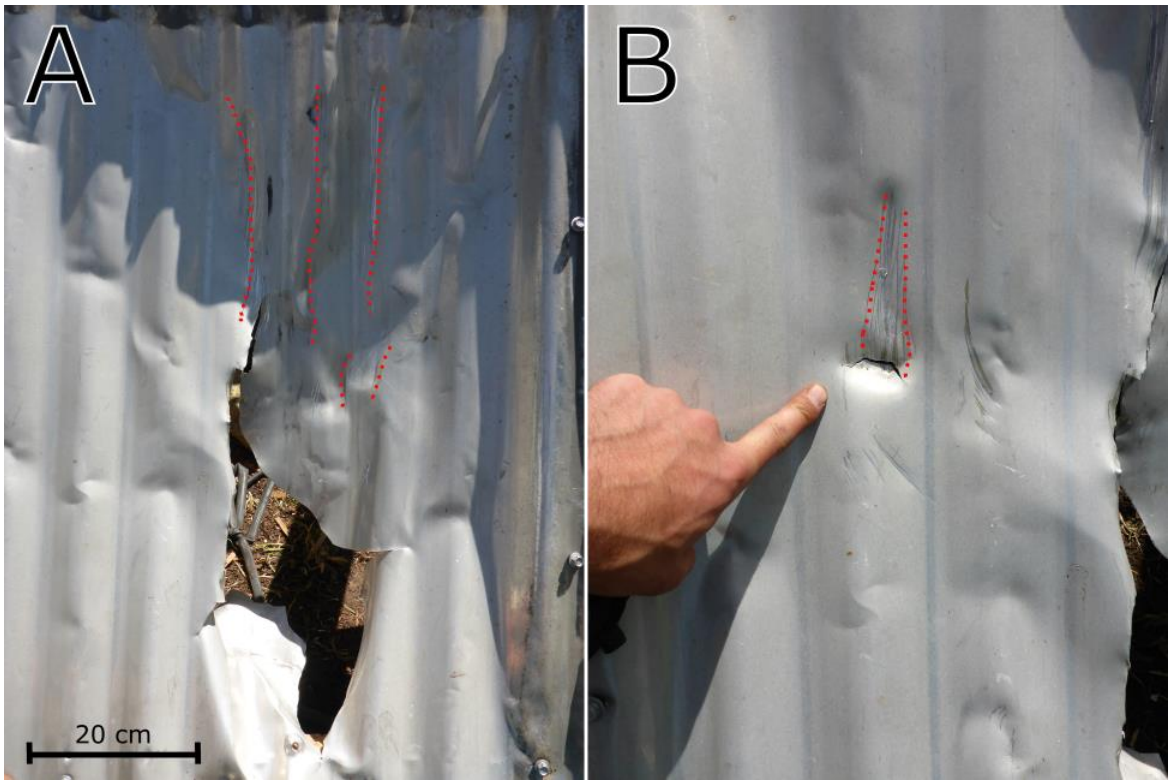

Figure 40: Scratches preceding main impact location of sheet metal following oblique block impact tests. A) Illustration of DS3 from Test 45: Original impact energy = 1372 J, Normal component impact energy = 343 J. B) Illustration of DS2 from Test 46: Original impact energy = 700 J, Normal component impact energy = 175 J.

3.3.3.2Weatherboard tests

The weatherboard tests were initially carried out with a 75° obliquity as this was the mean obliquity produced for ballistic-wall impacts in the ballistic hazard model used in the impact assessment (Chapter 4). Obliquity was reduced to 65° after five shots (two fired at the cannon's maximum air pressure) were unable to cause DS 3 damage (Figure 41). The raw data follows the same trend seen in the inclined sheet metal tests,

where increased obliquity results in lower damage states for impacts of the same energy. The bin plot for this data suggested the likelihood of DS3 being reached or exceeded went down with increased impact energy between the last two bins for these tests (Figure 42). This was likely due to an incomplete dataset as it is assumed that the probability of a given damage state occurring will never decrease for an increased hazard intensity. The DS3 function was adjusted to reflect this assumption.

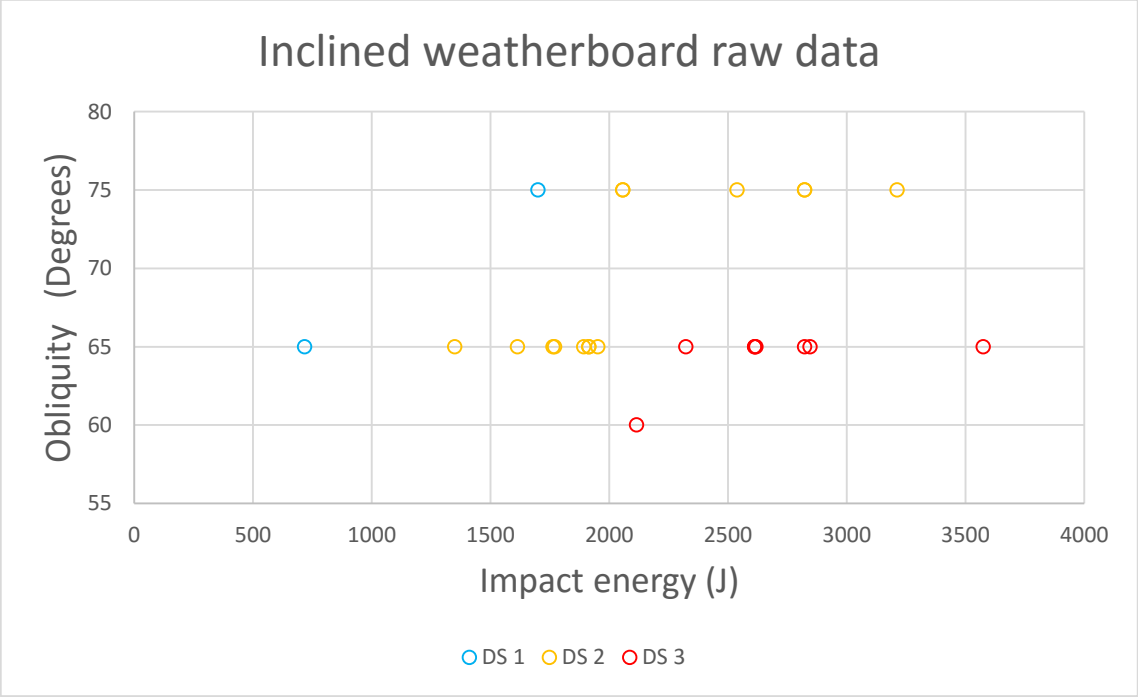

Figure 41: Raw data from weatherboard impact tests at various obliquities.

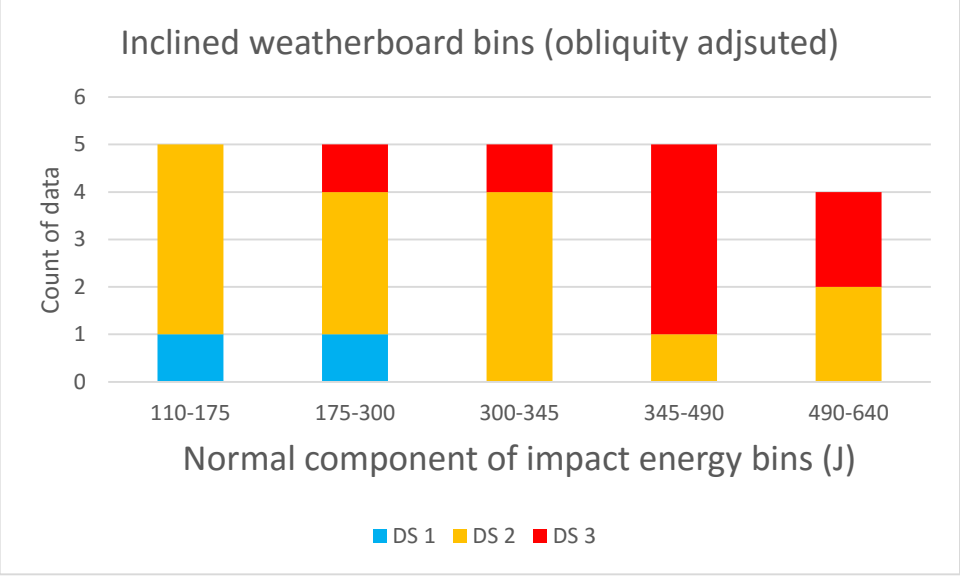

Figure 42: Bin plot of damage data for individual ballistic strikes to bevel back timber weatherboards. All impact energies have been calculated as normal component from impact obliquities of 60-75°.

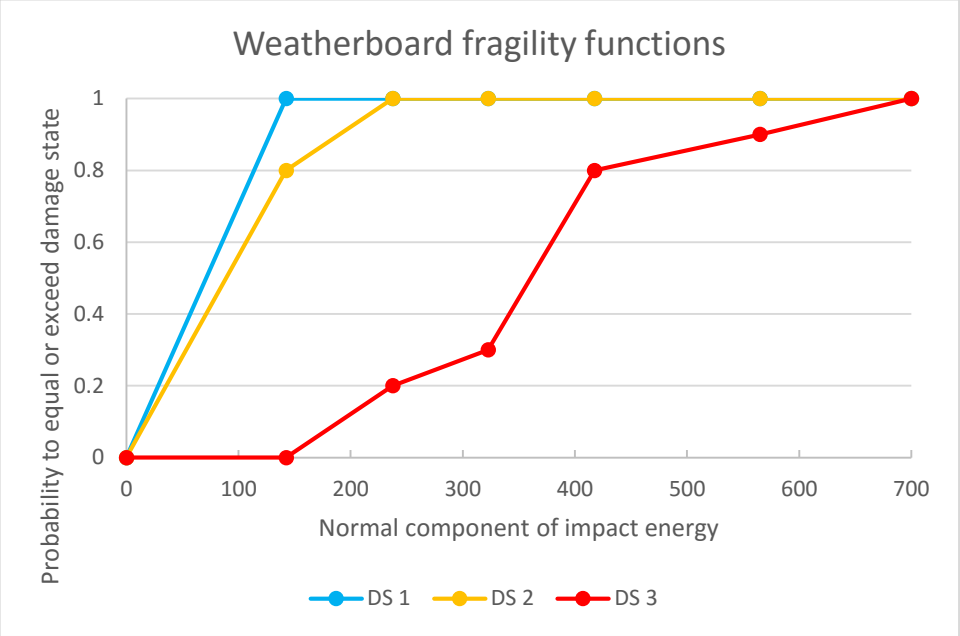

Figure 43: Fragility functions for individual ballistic strikes at impact obliquities of 60-75° to the plane of bevel back timber weatherboards.

3.3.3.3Reinforced Concrete slab tests

The RC slab tests consisted of 27 shots fired at 19 separate slabs (Figure 44). Due to the development of cracks and weakening of the slabs with successive shots, only the first shot fired at each slab has been used as a data point for this fragility function suite (Figure 45). Reinforced concrete was more resistant to impacts than all the other materials tested but results followed the same overall trends as for other materials in regards to higher impact energies being required to reach higher damage states and the relationship between obliquity and damage. Ballistic perforation was not achieved in any of the experiments due to the strength and spacing of the reinforcing bars but back-face scabbing (DS2) was able to occur for impact energies as low 1500 joules. Compared to the stronger more dense basaltic blocks, blocks from the TVZ showed a tendency to shatter into smaller fragments and cause less overall damage to the slabs. For example the only experiment resulting in DS0 used a TVZ block that shattered into a large number of small pieces, causing only cosmetic damage to the front-face of the slab despite having a moderately high 1700 J impact energy.

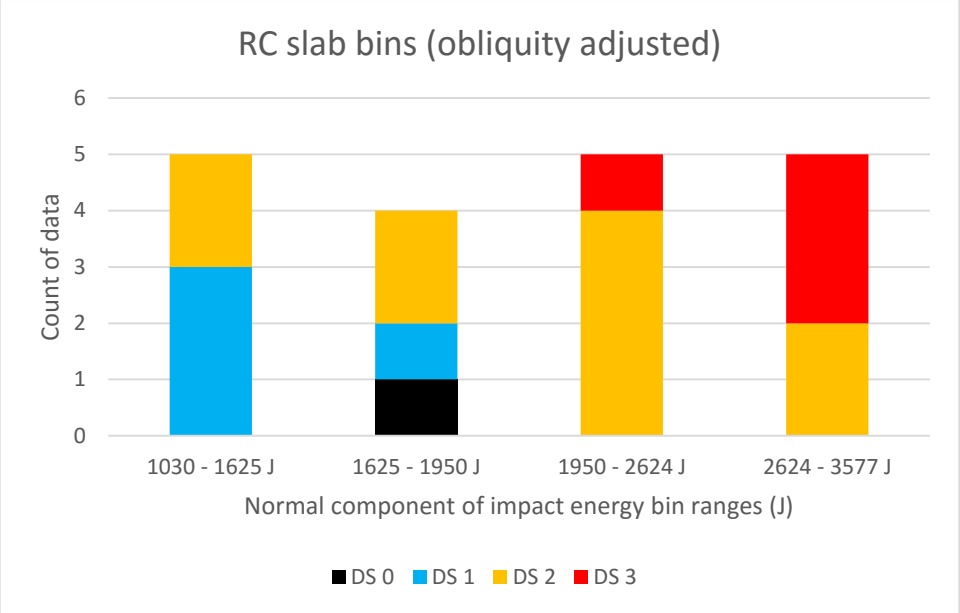

Figure 44: Bin plot of damage data for individual ballistic strikes at varying obliquities to the plane of RC slabs.

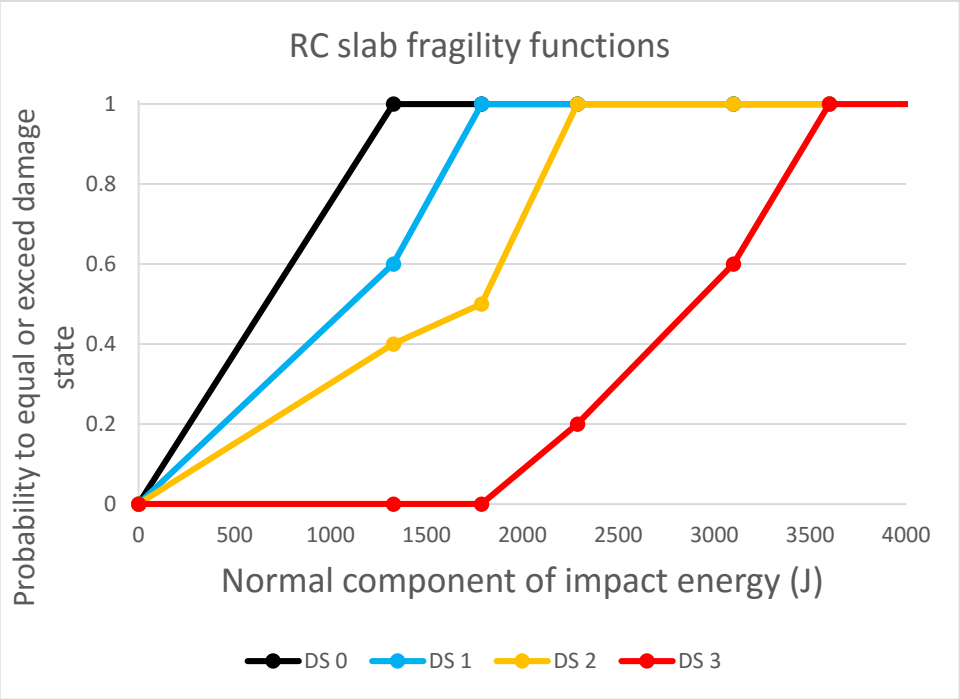

Figure 45: Fragility functions for individual ballistic strikes at varying obliquities to the plane of RC slabs.

The speed and impact energy of fragments ejected from the back-face of the slab was calculated using the same methodology as was used for the ballistics. The fragments moved significantly slower than the cannon fired ballistic. For DS 2 impacts, fragment velocities were on average, ~20% of the ballistic velocity. For DS 3 impacts, fragment velocities were on average, ~33% of the ballistic velocity. After weighing the largest individual fragments from each experiment, the impact energies of the fragments were calculated. All of the fragment impact energies were less than 1% of their ballistic's impact energy. The fragment with the highest impact energy of ~80 J (Figure 46) was only slightly below the 100 J threshold for lethal skull fractures suggested by Raymond et al. (2009).

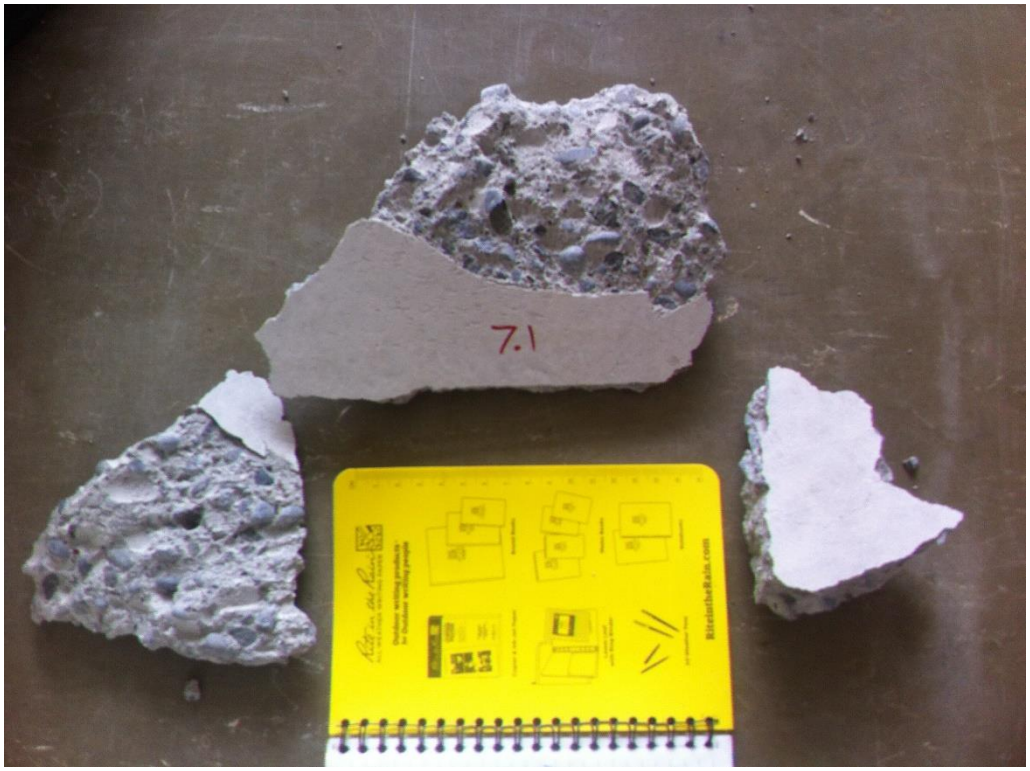

Figure 46: The largest three back-face fragments ejected during experiment 7.1. The largest of these, weighing 870 grams had an ejection velocity of 48 km/hour (13.5 m/s).

3.3.3.4Results Summary

The testing of sheet metal, timber framing, weatherboards and reinforced concrete in simulated ballistic block impacts found was used to develop fragility functions to quantify their vulnerability. Key patterns identified from the testing include:

1. Higher impact energies were required to reach higher damage states for all materials, making impact energy a suitable HIM for ballistic impact studies.

2. For perpendicular ballistic impacts, typical building claddings will only be able to resist perforation from ballistics at the lower end of the impact energy range (with energy being primarily controlled by the ballistic's terminal velocity and hence mass).
3. In all materials tested, the impact energy threshold for each damage state was significantly higher for strongly oblique impacts (>60°) than for perpendicular ones.
4. Fragments of building materials or ballistics that are ejected/ricocheted post-impact increase the area of ballistic hazard and have velocities that are potentially lethal.

3.3.4 Limitations

Fragility functions developed using the air cannon apparatus have a number of limitations associated with either the inaccurate simulation of ballistic impacts to buildings or a low number of experiment repetitions. The limitations in simulating impacts can be broken down into inaccurate simulation of ballistic hazard and the issues associated with using small sections of specific claddings to represent the walls and roofs of real buildings for an entire building stock. The air cannon has been specifically designed to launch rocks up to 10 kg at velocities up to 100 m/s, meaning this air cannon is more capable of simulating volcanic ballistic impacts than the apparatus used in both cyclone vulnerability and impact engineering studies. However, there are still aspects of real ballistic impacts that the cannon cannot simulate. First and foremost, the maximum speed achieved during testing was 39 m/s, about 1/3 of the velocity the blocks used in these tests could reach if they attained terminal velocity post eruption (Capaccioni and Cuccoli, 2005). However the speeds reached during these tests are appropriate for simulating the lower the terminal velocities of smaller blocks. These speeds are also appropriate for simulating bomb impacts from typical strombolian eruptions (Gaudin et al., 2014). Another aspect of ballistic hazard that the cannon does not reproduce is the spinning that occurs during the flight of pyroclasts (Vanderkluysen et al., 2012). The cannon launches rocks with minimal amounts of spin which is ideal for maintaining the same impact conditions over multiple tests but gives no insight to the different damage that may occur during spinning impacts. All of

the experiments have used relatively dense, solid rocks to represent ballistic block impacts. The damage and perforation thresholds associated with block impacts are likely to be significantly different from those of bombs. Bombs have visco-elastic properties, meaning they would be classed as non-rigid missiles which can deform considerably on impact compared to target deformation (Li et al., 2006).

The orientation of a block as it struck a test panel varied from test to test. As the blocks used were not spherical, different impact orientations affected the surface area connecting with a test panel, adding another variable that could affect observed damage. Testing of metal hurricane shutters impacted by concrete tiles found a strong relationship between the orientation of the projectile and the amount of deformation observed. Side impacts consistently caused more deformation than flat impacts where the same kinetic energy was being absorbed by a smaller area of the target (Fernandez et al., 2010). If a larger number of tests were to be carried out using the same block, the damage from tests of different impact orientations could be analysed separately, with different impact orientations classified using the mandrill attachment as a fixed reference point.

Aside from the concrete slabs, building materials used in these experiments were salvaged from houses scheduled for demolition. The materials tested are therefore likely to be older and weaker than the average cladding they represent in a real building stock and resulting fragility functions may be overestimating cladding vulnerability. The rimu weatherboards in particular are more prone to splintering than other types of weatherboards such as pine (Elkink, 2011). These properties should be noted considering the fragility curves derived from tests on rimu will be applied to all types of weatherboards during impact assessments. Rimu weatherboards have also not been commonly used in construction since the 1960s (Elkink, 2011) meaning another type of weatherboard may have been more appropriate as an average representative for modern building stocks.

With the limited supply of building materials available for testing, the fragility functions were derived from a relatively small number of data points. Rossetto et al (2014) suggest 30 buildings as the minimum requirement for low quality seismic fragility functions yet all of the functions presented here use between 14 and 24 data points, some of which gained from experiments where the same piece of cladding material

was impacted multiple times. To account for these limitations and uncontrolled variables in testing, the uncertainty bounds suggested by Jenkins and Spence (2009) that +/- 20% of a ballistic's impact energy be assigned as the 5th and 95th percentile values respectively.

3.4 Discussion

Despite this testing's limitations, it has made several important findings with implications for ballistic impacts to buildings and appropriate life safety actions for those forced to shelter-in place using unreinforced buildings. The test results and life safety actions are supported by our research group's recent post-eruption ballistic impact assessments in Japan.

This testing has found that exterior building claddings are highly vulnerable to impacts from solid ballistic blocks, especially if the impact is perpendicular to the face of the cladding. Oblique impacts required noticeably higher velocities and impact energies to perforate claddings compared to perpendicular strikes, particularly when obliquity increased over 60°. This means detailed ballistic-building risk assessments require a method for calculating impact obliquity and a method for determining whether a wall or roof of a building has been impacted as obliquity will vary considerably between the two (see section 4.3.2).

During the concrete testing, the weaker, lower desnsity TVZ blocks (relative to the basaltic blocks) all shattered on their first impact causing markedly less damage than basaltic block impacts of comparable impact energy. This suggests rock strength plays a role in determining the maximum damage a ballistic can cause when impacting relatively strong targets. This means the variation ballistic impacts to concrete structures may be predicted between different volcanoes based on lithology of the country rocks which are the source for ballistic blocks. The damage caused by different types of ballistics (blocks compared to 'mudbombs') was evident at Mt Usu. The strength of country rock is also important in terms of its influence on the density and fragmentation of country rock as these properties control ballistic distributions.

Based on 20 RC slab experiments, the velocity ratio between a ballistic and its backface fragments is roughly 4:1 (5:1 for DS2 impacts and 3:1 for DS3 impacts). If this ratio remains constant for higher velocity ballistic impacts then fragments from a

100 m/s ballistic impact would be travelling at 25 m/s (90 km/h). At this speed fragments weighing 0.5 kg carry a 90% chance of fatality (Baxter and Gresham, 1997).

From examination of the conical shape of backface impact craters on concrete slabs during post-eruption building surveys, it was thought that ejected fragments were likely to have exploded outwards from the point of impact. By analysing videos of the fragments ejected during experiments, their trajectories appear mostly confined to following the trajectory of the ballistic rather than exploding outwards from the point of impact as the conical shape of the craters might suggest. However, because these fragments are moving relatively slowly compared to velocities expected from real ballistic impacts, their trajectories are likely to be more strongly influenced by gravity giving the appearance they are simply following the vertical trajectory of the ballistic. Faster moving fragments from higher velocity impacts will be less influenced by gravity and may show greater lateral dispersion, increasing the area of hazard inside a concrete building impacted by ballistics. This is an area of research that requires more attention especially considering many ballistic shelters are made of concrete which may not have a high enough impact resistance to prevent high velocity backface scabbing

These experiments support the suggested life safety actions presented in section 3.2.2, that if people are required to shelter from ballistics in unreinforced buildings, they should put as many layers of the building envelope as possible in-between themselves and incoming ballistics. Fragments of rock and building materials produced in these experiments were too slow to be lethal but because ballistics can travel over three times faster than the ones in these tests, their fragments are also capable of higher velocities and may become lethal. This means additional cover should be sought behind any available furniture or barriers. (Figure 47).

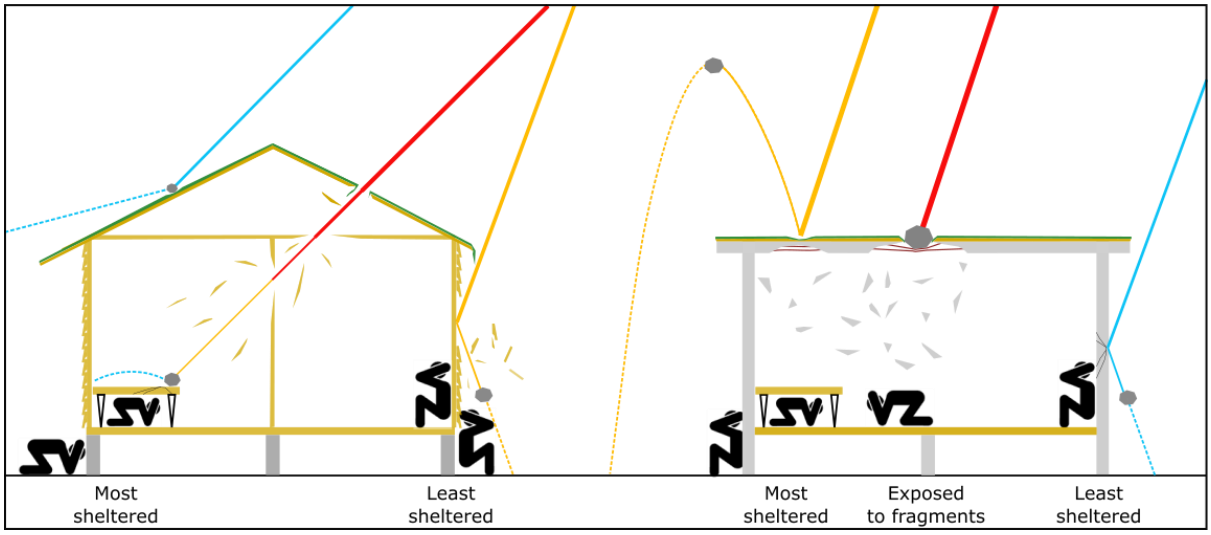

Figure 47: Illustration of the likely least sheltered and most sheltered areas of buildings impacted by ballistics based on findings from cannon experiments and post-eruption impact assessments. Line colour signifies impact's damage state (red, DS3; orange, DS2; blue, DS1), line thickness signifies impact energy.

Chapter 4 Tephra Impact Assessment

4.1 Introduction

This chapter outlines the development of an impact assessment methodology for tephra hazards and presents the results of a tephra hazard impact assessment to buildings in Auckland city. For urban environments in volcanically active areas such as Auckland city, tephra presents a significant hazard to buildings. The purpose of this impact assessment is to quantify the severity of damage to buildings so likely building repair costs and the loss of building functionality can be predicted. The approach uses a geographic information system (GIS) to model the interaction between hazard, exposure, and vulnerability (Figure 48), with a key feature being the use of fragility functions presented in Chapters 2 and 3. The chapter addresses risk analysis and risk evaluation stages of the risk management framework.

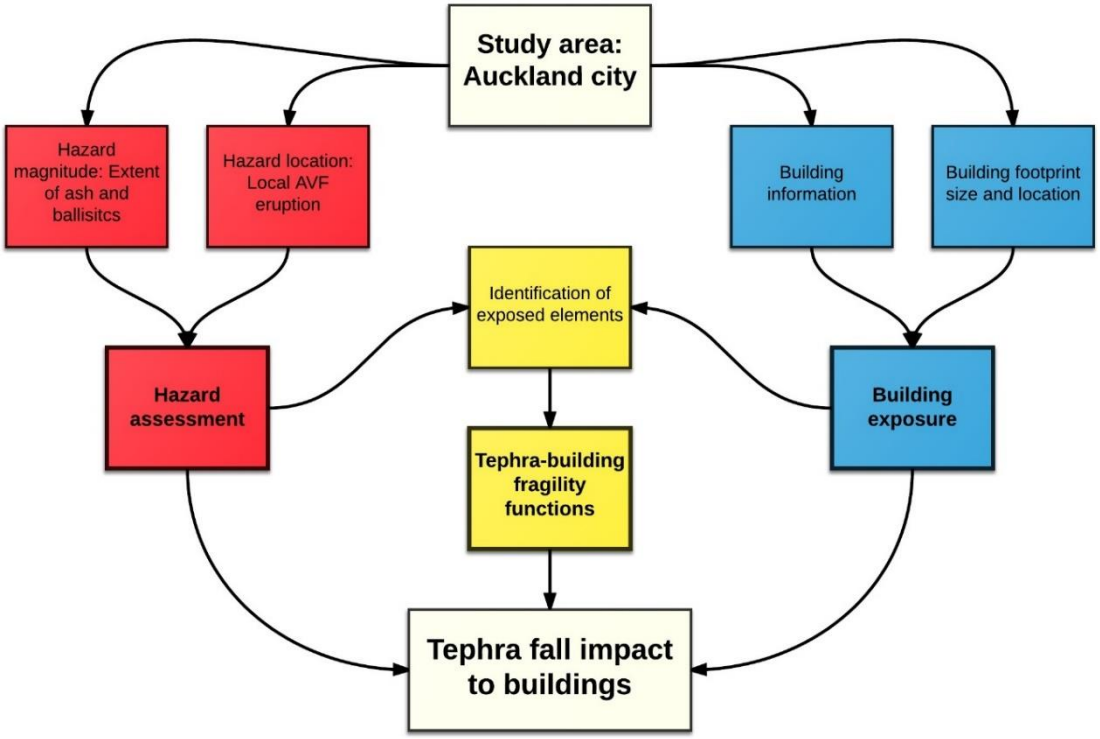

Figure 48: Tephra impact assessment conceptual approach.

4.2 Tephra impact assessment approach

For simplicity, a deterministic approach to hazard assessment was adopted to assess the distribution of ballistics and tephra fall using the Exercise Ruaumoko AVF eruption scenario (Lindsay et al., 2010). For exposure, a three-dimensional building exposure inventory was developed to determine which buildings would be impacted by tephra in this scenario. Vulnerability was then determined by assigning the appropriate fragility or vulnerability functions to each building in the exposure inventory.

4.2.1 Exposure inventory development

The first step taken to develop an exposure inventory for buildings is an initial identification of what essential building information is required to model ballistic and tephra fall impacts. The required information is then compared with the available databases and the information they contain to determine what additional data must be obtained and to justify the estimation of data that could not be obtained.

Building exposure attributes that influence tephra impacts to buildings have been identified in Chapter 2 (blue boxes in Figure 9 (tephra fall) and Figure 11 (ballistics)). The two databases used to develop this exposure inventory contain information on the majority (but not all) of these exposure attributes. The attributes that are not captured in the databases have been estimated based on building codes, building surveys and additional modelling. This exposure inventory was developed using building footprints from the Auckland Council Geospatial Team's building database combined with RiskScape's building asset database. The RiskScape programme has developed an asset database for buildings in Auckland and around New Zealand (Paulik, 2015). The database contains information on building attributes relevant to tephra impacts including (but not limited to) construction type, cladding type, roof pitch, contents value and replacement cost. The database was created primarily using data from Quotable Value NZ (QV) (King and Bell, 2009). The QV data was used because it covers all of New Zealand, but there is some data that is incomplete, inaccurate or uncertain due to on-going modification of buildings in the study area and data collection errors (King and Bell, 2009). An issue which required addressing was that the QV data is only gathered for buildings with a footprint over 30 square metres yet the Auckland Council's building footprints have been digitised for buildings smaller than this meaning the database has no data on these structures. To account for this in the

ballistic impacts scenario, any building without data was assumed to have the most common cladding and construction type from the database. For the tephra fall impact assessment, instead of having to assume the roof pitch, roof cladding, construction type and estimating the replacement cost of each structure, structures without RiskScape's data were omitted from the assessment. Other developments required to make the exposure inventory functional involved the accurate spatial representation of buildings, in two dimensions for tephra fall impacts and three dimensions for ballistic impacts. This required the merging and simple modification of the two databases, which is outlined below.

To spatially represent buildings for both the ballistic and tephra fall impact assessments the first step was to take RiskScape's building data points and expand them into a two-dimensional area across each point's corresponding footprint (Figure 49). As tephra fall is predominantly deposited on a building's roof, the building exposure inventory for this assessment can remain two-dimensional. For the ballistic impact assessment, impacts were recorded when a ballistic trajectory spatially intersected with a building and impacts to a building's walls or roof needed to be differentiated. This required building footprints to be extruded into three dimensions based on the building's height. To determine the height each building should be extruded to, information on each building's floor height and number of storeys was combined using the following equation:

$$H_{total} = H_{floor} + (S \times 2.5)$$

Where H_{total} is the total height in metres, H_{floor} is the floor height in metres and S is the number of storeys. This equation assumes an average of 2.5 metres per storey and produces three dimensional polygons with vertical 'walls' and flat horizontal 'floors' and 'roofs'.

Figure 49: Example of spatial representation of buildings: A) Buildings represented as points in the RiskScape building database. B) The same buildings represented as polygons from the Auckland Council Geospatial Team's building database. Note that the red building footprints contain no points as they are below the footprint size that RiskScape's database has information for.

At this stage the exposure inventory contains essential information on the spatial extent of each building, the building's construction type (e.g. light timber frame), and the type of claddings used on walls and roofs. This specific information is used to determine which fragility or vulnerability functions should be used to assess impact when the building exposure and tephra hazard models are combined. However, a major limitation of the Riskscape and Auckland Council database in terms of modelling ballistic impacts is that they do not provide information on the extent of roofs and walls which are made of highly vulnerable glass windows or significantly less vulnerable framing members. It is important to quantify the spatial extent of framing and windows so that ballistic impacts to either material can be differentiated.

One approach to quantifying the extent of framing is to refer to the New Zealand building code to calculate the area of the building envelope profile that may be composed of framing for a typical building. For standard roofs built to the New Zealand Building Code (in high wind zones) the maximum spacing for 90×45 mm rafters and purlins are 600 mm and 900 mm respectively (Department of Building and Housing, 2010). This means the smallest spacing between members is 600 mm and any ballistic with a diameter greater than this has a 100% chance of striking framing. Similarly for external walls 90 × 45 mm studs and dwangs are spaced at 480 mm and 1350 mm respectively. This configuration means any wall struck by a ballistic over 480 mm in

diameter must strike framing. To simply calculate the probability that a ballistic will strike faming, the ballistic diameter was divided by the minimum framing spacing. The average diameter of ballistics impacting buildings in this scenario is ~440 mm and oblique impacts have a reduced space through which they can pass between framing members compared to perpendicular impacts. This is likely to result in a large number of timber framed buildings receiving impacts directly to their framing. Each impact to framing is simply recorded as one impact. This can be considered a minimal value as ballistic strikes with high obliquities take a longer trajectory through the wall and therefore have a high chance of striking multiple framing components (e.g. Figure 19).

To account for wall areas made of windows, the proportion of wall area taken up by windows in the impacted zones was undertaken using photos from Google Streetview. A total of 20 buildings from different addresses which were impacted by ballistics were part of this analysis and although a more thorough analysis would have been preferable, due to time constraints, only residential buildings (the most common building use type in Auckland) were investigated. Buildings were chosen from different areas around Mangere in order to gain a representative sample of buildings from different socio-economic areas. Also an equal number of walls with different directional aspects were analysed to account for north-facing walls likely having a higher proportion of window coverage. The Streetview analysis calculated that windows make up ~20% of the area of walls for the houses assessed. The data and methodology of this analysis is presented in Appendix B5.

4.2.2 Tephra hazard modelling

In this impact assessment, tephra fall hazard was modelled using the advection-diffusion model TEPHRA2 (Bonadonna et al., 2005) and ballistic hazard was modelled using the 3D ballistic trajectory Tsunematsu model (Tsunematsu et al., 2014). Calculating the HIM for tephra fall (loading on roofs) required tephra deposit bulk density and thicknesses to be modelled. TEPHRA2 modelled thickness in different areas and two end-member densities were selected based on their previous use in the RiskScape programme. For ballistic hazard, the impact energy of ballistic strikes to buildings was calculated using the impact energy output from the Tsunematsu model, then the impact obliquity was found to resolve the normal component of impact energy.

4.2.2.1 Tephra fall hazard development

Using the TEPHRA2 model, two approaches to representing tephra thickness in ArcGIS include the use of rasters or isopachs (Figure 50: Tephra thickness representation methods using isopachs (black lines) with 11 different thickness ranges and using a raster grid with over 500 different tephra thicknesses (red to green grid squares).). To more accurately model thickness, a 50x50 m resolution raster grid was chosen over the isopachs. Once tephra fall thickness has been modelled, tephra fall deposits must be assigned a bulk density value to calculate loading. A dry tephra density value of 1000 kg/m^3 has been chosen for this impact assessment as it is the default value used in RiskScape and it has been used in previous tephra impact studies (e.g. Bonadonna et al. 2005; Biass and Bonadonna 2013). For tephra saturated by rain, density is increased by 50% to 1500 kg/m^3 as this is the value used for wet tephra in RiskScape (as opposed to a maximum, 100% density increase suggested by Macedonio and Costa (2012)).

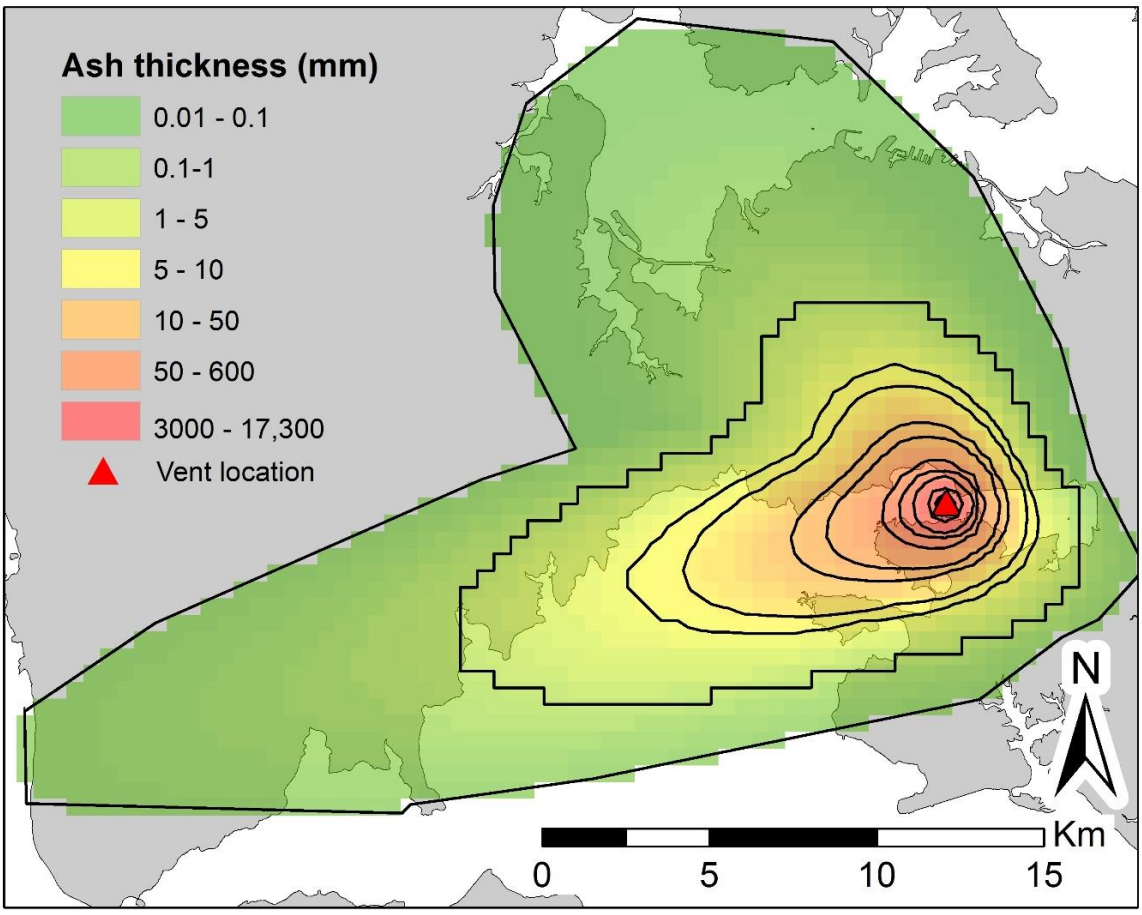

Figure 50: Tephra thickness representation methods using isopachs (black lines) with 11 different thickness ranges and using a raster grid with over 500 different tephra thicknesses (red to green grid squares).

4.2.2.2Ballistic hazard modelling

To assess the impact of ballistic projectiles in a GIS, the first step is to establish where ballistics will impact in space (i.e. create a ballistic hazard footprint). This can be completed by either mapping previous ballistics from an eruption, or by using a numerical model to estimate the distribution where ballistics may impact the ground surface. Ideally, each point (i.e. where the ballistic impacts the ground) will contain hazard intensity information which informs the degree of damage the ballistic may cause. This may include impact energy, temperature, trajectory, diameter, etc.. The Tsunematsu ballistic model used in this impact assessment provides this information and differs from most of its counterparts by considering the trajectory of multiple particles and their collisions in three dimensions, to output a two dimensional distribution of impacts on the ground (Tsunematsu et al., 2014). This model requires a set of input parameters to run and to model an appropriate ballistic distribution (i.e. one that is likely or expected to occur at the site of the impact assessment), the input parameters should be selected based on a literature review outlining the expected style and intensity of volcanism. In accordance with this, input parameters for two end member AVF eruption styles were chosen from a literature review into the ballistic hazard from past AVF eruptions and eruptions from other volcanoes which may be considered analogous.

Few ballistic deposits have been mapped in the AVF and attempting to map ballistic distributions from deposits has been made difficult due to urban development, quarrying and weathering of the deposits (Houghton et al., 1996). Due to there being limited research on the range of ballistic impacts, no mapped ballistic deposits and no observed eruptions in the AVF, analogous eruptions from more intensely studied volcanoes have also been used to parameterise the model (Table 14). The modelled distributions below represent the ballistic hazard for Strombolian and Vulcanian scale phreatic eruptions situated in Manukau Harbour (Figure 51 and Figure 52).

One parameter that can be well constrained from studying ballistic deposits within the AVF is particle density. Particle density for strombolian eruptions was modelled at 1300 kg/m^3 based on values of Strombolian deposits found around the AVF and from similar values from an analogue monogenetic volcano, Paricutin, Mexico (Houghton

et al., 1999; Pioli et al., 2008). For the Vulcanian phreatic eruption, mean particle density was modelled at 2000 kg/m^3 based on the densities of basaltic lavas and country rock around Auckland (1700 – 2000 and 2000 – 2200 kg/m^3 respectively) (Houghton et al., 1999; Kereszturi et al., 2013).

In regards to range of ballistic projectiles, Allen and Smith (1994) suggest the maximum range for ballistics in the AVF will be between 2-3 km of the vent for ballistics ejected during violent, 'wet' phreatomagmatic eruptions. The maximum range of ballistics from the 'wet' Vulcanian phreatic eruption is modelled as 1.7 km, so the range of ballistics in this scenario can be considered credible. The maximum range from the Strombolian eruption was < 500 m which constrained ballistics to fall within the harbour (Figure 51), so a full ballistic impact assessment was only carried out for the Vulcanian phreatic eruption. For further detail on the values used to parameterise the model, refer to Appendix A.

Table 14: Tsunematsu model input parameters for a Strombolian and a Vulcanian phreatic eruption. The literature review providing these input parameters was carried out by Rebecca Fitzgerald (90%) and myself (10%) and is presented in Appendix A.

	Strombolian		**Phreatic (Vulcanian)**	
Parameter	**Mean**	**Standard deviation**	**Mean**	**Standard deviation**
Particle density (kg/m³)	1300	200	2000	300
Particle diameter (m)	0.48	0.23 (0.064 - 4.59)	0.36	0.23 (0.064 - 3)
Magnitude of initial velocity (m/s)	50	50 (up to 400m/s)	200	50
Ballistic ejection angle (° from vertical)		20		50
Vent inclination angle (° from vertical)	0		0	
Displacement of ejection points from the vent centre (m)		5		5
Number of particles per burst	780		13000	
Number of bursts	38		11	
Direction (North is 0°)	0		0	
Flow velocity (m/s)	100		150	
Flow radius (m)	50		300	

Figure 51: Distribution of ballistics from a single Strombolian burst from Ruaumoko volcano (LINZ Auckland 0.5m Rural Aerial Photos (2010-2012)). Map produced by Rebecca Fitzgerald.

Figure 52: Distribution of ballistics from a Vulcanian eruption from Ruaumoko volcano (LINZ Auckland 0.5m Rural Aerial Photos (2010-2012)). Map produced by Rebecca Fitzgerald.

One advantage of using a three dimensional ballistics model for building impact assessment is that the trajectory of each ballistic can be imported directly into a GIS (in this case, ArcScene) to determine where it may have struck the building (i.e. roof, wall or the intersection between the two) as this will influence which fragility function is used, the obliquity calculation (and thus associated hazard intensity of the ballistic) and hence the overall damage (Figure 53).

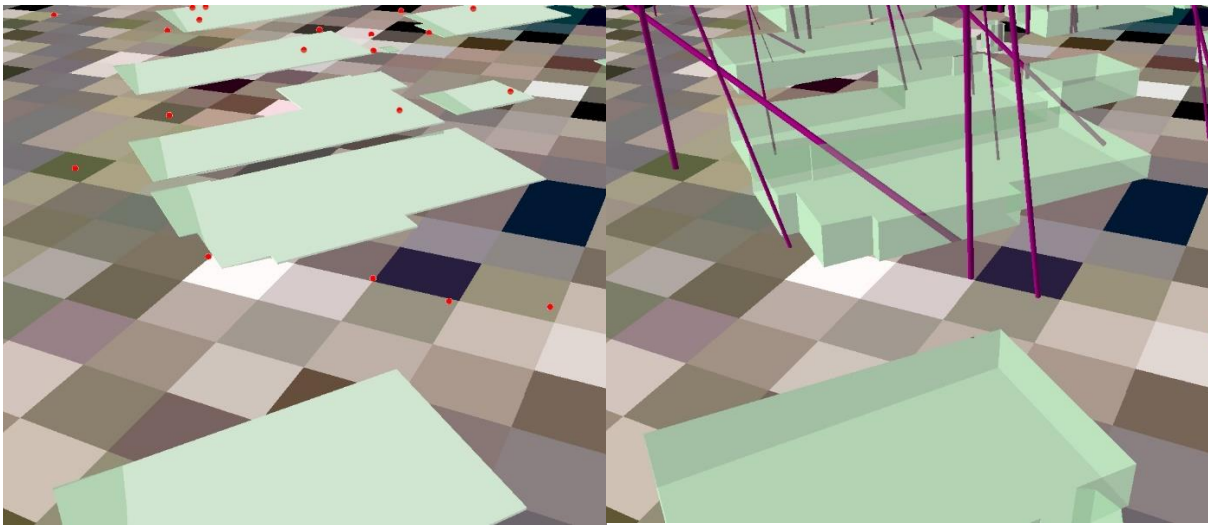

Figure 53: Two ArcScenes illustrating ballistic hazard and building exposure in 2D and 3D. In 2D, ballistic impact locations are represented using red dots. In 3D ballistic impact trajectories are represented using purple cylinders.

However, developing the model so that it can import 3D trajectories into ArcScene will require further collaboration with the model developers and was ultimately considered beyond the scope of a masters thesis. Therefore, a simplified approach was taken to model ballistic impact trajectories in three dimensions. Firstly a 2D line between each block's impact point and the vent was digitised (i.e. the flight path projected to the ground surface). Next trigonometry was used to add a Z coordinate to the vent end of the line so that this line's angle would be equal to its ballistic's impact angle (see example Figure 54). This assumes that the trajectory of a ballistic over its final ~5-20 metres of flight follows a straight line but it should be very similar to the trajectory at the end of a ballistics' flight.

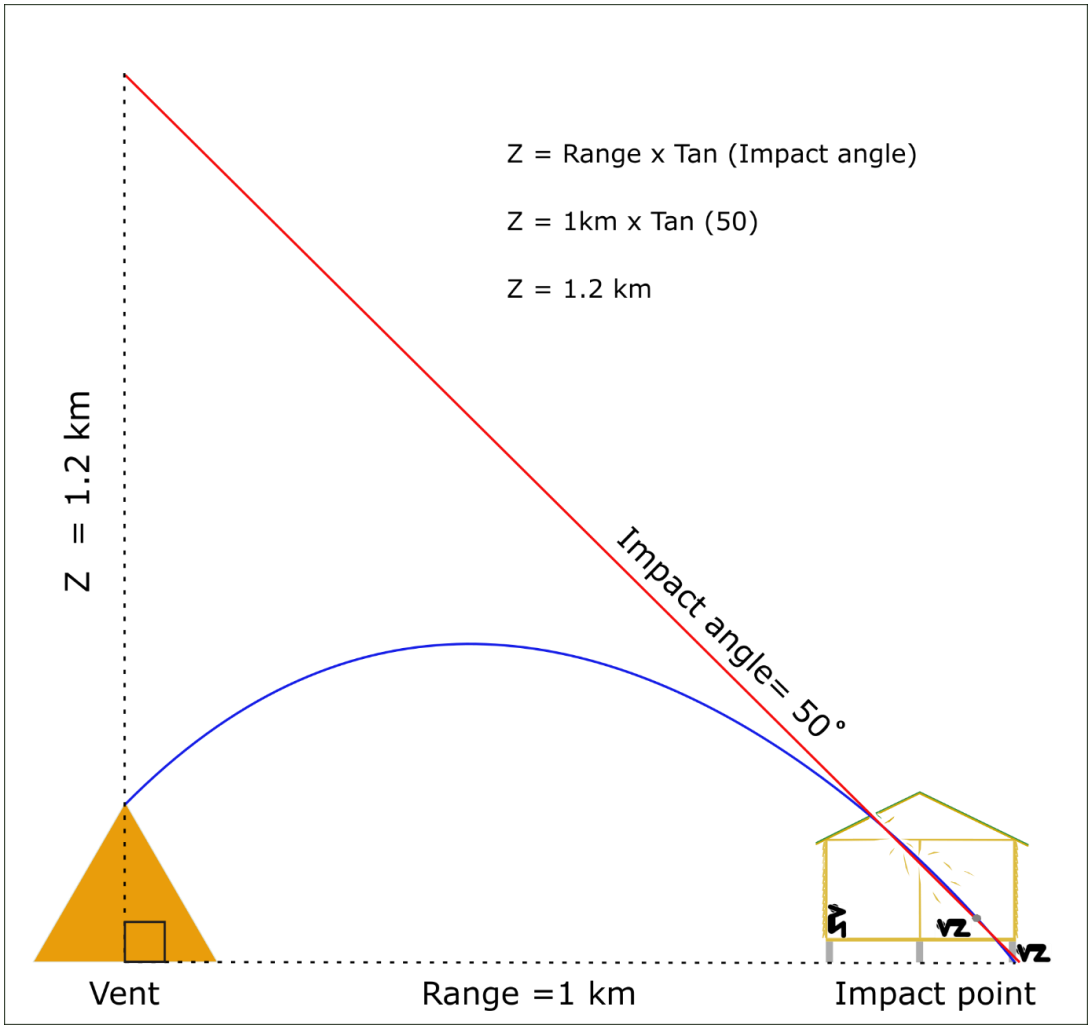

Figure 54: Example of the trigonometry used to approximately model the end of a ballistic's trjectory (red line) using its range and impact angle. Z is the height to which the vent end of the line must be raised so that the impact end of the line approximates the ballistic's true parabolic trajectory (blue line) which is calculated in Matlab using the Tsunematsu model.

4.2.3 Building vulnerability modelling

Once building exposure and tephra hazard have been characterised, fragility and vulnerability functions are used to relate these two components to determine impact (Figure 48). For functions to determine impact effectively they must be attributed to the building materials or building structure they have been developed for (i.e. a ballistic fragility function for reinforced concrete cannot accurately model impacts to a brick masonry wall). Therefore, building vulnerability has been modelled by assigning the appropriate set of fragility or vulnerability functions to each building in the exposure inventory based on attributes within the exposure inventory.

4.2.3.1 Assigning tephra fall functions to buildings

For tephra fall, construction type has been identified as the strongest indicator of building vulnerability (e.g. Spence et al., 1996; Jenkins et al., 2014; Maqsood et al., 2015). This means of all the building attributes within RiskScape's building asset database, 'construction class' has been chosen as the most suitable attribute for function assignment to be based on. From the selection of previously developed functions in section 2.4 the most widely applicable suite is arguably that from the United Nations Global Assessment of Risk 2015 (Maqsood et al., 2015). The relatively large number of different building typologies in the report's 'global building schema' (which ranges from adobe buildings through to engineered reinforced concrete buildings) contains several typologies that can be used to represent the range of buildings in Auckland and their vulnerability to tephra fall hazards. Also if the vulnerability functions are to be used within RiskScape in the future then they are also applicable from the point of view that similar vulnerability functions (in regards to damage ratio) have been used by RiskScape in the past (King and Bell, 2009). A final reason for the selection of vulnerability functions over fragility functions was because none of the previously developed tephra fall fragility functions have considered damage states below roof collapse meaning they would not be able model lesser damage at lower hazard intensities. Vulnerability functions on the other hand can be used to output an estimated dollar value for building repair cost across the full range of hazard intensity.

There are nine construction classes recognised within the database that are present in the Auckland building stock, however only six vulnerability functions have been selected to capture the likely differences in building performance (Figure 55). This has been done because although a the full range of different construction classes recognised in RiskScape's database may be relevant for modelling building performance under earthquake or flooding hazards, based on the description of building classes in Paulik (2015), several of the 12 classes are assumed to perform similarly under tephra loading meaning classes can be aggregated (Table 16**Error! Reference source not found.**). By assigning a function to each construction type in the database, vulnerability has been matched with exposure. This means once the tephra load on each building has been modelled for a particular eruption scenario, the impacts associated with that scenario can be calculated.

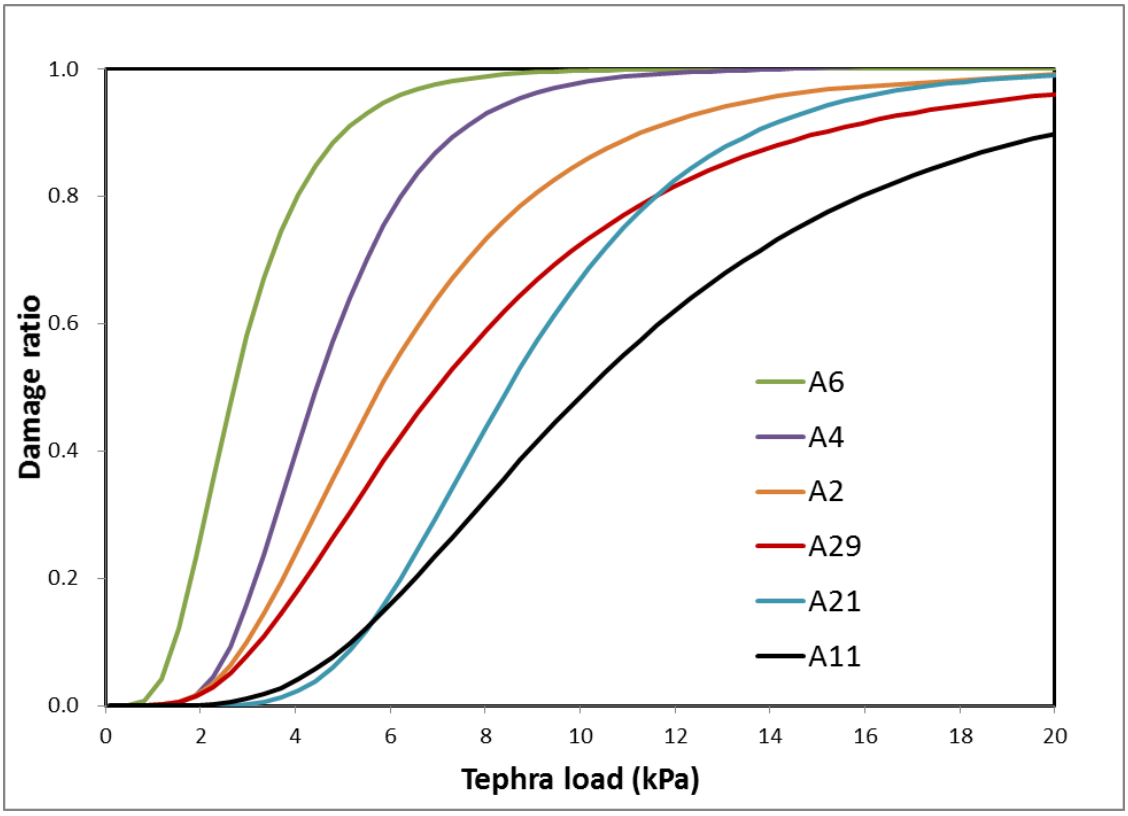

Figure 55: Building vulnerability functions for tephra loading. Typologies and function attributes given in Table 15.

Table 15: Building typologies and parameters of the functions in Figure 55. Note that low pitch roofs are angled less than 6 degrees, medium pitch roofs are between 6 and 35 degrees and high pitch roofs are over 35 degrees.

Building typology	GAR identifier	Median (θ)	Standard deviation (β)
Light timber frame, engineered, low rise, medium roof pitch	A2	5.8	0.52
Light timber frame, non-engineered, low rise, medium roof pitch	A4	4.45	0.4
Timber and light steel frame Industrial/Commercial, engineered, low rise, low roof pitch	A6	2.7	0.5
Concrete Frame/Reinforced Masonry, non-engineered, low rise, medium roof pitch	A11	10.2	0.53
Unreinforced Masonry Bearing Walls, non-engineered, low rise, medium roof pitch	A21	8.5	0.36
Concrete Frame with Unreinforced Masonry Infill Walls / Steel Moment Frame, engineered, low rise, low roof pitch	A29	7.0	0.6

Table 16: Attribution of typology-specific vulnerability functions to RiskScape construction classes.

GAR 15 Tephra Fall Function	RiskScape Construction Class No	RiskScape Construction Class Name	Percentage of Greater Auckland Building Stock
A11: Concrete Frame/Reinforced Masonry, non-engineered, low rise, medium pitch	1	Reinforced Concrete Shear Wall	4.30%
	2	Reinforced Concrete Moment Resisting Frame	1.40%
	10	Concrete Masonry	3.50%
A29: Steel Moment Frame, engineered, low rise, low roof pitch	3	Steel Braced Frame	0.00%
	4	Steel Moment Resisting Frame	0.00%
A4: Light timber frame, non-engineered, medium pitch, low rise	5	Light Timber	86.80%
	11	Unknown Residential	0.00%
	8	Advanced Design	0.00%
A6:Timber and light steel frame Industrial/Commercial, engineered, low rise, low pitch	6	Tilt Up Panel	0.80%
	7	Light Industrial	0.80%
A21: Unreinforced Masonry Bearing Walls, non-engineered, low rise, medium pitch	9	Brick Masonry	2.30%
	12	Unknown Commercial	0.00%

The tephra fall vulnerability functions have a cumulative lognormal distribution typical of functions used for other hazards (Baker, 2014; Maqsood et al., 2015). The functions are calculated using the following equation:

$$DI(IM = x) = \Phi \frac{\ln\left(\frac{x}{\theta}\right)}{\beta}$$

Where DI is the expected mean damage index reached when a structure is subjected to a tephra load x (measured in kPa), Φ is the standard normal cumulative distribution function, θ is the median of the fragility function (i.e. the tephra load corresponding to an IM of 0.5) and β is the standard deviation of lnIM. The uncertainty assigned to the mean damage index was decided by the Global Assessment project team to be +/-

30% of the mean damage index to the 5th and 95th percentile values of the damage index respectively.

4.2.3.2 Assigning ballistic functions to buildings

From ballistic cannon experiments and post-eruption impact assessments the amount of damage caused by ballistic impacts to buildings is primarily controlled by the ballistic's impact energy and the impact resistance of the cladding. Therefore, the most appropriate attributes within RiskScape's building asset database to base cladding specific ballistic fragility function assignment on are likely to be RiskScape's 'roof cladding class' and 'wall cladding class' attributes. In addition to 'cladding class', the 'construction class' attribute has also been used to determine what type of framing (if any exists) could be impacted by ballistics. Three dimensional modelling of exposure and hazard determines if a ballistic impact has struck a building's wall or roof and hence, which cladding function should be applied. However, cladding does not cover the entire surface of a building so once the impact location has been established there are still up to three different types of fragility functions (cladding, framing or window) that could be used to model damage from the impact. The process for deciding which of the three fragility functions is attributed to each individual impact is outlined in (Figure 56).

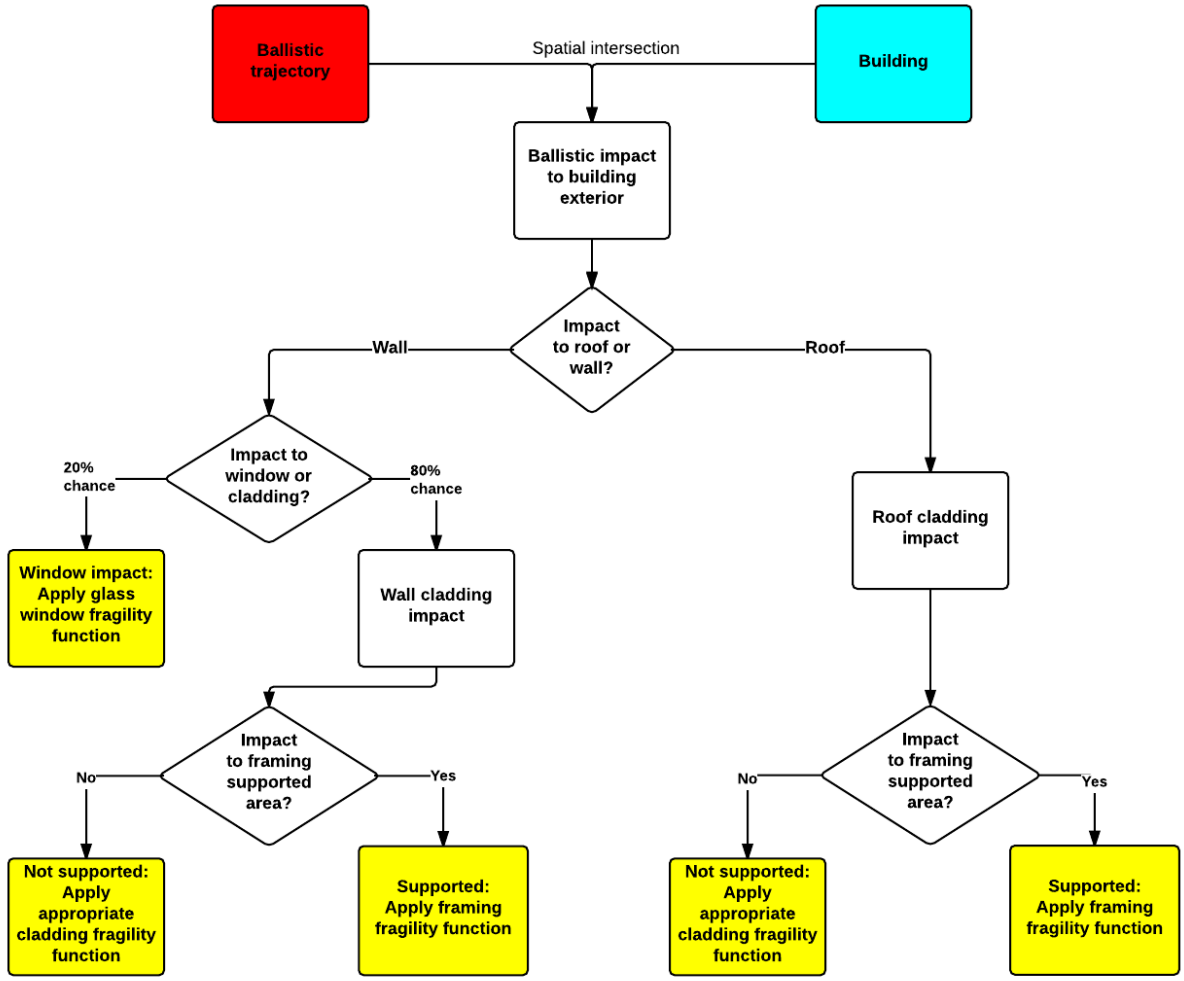

Figure 56: The decision making process for assigning the appropriate fragility functions based on building type and ballistic impact location. Colours signify whether an item pertains to hazard (red), exposure (blue) or vulnerability (yellow)

In RiskScape's building asset database, there are seven distinct roof cladding classes, six of which are impacted by ballistics in this eruption scenario. One suite of functions (i.e. DS1, DS2, DS3) has been assigned to each of the cladding classes impacted (Table 17). Wall claddings have been attributed functions in the same way by matching each cladding type listed in the exposure inventory with the most appropriate function suite. There are a total of 15 different wall cladding classes recognised in the database, nine of which are impacted by ballistics in this scenario (Table 18). If a window is impacted then the glass fragility function is used and if a building has framing that is modelled to have been impacted then the timber framing fragility functions are used. A full list of the function suites and the claddings they are assigned to is given in Appendix B5. This list also identifies claddings which are a priority to develop functions for during future ballistic-building vulnerability research.

Table 17: The six roof cladding classes impacted by ballistics in this impact assessment. Note the 'membrane' roof cladding class has been assigned the sheet metal fragility function suite because this type of roof cladding is simply a waterproofing layer usually placed over a steel deck.

RiskScape roof cladding class	Function suite attributed	Number of roof impacts	Percentage
1: Clay/Concrete Tile	Tile	109	16.4%
2: Concrete Slab	RC Slab	6	0.9%
3: Membrane	Sheet metal	1	0.2%
4: Metal Tile	Sheet metal	44	6.6%
6: Other - Light	Plywood	6	0.9%
7: Sheet Metal	Sheet metal	500	75.2%
Grand total		**665**	**100%**

Table 18: The nine wall cladding classes impacted by ballistics in this impact assessment.

RiskScape wall cladding class	Function suite attributed	Number of wall impacts	Percentage
1: Weatherboard	Weatherboard	66	41.8%
2: Stucco, Roughcast	Fibre RC sheet (5^{th} percentile)	11	7.0%
5: Fibre Cement Sheet	Fibre RC sheet	8	5.1%
6: Fibre Cement Plank	Fibre RC sheet (5^{th} percentile)	8	5.1%
7: Reinforced Concrete	RC slab	7	4.4%
8: Concrete Masonry	RC slab (95^{th} percentile)	14	8.9%
9: Brick	RC slab (95^{th} percentile)	38	24.1%
14: Other Sheet-Non Combustible	Sheet metal	2	1.3%
15: Other	Weatherboard	4	2.5%
Grand total		**158**	**100%**

4.2.4 Relating hazard, exposure, and fragility

To complete an impact assessment the three major components of the impact assessment need to be related to each other within a GIS to generate and analyse spatial data. The steps required to relate these components for ballistics and tephra fall are different.

4.2.4.1 Tephra fall impact assessment GIS process

The steps required to quantify building damage from tephra fall in ArcMap 10.2 are set out below:

1. Calculate the thickness of tephra on each impacted building. Total accumulated tephra thickness is dependent on the thickness of tephra deposited on the roof and the percentage of this tephra which sheds from the roof. In turn the percentage of tephra which sheds from the roof is dependent on roof pitch and cladding. Hampton (2015) conducted experiments measuring the percentage of tephra fall that would accumulate on corrugated iron roofing at four different roof pitches. By fitting a linear trend line to their experimental results, the percentage of tephra remaining on a pitched metal roof after deposition can be modelled using the following equation.

$$\%\ accumulated = -2.41x + 109$$
$$(3.7 \leq x \leq 90)$$

   Where the % accumulated is modelled as the remaining thickness of the tephra fall deposit on a metal roof with x pitch compared to the total tephra fall thickness in the area. The negative coefficient of x means that increasing pitch causes increased tephra shedding from roofs.

2. Calculate the tephra loading on each impacted building using the tephra fall loading equation below.

$$L_{AF} = \frac{\rho g h}{1000}$$

   Where L_{AF} is the tephra fall load (kPa), ρ is the tephra deposit's bulk density (kg/m^3), g is gravitational acceleration (9.81 m/s^2) and h is the tephra deposit thickness remaining on the roof (m).
3. Calculate the cost to repair: cost to replace damage ratio by inputting the tephra loading value on each building into that building's vulnerability function.
4. Calculate the repair cost in dollars by multiplying each building's damage ratio by the building replacement cost recorded in RiskScape's building asset database.

4.2.4.2 Ballistics impact assessment GIS process

As illustrated in Figure 56, the first step is to identify which buildings have been impacted and whether the impact is to the wall or roof. Once a fragility function is assigned to each impact, its damage state can be predicted reached by each impact are as follows:

1. Calculate the impact obliquity of each ballistic. Based on impact angle and angle of wall/roof surface being impacted.
2. Using the calculated obliquity value, calculate the normal component of impact energy for each ballistic.
3. Input the normal component of impact energy of each ballistic into its fragility function equation to determine the probability of it falling into a given damage state.
4. Compare the probability to a randomly generated number (between 1 and 0) to get a discrete number determining which damage state (DS1, DS2 or DS3) has occurred.
5. For buildings with cladding over a reinforced concrete frame, if an impact has resulted DS3 to cladding then the residual energy of the ballistic is calculated according to Kar (1979) and the damage to the concrete frame may also be modelled.

This type of ballistic impact assessment on its own can only predict the most likely damage state from individual impacts. It does not consider the potential for multiple impacts to have a compounding effect on damage nor does it consider loss of building functionality as a whole.

4.3 Tephra impact assessment results

Using the Exercise Ruaumoko eruption scenario, >162,000 buildings are impacted by tephra fall (>0.1 mm thick) and 468 buildings are impacted by ballistics. All of the buildings within the ballistic fallout zone were also impacted by at least 100 mm of tephra fall, therefore for an eruption with this large thickness of tephra fall near the vent, ballistics may have an effect on a building's tephra load bearing capacity but their impacts can be considered relatively insignificant compared to tephra fall impacts.

However, to assess the impact from each hazard individually, a summary for each is presented.

4.3.1 Tephra fall impact assessment results

Tephra from this eruption covers an area ~500 km^2 with a total of 162,108 buildings impacted by thicknesses at least 0.1 mm. Of these impacted buildings, 3-10% are modelled to have structural damage. The estimated repair cost associated with structural damage ranges from $1.3 to $2.4 billion. This large range is dependent on how the tephra loading is calculated for each building's roof (Table 19). Loading can be changed by varying tephra density (kg/m^3) or the thickness of deposits resulting from different tephra shedding dynamics. Buildings impacted by tephra can be separated to assess the number of buildings in different damage ratio ranges (Table 20). Table 20 shows that ~97% buildings impacted by tephra receive no structural damage. Figure 57 and Figure 58 show that for even the most vulnerable building types, structural damage does not begin to occur until tephra thicknesses of 20 -30 mm are reached (different thicknesses corresponding to 0.3 KPa loading for 1000 and 1500 kg/m^3 tephra densities respectively).

Table 19: Modelled structural building damage repair costs for four eruption scenarios with different combinations of tephra fall densities and tephra shedding dynamics.

Density	**Dry density (1000 kg/m3)**		**Wet density (1500 kg/m3)**	
Accumulation	**1. Maximum shedding**	**2. No shedding**	**3. Maximum shedding**	**4. No shedding**
Average damage ratio amongst damaged buildings	0.49	0.44	0.40	0.29
Number of buildings damaged	5621	9,542	7,895	15,986
Average repair cost for damaged buildings (NZD)	233,147	223,877	197,247	152,418
Total repair cost (NZD)	1,310,521,724	2,136,239,333	1,557,272,081	2,436,569,745

Table 20: The number of buildings of different use categories in given damage ratio ranges. These values are for scenario #1 in dynamics. Table (Maximum shedding, 1000 kg/m^2 tephra density).

Damage ratio range	Building type				Totals	%
	Residential	Commercial	Industrial	Other		
0-0.001	141293	4313	5465	6799	**157870**	**97.39%**
0.001-0.1	828	16	64	38	**946**	**0.58%**
0.1-0.2	178	3	9	9	**199**	**0.12%**
0.2-0.3	60	2	8	2	**72**	**0.04%**
0.3-0.4	85	1	5	1	**92**	**0.06%**
0.4-0.5	124	0	1	3	**128**	**0.08%**
0.5-0.6	188	0	2	10	**200**	**0.12%**
0.6-0.7	165	0	4	5	**174**	**0.11%**
0.7-0.8	125	2	10	2	**139**	**0.09%**
0.8-0.9	97	5	26	7	**135**	**0.08%**
0.9-1	1926	20	136	71	**2153**	**1.33%**
Grand Total	145069	4362	5730	6947	**162108**	**100.00%**

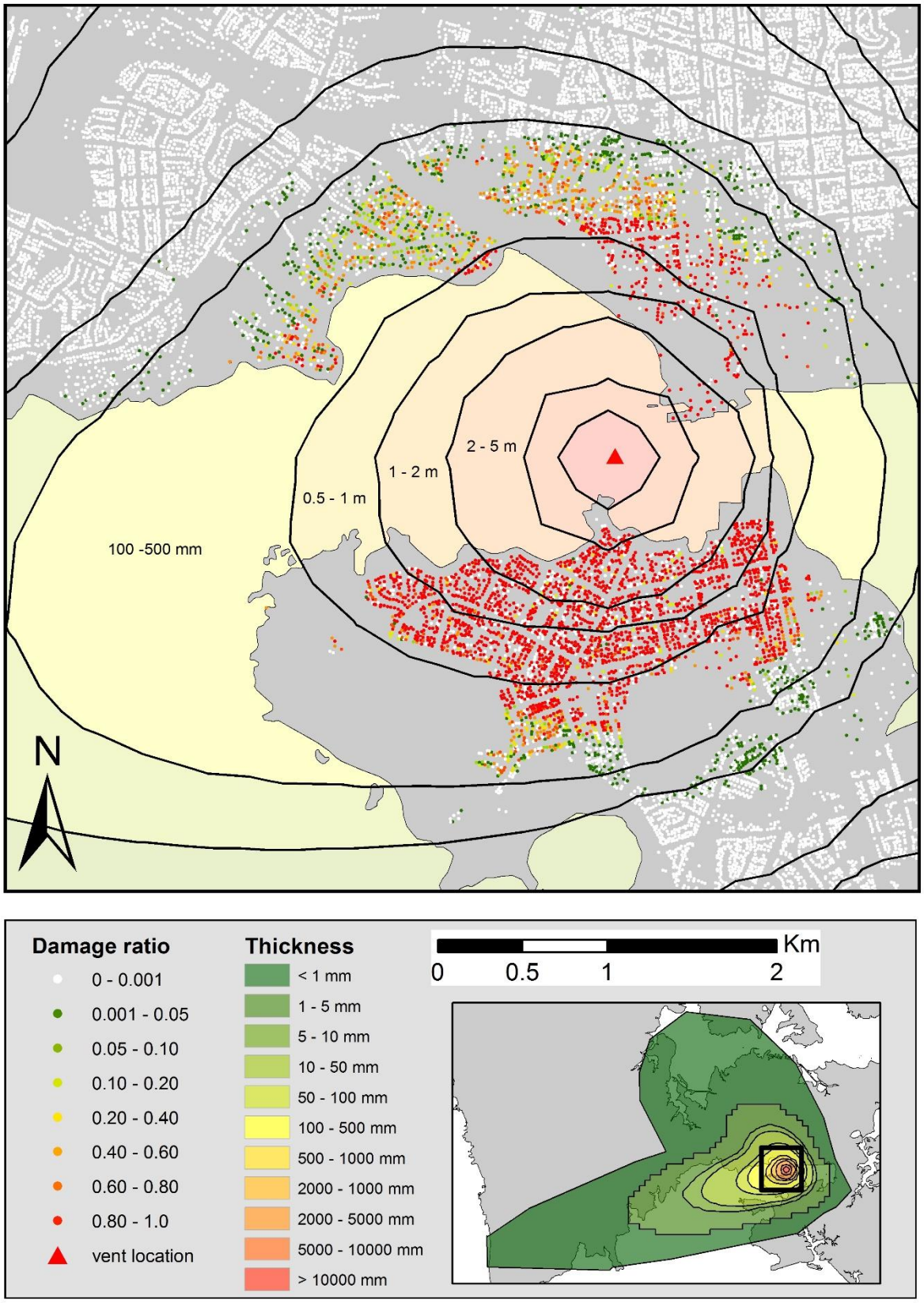

Figure 57: Tephra loading structural damage for scenario 1: Maximum shedding, 1000 kg/m^3 tephra density.

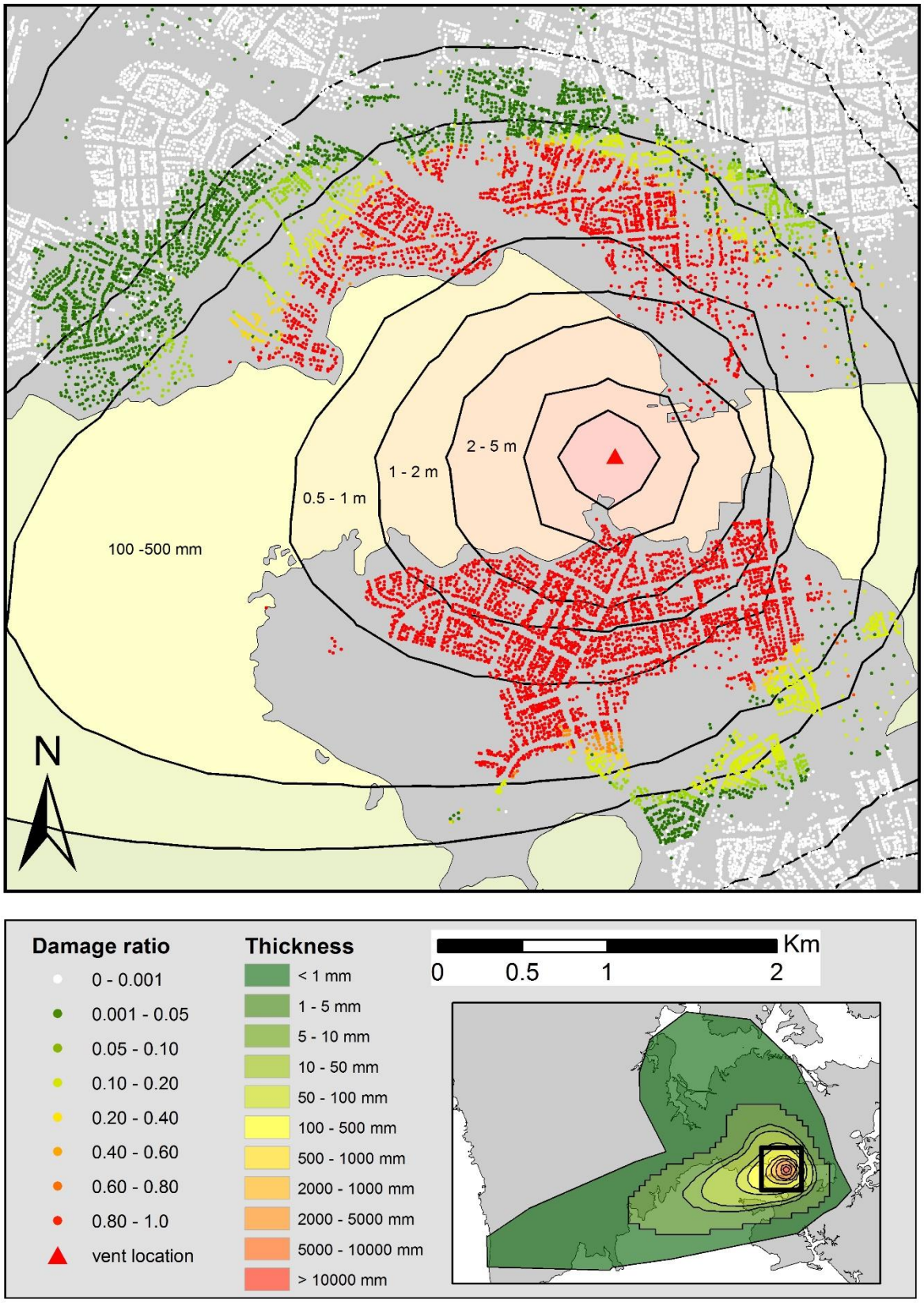

Figure 58: Tephra loading structural damage for scenario 4: No shedding, 1500 kg/m^3 tephra density.

Though tephra fall thicknesses of 20 mm or less are modelled to cause no structural damage, they will still cause significant disruption and damage to non-structural building components such as roof guttering, HVAC units, roof and wall coatings and satellite dishes. The exposure inventory used in this model doesn't explicitly identify which buildings have these non-structural building components and apart from HVAC units there are currently no published vulnerability of fragility functions for these components. This means any risk or impact assessment seeking to quantify non-structural damage must rely on numerous assumptions to account for incomplete exposure and vulnerability assessments (e.g. Magill et al., 2006). As the purpose of this chapter is to showcase how fragility and vulnerability functions are used in impact assessments, approaches relying heavily upon assumptions will not be adopted so non-structural building damage from tephra falls has not been modelled.

4.3.2 Ballistic impact assessment results

Ballistics in this scenario impact on residential and industrial areas up to 1.4 kilometres from the vent (Figure 59 and Figure 60). A total of 468 different buildings were impacted by 823 ballistics giving an average of ~1.8 hits per building impacted (Table 21). This scenario displays a pattern of decreasing impacts per unit area with increasing distance from the vent and the percentages of buildings being impacted decreases accordingly (Table 22). Although most buildings receive 1-2 impacts the building receiving the most impacts had 10 strikes to its roof (Figure 61).

Summary of impacts		Totals
Ballistic strikes to roofs	665	823
Ballistic strikes to walls	158	
Buildings with wall strikes	141	468
Buildings with roof strikes	446	

Table 21: Quick summary of individual ballistic impacts to buildings.

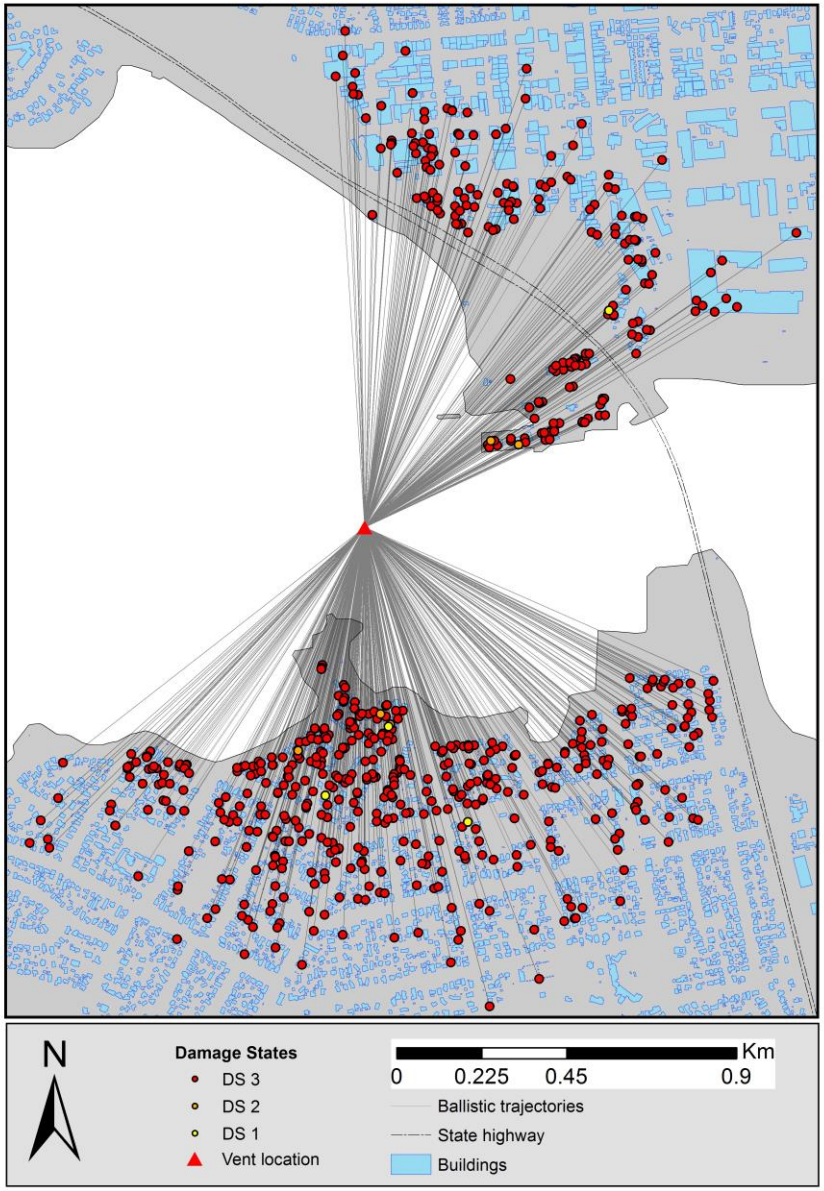

Figure 59: Damage states for direct ballistic impacts to roofs.

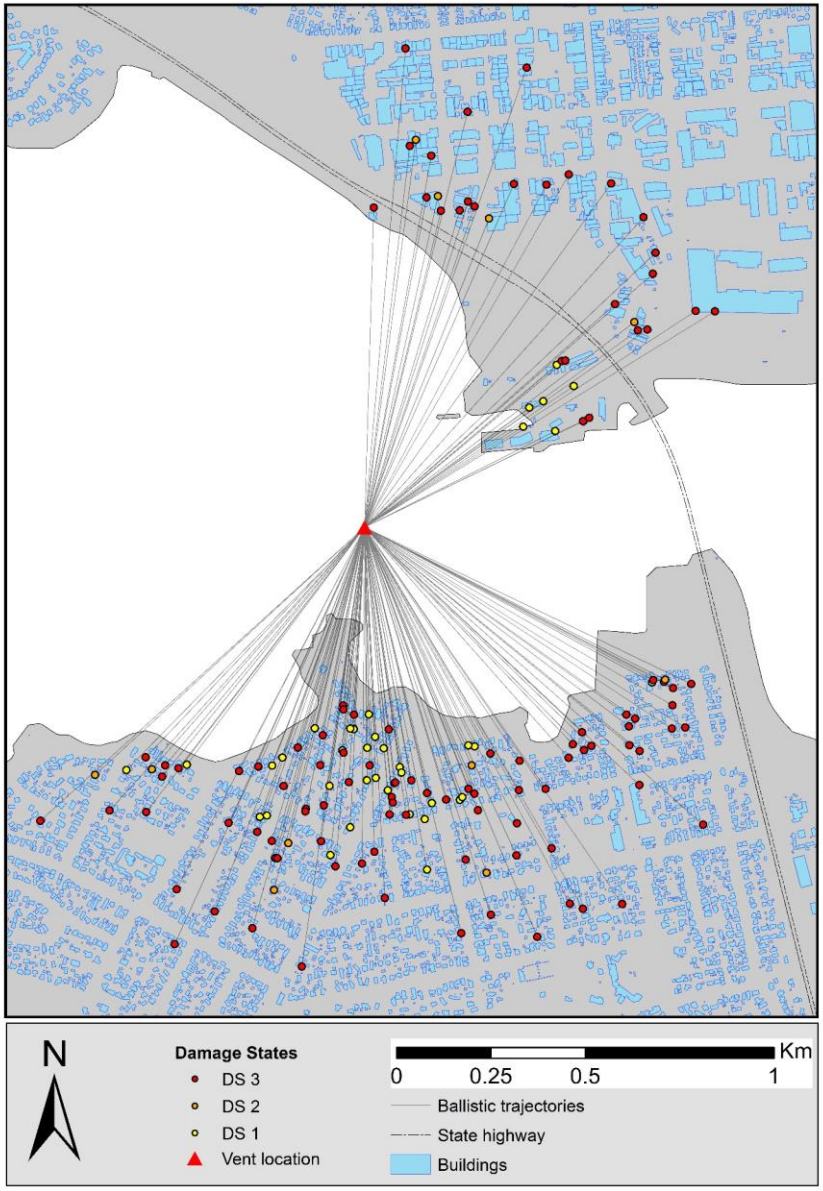

Figure 60: Damage states for direct ballistic impacts to walls.

Metres from vent	0-500	500-1000	1000-1500	0-1500 (total)
Area (hectares)	78.5	235.6	392.7	706.9
Ballistics	4134	8536	1018	13688
Ballistic per hectare	52.7	36.2	2.6	19.4
Total buildings	34	1233	3052	4319
Impacted buildings	15	352	101	468
Percentage impacted	44.12%	28.55%	3.31%	9.23%

Table 22: Ballistic impact density and percentage of buildings impacted in each zone.

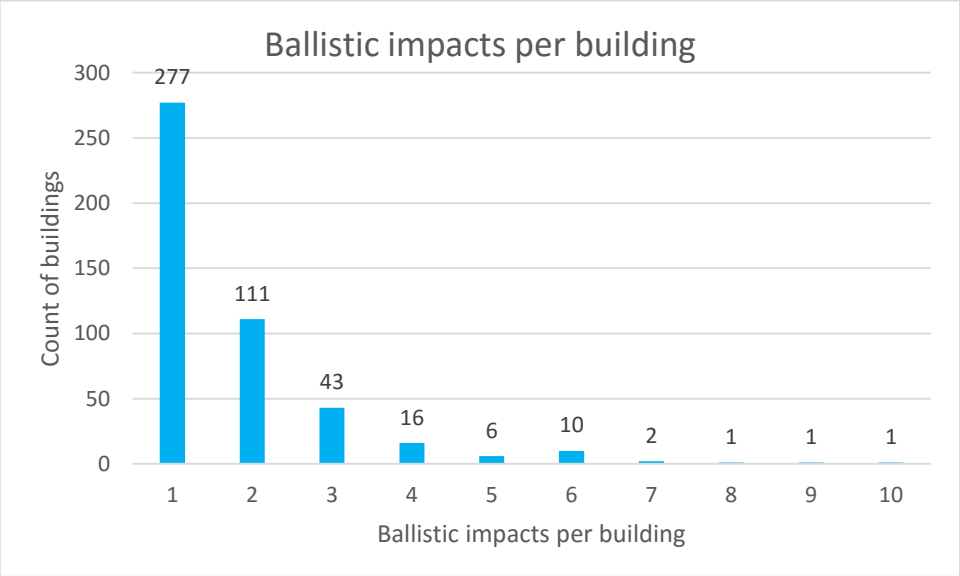

Figure 61: Ballistic impacts per building.

Of all the ballistic impacts to buildings, >92% were modelled to cause DS3 perforations to the buildings they impacted. However, there is a significant difference between roof and wall impacts where perforations occurred in 98% and 67.5% of impacts respectively (Table 23 and Table 24). The cause of this difference can be mostly attributed to two factors. The first being that wall impacts had higher obliquities than roof impacts, averaging to 66° and 29° respectively. In calculating the normal component of velocity a 66° obliquity equates to a 60% reduction in the normal component of velocity whereas a 29° obliquity equates to only a 12% reduction. The second factor contributing to a lower percentage of wall perforations is the higher proportion of relatively strong wall claddings made of reinforced concrete, concrete

masonry and bricks which are more resistant to perforation than the claddings used in roofs which are typically lighter (4% of walls compared to 0.8% of roofs).

Damage Type	Totals	%	% combined
Sum of Framing DS 1	4	0.6%	1.2%
Sum of Cladding DS 1	4	0.6%	
Sum of Framing DS 2	1	0.2%	0.8%
Sum of Cladding DS 2	4	0.6%	
Sum of Framing DS 3	355	53.4%	98.0%
Sum of Cladding DS 3	297	44.7%	
Totals	665	100.0%	100.0%

Table 23: Damage state distribution for ballistic impacts to roofs.

Damage type	Totals	%	% combined
Cladding DS 1	4	2.4%	24.1%
Framing DS 1	33	19.9%	
RC backing DS 1	3	1.8%	
Cladding DS 2	0	0.0%	8.4%
Framing DS 2	12	7.2%	
RC backing DS 2	2	1.2%	
Window DS 3	29	17.5%	67.5%
Cladding DS 3	38	22.9%	
Framing DS 3	42	25.3%	
RC backing DS 3	3	1.8%	
Totals	166	100.0%	100.0%

Table 24: Damage state distribution for ballistic impacts to walls.

Despite nearly all of the impacting ballistics being able to cause roof punctures the area of damage caused by these punctures may be relatively low. Using the diameter of each impacting ballistic, it was found that punctures caused by these sum to an average of <0.2% per building (assuming punctures are roughly the same size as the ballistic that caused them). The building with the highest coverage by ballistics was a small building impacted by one large, 63 centimetre diameter ballistic whose puncture would account for 1.3% of the house's footprint. Punctures to this quantity of a building's footprint are considered to be repairable so long as the impact doesn't strike in an area causing damage to key structural components of the building, such as purlins or king trusses (identified as important roof framing structures by Pomonis et al. (1999)). Aside from the repair cost of a roof, another impact metric to consider is the building's functionality. A complete puncture of the building envelope leaves a building more vulnerable to subsequent tephra contamination and moisture damage,

potentially for months or even years after the initial eruption should evacuation cordons remain in place for the duration of extended periods of volcanism.

4.4 Limitations and assumptions

The damage predictions from impact assessments such as these are useful for identifying and quantifying possible impacts to aid in future risk reduction measures. However, it is important to acknowledge the inherent limitations and assumptions of this impact assessment and the uncertainty they bring to any loss predictions. Some assumptions are required when modelling the interactions between tephra fall, ballistics and a large number of buildings. Every assumption reduces the accuracy of the model and is likely to contribute to either an underestimation or an overestimation of the overall impact to buildings. Assumptions for the tephra fall and ballistic impact assessments have been summarised in Table 25 and Table 26 respectively. A full explanation of these assumptions can be found in Appendix B7.

Table 25: Assumptions and limitations of different components of the tephra fall impact assessment and their implications for the model's results.

Assumption /limitation	Implication for loss estimates		
	Under estimation	Over estimation	Unknown
Hazard model			
Modelled eruption isopachs (not past eruption isopachs)			
Deterministic hazard assessment with unusual wind profile used in the modelling			
Changing density or grainsize distribution with distance from vent not modelled			
Exposure inventory			
Over 25% of building footprints have no data attributed			
Exposure of non-structural building components not captured			
Vulnerability model			
Functions produced solely using expert elicitation data and are yet to be validated			
Functions only consider structural damage (>100 mm/ 0.3 kPa)			
Functions ignore the higher load bearing capacity of steeply pitched roofs			
Relating hazard, exposure and vulnerability			
One end-member scenario models zero shedding (wet tephra)			
One end-member scenario models maximum shedding (dry tephra)			
Wind remobilisation of tephra from roofs not considered			
Roofs which shed all their tephra are modelled to receive 0 damage, even if buried			

Table 26: Assumptions and limitations of different components of the ballistic impact assessment and their implications for the model's results.

Assumption/limitation	Implication for loss estimates		
	Under estimation	Over estimation	Unknown
Hazard model			
No consideration of impact temperature and potential fire hazard			
No consideration of ballistic bomb impacts			
No particle collisions modelled			
No consideration water's effect on the initial flight path			
Only direct impacts modelled no modelling of ricocheting/bouncing ballistics			
Exposure inventory			
Most common claddings attributed to buildings with no roof cladding data			
Flat topped buildings with roofs not extruded into 3D			
Exposure of non-structural building elements not considered			
Window:cladding ratio for all buildings based on residential building analysis only			
Vulnerability model			
Some functions attributed to claddings they were not specifically made for			
Normal component of impact energy doesn't consider shear stress component			
Functions used were developed from limited data			
Relating hazard, exposure and vulnerability			
Impacts to successive layers (e.g. roof-floor or roof-wall) not modelled			
Residual energy = impact energy - perforation threshold			
Perforating ballistics assumed to stay fully intact			

4.5 Discussion

The repair cost of structural building damage from tephra fall and ballistic impacts for an eruption of this magnitude is likely to be in excess of $450 million, with the majority of this cost being from tephra fall. In addition to structural damages, non-structural damages caused by light tephra loads are expected to be widespread and therefore their total cumulative cost is likely to be significant.

Of all the buildings impacted by tephra fall in this scenario, less than 3% experience structural damage. This highlights the need for quantification of non-structural building components' vulnerability to light tephra falls. The cost of non-structural damage is likely to be relatively low for individual properties but because of the large numbers of impacted buildings it is important that these estimates be as accurate as possible as they have important implications for insurance and construction sectors and for the large number of affected communities.

More research is required to quantify non-structural damage caused by tephra fall without relying heavily on assumptions as previous work has done (e.g. Magill et al 2006). In particular this requires the development of fragility functions for several key building components which are vulnerable to impacts from light tephra falls (outlined in Table 3). To match improvements in the development of vulnerability, exposure inventories must also be enhanced with additional information regarding which buildings actually have these vulnerable building components.

Another aspect of tephra impacts to buildings that this impact assessment has identified as an area for future research is the relationship between roof pitch and a roof's ability to facilitate tephra shedding. This has implications not only for structural damage from tephra loading to roofs but also for non-structural damage to the gutters which tephra is shed into.

From the ballistic impact assessment, it has become apparent that in order to provide a more meaningful prediction of possible impacts, there is a need to translate specific damages (e.g. number of perforations per building footprint area), into an overall impact state for buildings as a whole (e.g. minor roof repair required or building uninhabitable). This could utilise an approach where vulnerability is modelled using two sets of fragility functions in succession. The first set would predict the specific damage state from each ballistic impact as the functions produced in this thesis do. A

second set would predict what generic impact state each building falls into based on the damage it has received. This approach would be especially useful in eruption scenarios such as this one where over 90% of ballistic strikes are modelled to have caused perforation of the building envelope. For this second set of fragility functions, perforation density per building footprint area could be used as the HIM. Using this HIM, one approach to developing impact state fragility functions may be to base impact state exceedance probabilities on the probability that a given perforation density will have individual ballistics striking critical areas of a building. These may be areas where a ballistic perforation destroys a critical section of the building's framing or destroys plumbing or ruptures gas lines and water cylinders *etc.*

Another area of future work for any ballistic impact assessment is to automate the modelling process so that it may be repeated with enough iterations to complete a Monte Carlo analysis and allow this work to develop from a deterministic impact assessment into a probabilistic risk assessment. Also further modelling and research is required to assess the multi-hazard impacts of ballistics and tephra fall (and other near vent hazards) combined. Ballistic and tephra fall hazards have been observed to interact and influence the total building damage a building receives but thus far this research is only anecdotal (e.g. increased tephra ingress through ballistic perforations (Mt Usu, 2000) or tephra deposits shielding roofs from ballistic perforation (Mt Ontake, 2014) (Fitzgerald et al. in prep)). Other possible interactions are only theoretical at this stage, such as the potential for a building already weakened by ballistics to have a lower tephra load bearing capacity or the potential for perforations to increase a building's vulnerability to damage from high internal pressures caused by pyroclastic density currents (as is the case for wind loading on windborne debris perforations in hurricanes (Herbin and Barbato, 2012)). The large number of combinations and the temporal aspects of multi-hazard impacts means fragility functions with a single hazard intensity measure are not well suited to modelling impacts. Instead of using functions, multi-hazard impacts may instead rely on expert judgement to apply a set of logical rules that model the most likely impacts.

Chapter 5 Conclusions and recommendations

5.1 Conclusions

The aim of this thesis is to quantitatively assess the vulnerability of Auckland city's buildings to tephra hazards. To achieve this aim, the objectives stated in Chapter 1 have been completed (Table 27). The thesis reviews previous instances of tephra impacts to buildings, identifying research gaps in building vulnerability for both ballistic and tephra fall hazards. The thesis focuses on ballistic impacts to buildings by: a) summarising the findings of a post-eruption ballistic impact assessment trip to Japan to characterise ballistic impacts to a built up areas and to identify appropriate life safety actions; and b) undertaking and analysing novel ballistic cannon experiments to quantify building vulnerability. This research was used to inform fragility and vulnerability functions used for a tephra-building impact assessment in Auckland city, New Zealand.

Table 27: Objectives stated in Chapter 1 and their outcomes.

	Objectives	**Outcomes**
Objective 1	To develop a framework that guides the derivation of tephra fall and ballistic fragility functions for buildings	Framework developed and research gaps identified
Objective 2	To improve understanding of building vulnerability to tephra hazard	Derived new ballistic fragility functions and identified tephra fall vulnerability functions applicable to New Zealand buildings
Objective 3	To conduct a tephra-building impact assessment using a typical AVF eruption scenario	Quantitative impact assessment conducted applying new fragility and vulnerability functions to Auckland buildings

5.1.1 Quantifying ballistic impacts and building vulnerability

This thesis has taken a significant step to improve knowledge of ballistic impacts to buildings, particularly in terms of quantitative impact/risk assessments. Ballistic impacts to buildings have been largely overlooked by researchers because of (1) their relatively limited range, and volcanic risk management's focus on life safety and

evacuation, and (2) the incorrect perception that ballistics have binary impacts to buildings, wherein any impact to a building will result in its destruction. Observation of ballistic impacts in the field and in the literature show that this is not the case. Our data from Japan shows that a building can experience multiple impacts without being destroyed and even though our testing found that building materials are highly vulnerable to perforation by large dense blocks, ballistic impacts per area are rarely high enough to cause complete destruction of a building.

As part of quantifying building vulnerability to ballistic impacts this thesis has developed the first ballistic-building fragility functions (to the best of the author's knowledge). Claddings tested were found to be most vulnerable to perpendicular impacts but increasing impact obliquity sharply reduced the probability of a ballistic strike resulting in perforation (yet lower damage states still occurred at surprisingly low energies). As expected, reinforced concrete roof slabs were the most resilient cladding material tested and no ballistics were able to fully perforate slabs due to the strength of reinforcing bars. However impacts were strong enough to eject fragments from the back face with velocities equal to ~25% the velocity of the impacting ballistic, fast enough to threaten lives and damage property inside reinforced concrete buildings. In addition to developing fragility functions, testing and post eruption impact assessments were able to provide information on appropriate life safety actions people should take if sheltering from ballistic impacts in buildings.

5.1.2 Ballistics and tephra fall impact assessment

A ballistic impact assessment has been carried out for buildings in Auckland following a Vulcanian phreatic eruption from 'Ruaumoko Volcano'. In this particular scenario, over 400 buildings were impacted by 844 ballistics and fragility functions predicted over 90% of impacts resulted in perforation. Despite this, the overall damaged area on each impacted building was low enough that they could probably all be economically repaired, assuming no significant further damage was sustained from hazards.

Tephra impacts to buildings were also assessed for this eruption from a different approach of using vulnerability functions. Impacts from tephra fall were found to be significantly more widespread and severe than for ballistics with >0.1mm of tephra impacting over 200,000 buildings in Greater Auckland. For 2000-3000 buildings, modelled tephra loads were high enough to cause structural damage with repair costs

ranging from $450 million to $1.2 billion depending on tephra density and the percentage of tephra fall remaining accumulated on roofs. As the tephra fall-building vulnerability functions only record structural damage, buildings receiving tephra loads of less than 0.3 kPa (equivalent thickness 20 – 30 mm) were modelled to have sustained no damage. Buildings in this category represent over 95% of all buildings impacted by tephra for this eruption, but because tephra fall vulnerability research has yet to quantify the vulnerability of non-structural building components to light tephra falls, losses have not been modelled for this large majority of buildings.

5.2 Recommendations

5.2.1 General guidelines for designing tephra resistant buildings and sheltering in place from ballistics

For buildings to increase their resistance to tephra impacts they should have several of the following design features including:

- Steeply pitched roofs, (over 35°) made of a smooth material with a relatively high impact resistance to ballistic strikes such as corrugated iron. This will facilitate tephra shedding and increase the overall load the building can support.
- Well-constructed doorways and windows with tight seals to minimise ash ingress following an eruption.
- Gutters that are easily detachable so they may be completely removed prior to eruptions or
- Sections of the building exterior against which a ladder can be safely placed so tephra removal from the roof can be carried out without risk of crushing gutters.

Though reinforced concrete showed a significantly higher impact resistance than all other materials tested, the cost of concrete compared to typical timber framed construction makes it unfeasible to advise Auckland's future buildings be constructed using RC slabs. However in the event of a short lead in time for a future AVF eruption where evacuations cannot be fully conducted prior to the eruption, it would be beneficial for emergency planners to have already identified buildings across Auckland which are exceedingly resistant to ballistic strikes and other volcanic hazards. Such buildings would ideally have multiple storeys of reinforced concrete (e.g. parking buildings).

Should people be forced to shelter from ballistics inside unreinforced buildings, they should seek to put as many layers of building materials as possible between themselves and incoming ballistics by positioning themselves behind, under or inside robust furniture on the side of the building furthest from the erupting vent.

5.2.2 Future research directions

Research directions related to tephra fall-building vulnerability which can contribute towards disaster risk reduction have been identified:

1. The vulnerability of non-structural building components to tephra fall hazards still needs to be assessed. To better understand potential impacts and the costs associated with repairs, further research into the factors influencing impacts and fragility/vulnerability function development for each component would be beneficial.
2. A better understanding in-particular of how susceptible New Zealand buildings are to interior contamination by ash and how easily gutters become blocked/broken by tephra shedding off different roof claddings will provide useful information for assessment of structural and non-structural building damage.

As knowledge of ballistic hazard and risk is relatively immature there are a number of research directions that can be taken to contribute towards overall volcanic disaster risk reduction. Several research directions have been identified:

1. It has been demonstrated that depending on their mass, the majority of ballistic impacts will cause perforation to the building envelope of unreinforced buildings. In light of this, it would be beneficial to develop a second tier of ballistic-building fragility functions which express the conditional probability of the building falling into a specific impact state (e.g. minor repairs required, building partially collapsed) in relation to its perforation density (e.g. number of perforations per unit area).
2. In terms of ballistic hazard modelling, now that ballistic trajectories can be modelled accounting for the collision of one ballistic with another, this capacity

should be extended to model the potential bounce, ricochet or shattering of a ballistic after it collides with the ground or with a building. This additional modelling will give a clearer picture of the area of ballistic hazard on the ground, rather than simply representing the hazard from each ballistic using only its initial impact point.

3. The ballistic impact assessment in this thesis has been carried in only one location using one eruption scenario. Ideally for situations such as Auckland's, where the locations of future eruptions are unknown, a probabilistic risk assessment would be carried out using a range of eruption scenarios producing ballistics in different locations within the AVF to identify areas at greatest risk. In order to repeat this assessment thousands of times as part of probabilistic risk assessment, the process of assigning fragility functions and measuring impacts must first be automated.
4. While the impacts of ballistic blocks to building claddings have been investigated in this thesis, the impact of ballistic bombs remains uncertain, both in terms of a typically slower moving and deformable ballistic's ability to perforate claddings and in terms of the fire risk they present due to their high thermal energies.
5. Testing has been carried out using an air cannon which cannot simulate the speeds of most ballistics from real eruptions and it has only tested sections of wall claddings rather than claddings which are part of a real building. To produce higher quality ballistic-building vulnerability data a larger cannon is being built, capable of launching rocks at over 100 m/s and relationships have been established with a local Christchurch demolition company to procure a residential building for destructive testing with the new cannon.

References

Alatorre-Ibargüengoitia, M. A., & Delgado-Granados, H. (2006). Experimental determination of drag coefficient for volcanic materials: Calibration and application of a model to Popocatépetl volcano (Mexico) ballistic projectiles. *Geophysical Research Letters*, *33*, 1–5. doi:10.1029/2006GL026195

Alatorre-Ibargüengoitia, M. A., Delgado-Granados, H., & Dingwell, D. B. (2012). Hazard map for volcanic ballistic impacts at Popocatépetl volcano (Mexico). *Bulletin of Volcanology*, *74*, 2155–2169. doi:10.1007/s00445-012-0657-2

Alatorre-Ibargüengoitia, M. A., Morales-Iglesias, H., Ramos-Hernández, S. G., Jon-Selvas, J., & Jiménez-Aguilar, J. M. (2016). Hazard zoning for volcanic ballistic impacts at El Chichón Volcano (Mexico). *Natural Hazards*. doi:10.1007/s11069-016-2152-0

Allen, S. R., & Smith, I. (1994). Eruption styles and volcanic hazard in the Auckland Volcanic Field, New Zealand. *Geosc Rep Shizuoka Univ*.

Alphonso, T. C., & Barbato, M. (2014). Experimental fragility curves for aluminum storm panels subject to windborne debris impact. *Journal of Wind Engineering and Industrial Aerodynamics*, *134*, 44–55. doi:10.1016/j.jweia.2014.08.010

Alpsdake. (2014). Mountain huts on Mount Ontake. Retrieved February 21, 2016, from https://commons.wikimedia.org/wiki/Category:Mountain_huts_on_Mount_Ontake#/media/File:Mount_Ontake_top_huts_and_Kengamine_huts_2013-07-09.JPG

Aspinall, W., & Cooke, R. (2013). Quantifying scientific uncertainty from expert judgement elicitation. In J. Rougier, R. S. J. Sparks, & L. Hill (Eds.), *Risk and uncertainty assessment for natural hazards* (p. 588). Cambridge: Cambridge University Press.

Auker, M. R., Sparks, R. S. J., Siebert, L., Crosweller, H. S., & Ewert, J. (2013). A statistical analysis of the global historical volcanic fatalities record. *Journal of Applied Volcanology*, *2*, 2. doi:10.1186/2191-5040-2-2

Baker, J. W. (2014). Efficient analytical fragility function fitting using dynamic structural analysis. *Earthquake Spectra*, (31), 579–599.

Barbato, M., Petrini, F., Unnikrishnan, V. U., & Ciampoli, M. (2013). Performance-Based Hurricane Engineering (PBHE) framework. *Structural Safety*, *45*, 24–35. doi:10.1016/j.strusafe.2013.07.002

Barnard, S. T. (2009). *The Vulnerability of New Zealand Lifelines Infrastructure to Ashfall. Unpublished PhD Thesis*. University of Canterbury, Christchurch, New Zealand.

Baxter, P. J., & Gresham, A. (1997). Deaths and injuries in the eruption of Galeras Volcano, Colombia, 14 January 1993. *Journal of Volcanology and Geothermal Research*, *77*(96), 325–338. doi:10.1016/S0377-0273(96)00103-5

Beppu, M., Miwa, K., Itoh, M., Katayama, M., & Ohno, T. (2008). Damage evaluation

of concrete plates by high-velocity impact. *International Journal of Impact Engineering*, *35*(12), 1419–1426. doi:10.1016/j.ijimpeng.2008.07.021

Biass, S., & Bonadonna, C. (2013). A fast GIS-based risk assessment for tephra fallout: The example of Cotopaxi volcano, Ecuador: Part I: Probabilistic hazard assessment. *Natural Hazards*, *65*, 477–495. doi:10.1007/s11069-012-0378-z

Blake, D. M., Wilson, G., Stewart, C., Craig, H., Hayes, J., Jenkins, S. F., … Cronin, S. (2015). *Impacts of the 2014 eruption of Kelud volcano, Indonesia, on infrastructure, utilities, agriculture and health. GNS Science Report 2015/15* (p. 131).

Blake, S., Wilson, C. J. N., Smith, I. E. M., & Leonard, G. S. (2006). *Lead times and precursors of eruptions in the Auckland Volcanic Field, New Zealand: Indications from historical analogues and theoretical modelling*. *GNS Science Report 2006/34* (p. 22).

Blong, R. (1981). Some effects of tephra falls on buildings. In S. Self & R. S. J. Sparks (Eds.), *Tephra Studies* (pp. 405–420). Reidel, Dordrecht.

Blong, R. (1984). *Volcanic hazards: a sourcebook on the effects of eruptions*. Elsevier (p. 424).

Blong, R. (2000). Volcanic Hazards and Risk Management. In H. Sigurdsson, B. F. Houghton, S. R. McNutt, H. Rymer, & J. Stix (Eds.), *Encylopedia of Volcanoes* (pp. 1215–1227). Elsevier Inc.

Blong, R. (2003). Building damage in Rabaul, Papua New Guinea, 1994. *Bulletin of Volcanology*, *65*, 43–54. doi:10.1007/s00445-002-0238-x

Bonadonna, C., Connor, C. B., Houghton, B. F., Connor, L., Byrne, M., Laing, a., & Hincks, T. K. (2005). Probabilistic modeling of tephra dispersal: Hazard assessment of a multiphase rhyolitic eruption at Tarawera, New Zealand. *Journal of Geophysical Research B: Solid Earth*, *110*(3), 1–21. doi:10.1029/2003JB002896

Bonadonna, C., & Houghton, B. F. (2005). Total grain-size distribution and volume of tephra-fall deposits. *Bulletin of Volcanology*, *67*(June 1996), 441–456. doi:10.1007/s00445-004-0386-2

Booth, B. (1979). Assessing volcanic risk. *Journal of the Geological Society*, *136*, 331–340. doi:10.1144/gsjgs.136.3.0331

Børvik, T., Forrestal, M. J., Hopperstad, O. S., Warren, T. L., & Langseth, M. (2004). Perforation of AA5083-H116 aluminium plates with conical-nose steel projectiles - Calculations. *International Journal of Impact Engineering*, *36*(3), 426–437. doi:10.1016/j.ijimpeng.2008.02.004

Breard, E. C. P., Lube, G., Cronin, S. J., Fitzgerald, R. H., Kennedy, B., Scheu, B., … Moebis, A. (2014). Using the spatial distribution and lithology of ballistic blocks to interpret eruption sequence and dynamics: August 6 2012 Upper Te Maari eruption, New Zealand. *Journal of Volcanology and Geothermal Research*. doi:10.1016/j.jvolgeores.2014.03.006

Bruce, E. P. (1962). Review and analysis of high velocity impact data. In *5th*

Symposium on Hyper Velocity (p. 439).

Bryan, G. M. (1962). Oblique impact of high velocity steel pellets on lead targets. In *5th Symposium on Hyper Velocity* (p. 511).

Capaccioni, B., & Cuccoli, F. (2005). Spatter and welded air fall deposits generated by fire-fountaining eruptions: Cooling of pyroclasts during transport and deposition. *Journal of Volcanology and Geothermal Research*, *145*(263), 263–280. Retrieved from http://ac.els-cdn.com.ezproxy.canterbury.ac.nz/S0377027305000600/1-s2.0-S0377027305000600-main.pdf?_tid=5114264e-c13d-11e4-9a5a-00000aacb35d&acdnat=1425343162_5b73d5d14fd74058a73f06a6640ad2ab

Carey, S., & Bursik, M. (2000). Volcanic plumes. In H. Sigurdsson, B. F. Houghton, S. R. McNutt, H. Rymer, & J. Stix (Eds.), *Encyclopedia of Volcanoes* (p. 1417). San Diego: Elsevier Inc.

Carey, S., & Sparks, R. S. J. (1986). Quantitative models of the fallout and dispersal of tephra from volcanic eruption columns. *Bulletin of Volcanology*, *48*(2-3), 109–125. doi:10.1007/BF01046546

Cas, R., & Wright, J. V. (2012). *Volcanic successions modern and ancient: A geological approach to processes, products and successions*. Springer Science (p. 528).

Cashman, K. V., Sturtevant, B., Papale, P., & Navon, O. (2000). Magmatic fragmentation. In H. Sigurdsson, B. F. Houghton, S. R. McNutt, H. Rymer, & J. Stix (Eds.), *Encyclopedia of Volcanoes* (p. 1417). San Diego: Elsevier Inc.

Chen, W., & Hao, H. (2015). Performance of structural insulated panels with rigid skins subjected to windborne debris impacts – Experimental investigations. *Construction and Building Materials*, *77*, 241–252. doi:10.1016/j.conbuildmat.2014.12.112

Chen, X. W., Fan, S. C., & Li, Q. M. (2004). Oblique and normal perforation of concrete targets by rigid projectiles.pdf. *International Journal of Impact Engineering*, *30*, 617–637. doi:10.1016/j.ijimpeng.2003.08.003

Chen, X. W., Li, Q., & Fan, S. (2006). Oblique perforation of thick metallic plates by rigid projectiles. *Acta Mechanica Sinica/Lixue Xuebao*, *22*(4), 367–376. doi:10.1007/s10409-006-0015-8

Cook, S. (2015). *A 2015 Engineering Geology Model of the Crater Lake Outlet, Mt Ruapehu, New Zealand. Unpublished Engineering Geology Dissertation*. University of Canterbury, Christchurch, New Zealand.

Crozier, M., & Glade, T. (2006). Landslide Hazard and Risk: Issues, Concepts and Approaches. In T. Glade, M. G. Anderson, & M. J. Crozier (Eds.), *Landslide Hazard and Risk* (pp. 1–41). Chichester, England: Wiley.

De'Michieli Vitturi, M., Neri, a., Esposti Ongaro, T., Lo Savio, S., & Boschi, E. (2010). Lagrangian modeling of large volcanic particles: Application to Vulcanian explosions. *Journal of Geophysical Research: Solid Earth*, *115*(8), 1–18. doi:10.1029/2009JB007111

Deguchi, K. (1990). Development of a ventilation system against volcanic ash fall in

Kagoshima. *Energy and Buildings*, *15-16*, 663–671.

Department of Building and Housing. (2010). *Simple House, Acceptable Solution: Compliance document for New Zealand Building Code*. Wellington: The Department of Building and Housing. Retrieved from http://www.dbh.govt.nz/userFiles/file/publications/building/compliance-documents/simple-house-acceptable-solution.pdf

Department of Building and Housing. (2011). *E2 External Moisture: Compliance document for New Zealand Building Code*. Wellington: The Department of Building and Housing. Retrieved from http://www.building.govt.nz/userfiles/file/publications/building/compliance-documents/e2-external-moisture-effective-24-december-2011.pdf

Dillman, J., & Roberts, M. (1982). The impact of the May 18 Mount St. Helens ashfall: Eastern Washington residents report on housing-related damage and cleanup. In S. A. C. Keller (Ed.), *Mount St . Helens: One year later* (pp. 191–198). Cheney: Eastern Washington University Press.

Doherty, E. (2011). Economic effects of the Canterbury earthquakes. Retrieved March 14, 2015, from http://www.parliament.nz/en-nz/parl-support/research-papers/00PlibCIP051/economic-effects-of-the-canterbury-earthquakes

Donovan, A., Oppenheimer, C., & Bravo, M. (2012). Science at the policy interface : volcano-monitoring technologies and volcanic hazard management, 1005–1022. doi:10.1007/s00445-012-0581-5

Douglas, J. (2007). Physical vulnerability modelling in natural hazard risk assessment. *Natural Hazards and Earth System Sciences*, *7*(2), 283–288. doi:10.5194/nhess-7-283-2007

Elkink, A. (2011). BRANZ Renovate 1970s (p. 122). Porirua: BRANZ.

ESCAP. (1999). Geology-related hazards, resources and management for disaster reduction in Asia. Proceedings of the IDNDR-ESCAP Regional meeting for Asia: risk reduction & society in the 21st century, Bangkok, Thailand.

Fagents, S. a, & Wilson, L. (1993). Explosive volcanic eruptions- VII. The ranges of pyroclasts ejected in transient volcanic explosions. *Geophysical Journal International*, *113*, 359–370.

Fagents, S. A., Gregg, T. K. P., Lopes, R. M. C., & Clarke, A. B. (2013). Chapter 7 Unsteady explosive activity : vulcanian eruptions. In S. A. Fagents, T. K. P. Gregg, & R. M. C. Lopes (Eds.), *Modeling Volcanic Processes: The Physics and Mathematics of Volcanism* (pp. 129–152). Cambridge University Press. doi:http://dx.doi.org.ezproxy.canterbury.ac.nz/10.1017/CBO9781139021562

Federal Emergency Management Agency (FEMA). (2003). *HAZUS-MH MR4 Technical Manual*. *National Institute of Building Sciences and Federal Emergency Management Agency (NIBS and FEMA)* (p. 712).

Fernandez, G., Masters, F. J., & Gurley, K. R. (2010). Performance of hurricane shutters under impact by roof tiles. *Engineering Structures*, *32*(10), 3384–3393. doi:10.1016/j.engstruct.2010.07.012

Fisher, R. ., & Schmincke, H.-U. (1984). *Pyroclastic Rocks*. Berlin: Springer Verlag (p. 472).

Fitzgerald, R. H., Kennedy, B. M., Leonard, G. S., Wilson, T. M., & Williams, G. T. (in prep.). *Post-eruption ballistic impact assessments for the 2014 eruption of Mount Ontake and the 2000 eruption of Mount Usu, Japan - EQC report*.

Fitzgerald, R. H., Tsunematsu, K., Kennedy, B. M., Breard, E. C. P., Lube, G., Wilson, T. M., … Cronin, S. J. (2014). The application of a calibrated 3D ballistic trajectory model to ballistic hazard assessments at Upper Te Maari, Tongariro. *Journal of Volcanology and Geothermal Research*, *286*, 248–262. doi:10.1016/j.jvolgeores.2014.04.006

Fowler, W. B., & Lopushinsky, W. (1986). Wind-blown volcanic ash in forest and agricultural locations as related to meteorological conditions. *Atmospheric Environment (1967)*, *20*(3), 421–425. doi:10.1016/0004-6981(86)90081-8

Gaudin, D., Taddeuci, J., Scarlato, P., Moroni, M., Freda, C., Gaeta, M., & Paladino, D. M. (2014). Pyroclast Tracking Velocimetry illuminates bombejection and explosion dynamics at Stromboli(Italy) and Yasur (Vanuatu) volcanoes. *Journal of Geophysical Research : Solid Earth*, *119*(7), 5384–5397. doi:10.1002/2015JB012061.

Green, B. D., & Rose, W. I. (2005). Volcanic Risk Map for Santa Mara, Guatemala: What can Risk Maps Contribute to Volcanic Hazard Communications? Retrieved February 12, 2016, from http://www.geo.mtu.edu/volcanoes/

Green, R. M., Bebbington, M. S., Cronin, S. J., & Jones, G. (2014). Automated statistical matching of multiple tephra records exemplified using five long maar sequences younger than 75ka, Auckland, New Zealand. *Quaternary Research (United States)*, *82*(2), 405–419. doi:10.1016/j.yqres.2014.06.004

Gurioli, L., Harris, a. J. L., Colò, L., Bernard, J., Favalli, M., Ripepe, M., & Andronico, D. (2013). Classification, landing distribution, and associated flight parameters for a bomb field emplaced during a single major explosion at Stromboli, Italy. *Geology*, *41*(March), 559–562. doi:10.1130/G33967.1

Haldar, A., & Miller, F. J. (1982). Penetration Depth in Concrete for Nondeformable Missiles. *Nuclear Engineering and Design*, *71*, 79–88.

Hampton, S. J., Cole, J. W., Wilson, G., Wilson, T. M., & Broom, S. (2015). Volcanic ashfall accumulation and loading on gutters and pitched roofs from laboratory empirical experiments: Implications for risk assessment. *Journal of Volcanology and Geothermal Research*, *304*, 237–252. doi:10.1016/j.jvolgeores.2015.08.012

Haneberg, W. C. (2000). Deterministic and probabilistic approaches to geologic hazard assessment. *Environmental and Engineering Geoscience*, *6*(3), 209–226. Retrieved from http://www.scopus.com/inward/record.url?eid=2-s2.0-0034431887&partnerID=tZOtx3y1

Harris, A. J. L., Ripepe, M., & Hughes, E. a. (2012). Detailed analysis of particle launch velocities, size distributions and gas densities during normal explosions at Stromboli. *Journal of Volcanology and Geothermal Research*, *231-232*, 109–131. doi:10.1016/j.jvolgeores.2012.02.012

Hayes, J. (2014). *Tephra clean-up in Auckland City, New Zealand : quantitative impact assessment and response planning, Unpublished MSc thesis.* University of Canterbury, Christchurch, New Zealand (p. 106).

Herbin, A. H., & Barbato, M. (2012). Fragility curves for building envelope components subject to windborne debris impact. *Journal of Wind Engineering and Industrial Aerodynamics*, *107-108*, 285–298. doi:10.1016/j.jweia.2012.05.005

Horspool, N. a., Savage, M. K., & Bannister, S. (2006). Implications for intraplate volcanism and back-arc deformation in northwestern New Zealand, from joint inversion of receiver functions and surface waves. *Geophysical Journal International*, *166*(3), 1466–1483. doi:10.1111/j.1365-246X.2006.03016.x

Houghton, B. F., Bonadonna, C., Gregg, C. E., Johnston, D. M., Cousins, W. J., Cole, J. W., & Del Carlo, P. (2006). Proximal tephra hazards: Recent eruption studies applied to volcanic risk in the Auckland volcanic field, New Zealand. *Journal of Volcanology and Geothermal Research*, *155*, 138–149. doi:10.1016/j.jvolgeores.2006.02.006

Houghton, B. F., Wilson, C. J. N., Rosenberg, M. R., Smith, I. E. M., & Parker, R. J. (1996). Mixed deposits of complex magmatic and phreatomagmatic volcanism: an example from Crater Hill, Auckland, New Zealand. *Bulletin of Volcanology*, *58*, 59–66. doi:10.1007/s004450050126

Houghton, B. F., Wilson, C. J. N., & Smith, I. E. M. (1999). Shallow-seated controls on styles of explosive basaltic volcanism: A case study from New Zealand. *Journal of Volcanology and Geothermal Research*, *91*, 97–120. doi:10.1016/S0377-0273(99)00058-X

Hurst, T., & Smith, W. (2010). Volcanic ashfall in New Zealand – probabilistic hazard modelling for multiple sources. *New Zealand Journal of Geology and Geophysics*, *53*(1), 1–14. doi:10.1080/00288301003631129

Imran Latif, Q. B. A., Rahman, I. A., Ahmad Zaidi, A. M., & Latif, K. (2015). Critical impact energy for spalling, tunnelling and penetration of concrete slab impacted with hard projectile. *KSCE Journal of Civil Engineering*, *19*(1), 265–273. doi:10.1007/s12205-012-0489-9

Jenkins, S. F., Spence, R. J. S., Fonseca, J. F. B. D., Solidum, R. U., & Wilson, T. M. (2014). Volcanic risk assessment: Quantifying physical vulnerability in the built environment. *Journal of Volcanology and Geothermal Research*, *276*, 105–120. doi:10.1016/j.jvolgeores.2014.03.002

Jenkins, S., & Spence, R. (2009). Vulnerability curves for buildings and agriculture. *A Report for MIA-VITA*, 61.

Johnson, W., Sengupta, A. K., & Ghosh, S. K. (1982). High velocity oblique impact and ricochet mainly of long rod projectiles: An overview. *International Journal of Mechanical Sciences*, *24*(7), 425–436. doi:10.1016/0020-7403(82)90052-2

Johnston, D. M. (1997). *Physical and Social Impacts of Past and Future Volcanic Eruptions in New Zealand, Unpublished PhD thesis*. Massey University, Palmerston North, New Zealand (p. 288).

Kar, A. (1979). Residual velocity for projectiles. *Nuclear Engineering and Design*, *53*,

87–95. doi:10.1016/0029-5493(79)90042-6

Kaye, G. (2008). Volcanic hazard risk assessment for the riskscape program, with test application in Rotorua, New Zealand, and Mammoth Lakes, USA. *Unpublished PhD Thesis, University of Canterbury, Christchurch, New Zealand.*

Kereszturi, G., Németh, K., Cronin, S. J., Agustín-Flores, J., Smith, I. E. M., & Lindsay, J. M. (2013). A model for calculating eruptive volumes for monogenetic volcanoes - Implication for the Quaternary Auckland Volcanic Field, New Zealand. *Journal of Volcanology and Geothermal Research*, *266*, 16–33. doi:10.1016/j.jvolgeores.2013.09.003

King, A., & Bell, R. (2009). *RiskScape Project: 2004 - 2008. GNS Science Consultancy Report 2009/247*.

Le Maitre, R. W. (2002). *Igneous rocks: A classification and glossary of terms - Recomendations of the Union International of Geological Sciences Subcommision on the Systematics of Igneous Rocks*. Cambridge: Cambridge University Press.

Li, J., & Hao, H. (2014). Numerical study of concrete spall damage to blast loads. *International Journal of Impact Engineering*, *68*, 41–55. doi:10.1016/j.ijimpeng.2014.02.001

Li, Q. M., Reid, S. R., Wen, H. M., & Telford, a. R. (2006). Local impact effects of hard missiles on concrete targets. *International Journal of Impact Engineering*, *32*(1-4), 224–284. doi:10.1016/j.ijimpeng.2005.04.005

Lindsay, J., Marzocchi, W., Jolly, G., Constantinescu, R., Selva, J., & Sandri, L. (2010). Towards real-time eruption forecasting in the Auckland Volcanic Field: Application of BET_EF during the New Zealand National Disaster Exercise “Ruaumoko.” *Bulletin of Volcanology*, *72*, 185–204. doi:10.1007/s00445-009-0311-9

Macedonio, G., & Costa, a. (2012). Brief communication: Rain effect on the load of tephra deposits. *Natural Hazards and Earth System Science*, *12*(4), 1229–1233. doi:10.5194/nhess-12-1229-2012

Maeda, Y., Kato, A., Terakawa, T., Yamanaka, Y., Horikawa, S., Matsuhiro, K., & Okuda, T. (2015). Source mechanism of a VLP event immediately before the 2014 eruption of Mt. Ontake, Japan. *Earth, Planets and Space*, *67*(1), 187. doi:10.1186/s40623-015-0358-0

Magill, C., & Blong, R. (2005). Volcanic risk ranking for Auckland, New Zealand. I: Methodology and hazard investigation. *Bulletin of Volcanology*, *67*, 331–339. doi:10.1007/s00445-004-0374-6

Magill, C., Blong, R., & McAneney, J. (2006). VolcaNZ: A volcanic loss model for Auckland, New Zealand. *Journal of Volcanology and Geothermal Research*, *149*(3-4), 329–345. doi:10.1016/j.jvolgeores.2005.09.004

Magill, C. R., Hurst, T., Hunter, L. J., & Blong, R. J. (2006). Probabilistic tephra fall simulation for the Auckland Region, New Zealand. *Journal of Volcanology and Geothermal Research*, *153*(3-4), 370–386. doi:10.1016/j.jvolgeores.2005.12.002

Maqsood, T., Wehner, M., Ryu, H., Edwards, M., Dale, K., & Miller, V. (2015). *GAR15*

Vulnerability Functions: Reporting on the UNISDR/GA SE Asian Regional Workshop on Structural Vulnerbility Models for the GAR Global Risk Assessment, 11-14 November, 2013. Canberra: Geoscience Australia. Retrieved from http://www.preventionweb.net/english/hyogo/gar/2015/en/bgdocs/risk-section/Geoscience Australia (GA), GAR15 Regional Vulnerability Functions Reporting on the Asian Regional Workshop.pdf

Marti, J., Spence, R., Calogero, E., Ordoñez, A., Felpeto, A., & Baxter, P. (2008). Estimating building exposure and impact to volcanic hazards in Icod de los Vinos, Tenerife (Canary Islands). *Journal of Volcanology and Geothermal Research*, *178*(3), 553–561. doi:10.1016/j.jvolgeores.2008.07.010

Masters, F. J., Gurley, K. R., Shah, N., & Fernandez, G. (2010). The vulnerability of residential window glass to lightweight windborne debris. *Engineering Structures*, *32*(4), 911–921. doi:10.1016/j.engstruct.2009.12.016

Mastin, L. G. (2001). *A Simple Calculator of Ballistic Trajectories for Blocks Ejected During Volcanic Eruptions, U.S. GEOLOGICAL SURVEY Open-File Report 01-45, Version 1.2*. Retrieved from http://vulcan.wr.usgs.gov/Projects/Mastin

McDonald, J. R. (1990). Impact Resistance of Common Building Materials to Tornado Missiles. *Journal of Wind Engineering and Industrial Aerodynamics*, *36*, 717–724.

Minakami, T. (1942). On the distribution of volcanic ejecta (Part I.): The distributions of volcanic bombs ejected by the recent explosions of Asama. *Bulletin of Earthquake Research Institute*, *20*, 65 – 92.

Murase, M., Kimata, F., Yamanaka, Y., Horikawa, S., Matsuhiro, K., Matsushima, T., … Nakamichi, H. (2016). Preparatory process preceding the 2014 eruption of Mount Ontake volcano, Japan: insights from precise leveling measurements. *Earth, Planets and Space*, *68*(1), 9. doi:10.1186/s40623-016-0386-4

Nairn, I. A. (1975). *Immediate report, field investigations of 1975 April 24 and 27 Ruapehu eruptions. New Zealand Geological Survey Preliminary Report*.

Nairn, I. a., & Self, S. (1978). Explosive eruptions and pyroclastic avalanches from Ngauruhoe in February 1975. *Journal of Volcanology and Geothermal Research*, *3*(1-2), 39–60. doi:10.1016/0377-0273(78)90003-3

Newhall, C., Aramaki, S., Barberi, F., Blong, R., Calvache, M., Cheminee, J. L., … Tjetjep, W. (1999). Professional conduct of scientists during volcanic crises. *Bulletin of Volcanology*, *60*(5), 323–334. doi:10.1007/s004450050236

Newhall, C., & Hoblitt, R. (2002). Constructing event trees for volcanic crises. *Bulletin of Volcanology*, *64*(1), 3–20. doi:10.1007/s004450100173

NipponNewsNet. (2014). 御嶽山噴火 - Mount Ontake erupts. Retrieved February 22, 2016, from https://www.youtube.com/watch?v=ODiqlpUwcVM

New Zealand Standards. (2006). *NZS:3101 Concrete structures standard - Part 1: The Design of Concrete Structures* (p. 309).

Oze, C., Cole, J., Scott, A., Wilson, T., Wilson, G., Gaw, S., … Li, Z. (2014). Corrosion of metal roof materials related to volcanic ash interactions. *Natural Hazards*, *71*(1), 785–802. doi:10.1007/s11069-013-0943-0

Paton, D., Smith, L., Daly, M., & Johnston, D. (2008). Risk perception and volcanic hazard mitigation: Individual and social perspectives. *Journal of Volcanology and Geothermal Research*, *172*(3-4), 179–188. doi:10.1016/j.jvolgeores.2007.12.026

Paulik, R. (2015). New Zealand Building Inventory - RiskScape Wiki. Retrieved February 22, 2016, from https://wiki-riskscape.niwa.co.nz/index.php/File:New_Zealand_Building_Inventory.pdf

Peng, Y., Wu, H., Fang, Q., Gong, Z. M., & Kong, X. Z. (2015). A note on the deep penetration and perforation of hard projectiles into thick targets. *International Journal of Impact Engineering*, *85*, 37–44. doi:10.1016/j.ijimpeng.2015.06.013

Pioli, L., Erlund, E., Johnson, E., Cashman, K., Wallace, P., Rosi, M., & Delgado Granados, H. (2008). Explosive dynamics of violent Strombolian eruptions: The eruption of Paricutin Volcano 1943-1952 (Mexico). *Earth and Planetary Science Letters*, *271*, 359–368. doi:10.1016/j.epsl.2008.04.026

Pomonis, A., Spence, R., & Baxter, P. (1999). Risk assessment of residential buildings for an eruption of Furnas Volcano, Sao Miguel, the Azores. *Journal of Volcanology and Geothermal Research*, *92*, 107–131. doi:10.1016/S0377-0273(99)00071-2

Porter, K., Kennedy, R., & Bachman, R. (2007). Creating fragility functions for performance-based earthquake engineering. *Earthquake Spectra*, *23*(2), 471–489. doi:10.1193/1.2720892

Pyle, D. (1989). The thickness, volume and grain size of tephra fall deposits. *Bulletin of Volcanology*, *51*, 1–15.

Raymond, D., Van Ee, C., Crawford, G., & Bir, C. (2009). Tolerance of the skull to blunt ballistic temporo-parietal impact. *Journal of Biomechanics*, *42*(15), 2479–2485. doi:10.1016/j.jbiomech.2009.07.018

Rose, W., Bluth, G., Schneider, D., Ernst, G., Riley, C., Henderson, L., & McGimsey, R. (2001). Observations of Volcanic Clouds in Their First Few Days of Atmospheric Residence: The 1992 Eruptions of Crater Peak, Mount Spurr Volcano, Alaska. *The Journal of Geology*, *109*(4), 677–694.

Rossetto, T., & Elnashai, A. (2003). Derivation of vulnerability functions for European-type RC structures based on observational data. *Engineering Structures*, *25*(10), 1241–1263. doi:10.1016/S0141-0296(03)00060-9

Rossetto, T., Ioannou, I., Grant, D. N., & Maqsood, T. (2014). Guidelines for Empirical Vulnerability Assessment Report produced in the context of the Vulnerability Global Component project.

Sandri, L., Jolly, G., Lindsay, J., Howe, T., & Marzocchi, W. (2012). Combining long- and short-term probabilistic volcanic hazard assessment with cost-benefit analysis to support decision making in a volcanic crisis from the Auckland Volcanic Field, New Zealand. *Bulletin of Volcanology*, *74*(3), 705–723. doi:10.1007/s00445-011-0556-y

Schultz, M. T., Gouldby, B. P., Simm, J. D., & Wibowo, J. L. (2010). Beyond the Factor of Safety : Developing Fragility Curves to Characterize System Reliability-US Army Corps of Engineers, (July), 51.

Self, S., Kienle, J., & Huot, J.-P. (1980). Ukinrek Maars, Alaska, II. Deposits and formation of the 1977 craters. *Journal of Volcanology and Geothermal Research*, *7*(1-2), 39–65. doi:10.1016/0377-0273(80)90019-0

Simkin, T., Siebert, L., & Blong, R. (2001). Volcano Fatalities: Lessons from the Historical Record. *Science*, *291*(255), 21–22.

Spence, R. J. S., Kelman, I., Baxter, P. J., Zuccaro, G., & Petrazzuoli, S. (2005). Residential building and occupant vulnerability to tephra fall. *Natural Hazards and Earth System Science*, *5*, 477–494. doi:10.5194/nhess-5-477-2005

Spence, R. J. S., Kelman, I., Calogero, E., Toyos, G., Baxter, P. J., & Komorowski, J.-C. (2005). Modelling expected physical impacts and human casualties from explosive volcanic eruptions. *Natural Hazards and Earth System Science*, *5*, 1003–1015. doi:10.5194/nhess-5-1003-2005

Spence, R. J. S., Pomonis, A., Baxter, P. J., Coburn, A. W., White, M., & Dayrit, M. (1996). Building damage caused by the Mt. Pinatubo eruption of June 14–15, 1991. In C. G. Newhall & R. Punongbayan (Eds.), *Fire and Mud: Eruptions and Lahars of Mount Pinatubo, Phillipines*. University of Washington Press.

Steinberg, G. S., & Babenko, J. I. (1978). Experimental velocity and density determination of volcanic gases during eruption. *J. Volcanol. Geoth. Res.*, *3*(1-2), 89–98. doi:10.1016/0377-0273(78)90005-7

Stephenson, A. E., Sliter, G. E., & Burdette, E. G. (1978). Full-scale tornado-missile impact tests. *Nuclear Engineering and Design*, *46*(1), 123–143. doi:10.1016/0029-5493(78)90178-4

Stewart, C., Johnston, D. M., Leonard, G. S., Horwell, C. J., Thordarson, T., & Cronin, S. J. (2006). Contamination of water supplies by volcanic ashfall: A literature review and simple impact modelling. *Journal of Volcanology and Geothermal Research*, *158*(3-4), 296–306. doi:10.1016/j.jvolgeores.2006.07.002

Taddeucci, J., Scarlato, P., Capponi, a., Del Bello, E., Cimarelli, C., Palladino, D. M., & Kueppers, U. (2012). High-speed imaging of Strombolian explosions: The ejection velocity of pyroclasts. *Geophysical Research Letters*, *39*, 1–6. doi:10.1029/2011GL050404

Takarada, S. (2003). Field Trip Guidebook B1: The Usu 2000 Eruption. In *XXII General Assembly of the International Union of Geodesy and Geophysics* (pp. 226–241). Sapporo, Japan.

Takarada, S., & Hasaka, T. (2000). *Preliminary report of the Mt Usu 2000 eruption contributed by Hokkaido Branch*.

Takarada, S., Hoshizumi, H., Miyagi, I., Nishimura, Y., Miura, D., & Kawanabe, Y. (2002). Proxmial deposits of the Usu 2000 eruption. *Bulletin of Volcanological Society Japan*, *47*, 645–661.

Tarbotton, C., Dall'Osso, F., Dominey-Howes, D., & Goff, J. (2015). The use of empirical vulnerability functions to assess the response of buildings to tsunami impact: Comparative review and summary of best practice. *Earth-Science Reviews*, *142*, 120–134. doi:10.1016/j.earscirev.2015.01.002

Trebilco, N. L. (1997). *Ruapehu Ash and Residential Buildings. BRANZ Report DC003*.

Tsunematsu, K., Chopard, B., Falcone, J. L., & Bonadonna, C. (2014). A numerical model of ballistic transport with collisions in a volcanic setting. *Computers and Geosciences*, *63*, 62–69. doi:10.1016/j.cageo.2013.10.016

Ulusay, R., & Hudson, J. A. (2007). *The complete ISRM suggested methods for rock characterization, testing and monitoring: 1974-2006*.

Vanderkluysen, L., Harris, A. J. L., Kelfoun, K., Bonadonna, C., & Ripepe, M. (2012). Bombs behaving badly: Unexpected trajectories and cooling of volcanic projectiles. *Bulletin of Volcanology*, *74*, 1849–1858. doi:10.1007/s00445-012-0635-8

Wang, E. (2014). Japan volcano death toll hits 36. Retrieved February 21, 2016, from http://www.wvgazettemail.com/article/20140929/ARTICLE/140929196

Wardman, J., Sword-Daniels, V., Stewart, C., & Wilson, T. M. (2012). *Impact assessment of the May 2010 eruption of Pacaya volcano, Guatemala, GNS Science Report 2012/09*. (p. 90).

Warren, T. L., Fossum, A. F., & Frew, D. J. (2004). Penetration into low_strength 23 MPa concrete_ target characterization and simulations.pdf. *International Journal of Impact Engineering*, *30*, 477–503. doi:10.1016/S0734-743X(03)00092-7

Wilson, G. (2011). *Ash , Gas and Computers : the vulnerability of laptop computers to volcanic hazards, Unpublished MSc thesis*. University of Canterbury, Christchurch, New Zealand.

Wilson, G. (2015). *Vulnerability of critical infrastructure to volcanic hazards, Unpublished PhD thesis*. University of Canterbury, Christchurch , New Zealand (p. 317).

Wilson, G., Wilson, T. M., Deligne, N. I., Blake, D. M., & Cole, J. W. (in review). Framework for developing volcanic fragility and vulnerability functions for critical infrastructure. *Journal of Applied Volcanology*.

Wilson, G., Wilson, T. M., Deligne, N. I., & Cole, J. W. (2014). Volcanic hazard impacts to critical infrastructure : A review. *Journal of Volcanology and Geothermal Research*, *286*, 148–182. doi:10.1016/j.jvolgeores.2014.08.030

Wilson, T. M., Cole, J. W., Stewart, C., Cronin, S. J., & Johnston, D. M. (2011). Ash storms: Impacts of wind-remobilised volcanic ash on rural communities and agriculture following the 1991 Hudson eruption, southern Patagonia, Chile. *Bulletin of Volcanology*, *73*(3), 223–239. doi:10.1007/s00445-010-0396-1

Wilson, T. M., Jenkins, S., & Stewart, C. (2015). Impacts from Volcanic Ash Fall. In P. Papale & J. F. Shroder (Eds.), *Volcanic Hazards, Risks and Disasters* (pp. 47–86). Elsevier. doi:10.1016/B978-0-12-396453-3.00003-4

Wilson, T. M., Stewart, C., Bickerton, H., Baxter, P., Outes, V., Villarosa, G., & E, R. (2013). *Impacts of the June 2011 Puyehue-Cordón Caulle volcanic complex eruption on urban infrastructure, agriculture and public health*. *GNS Science Report 2012/20*.

Wilson, T. M., Stewart, C., Sword-Daniels, V., Leonard, G. S., Johnston, D. M., Cole, J. W., … Barnard, S. T. (2012). Volcanic ash impacts on critical infrastructure. *Physics and Chemistry of the Earth*, *45-46*, 5–23. doi:10.1016/j.pce.2011.06.006

Yankelevsky, D. Z. (1997). Local response of concrete slabs to low velocity missile impact. *International Journal of Impact Engineering*, *19*(4), 331–343. doi:10.1016/S0734-743X(96)00041-3

Standards New Zealand (2009). *Risk Management: principles and guidelines (AS/NZS ISO 31000:2009)*.

Zobin, V. M., Luhr, J. F., Taran, Y. a., Bretón, M., Cortés, a., De La Cruz-Reyna, S., … Santiago, H. (2002). Overview of the 1997-2000 activity of Volcán de Colima, México. *Journal of Volcanology and Geothermal Research*, *117*(1-2), 1–19. doi:10.1016/S0377-0273(02)00232-9

Zuccaro, G., Cacace, F., Spence, R. J. S., & Baxter, P. J. (2008). Impact of explosive eruption scenarios at Vesuvius. *Journal of Volcanology and Geothermal Research*, *178*(3), 416–453. doi:10.1016/j.jvolgeores.2008.01.005

Appendix A – Formation and Dispersal of Tephra

Tephra is the collective term used to describe all lava and rock fragments ejected by explosive volcanic eruptions (Le Maitre, 2002). Explosions are driven by the expansion of exsolved magmatic gasses as they rise to the surface (Cashman et al., 2000). The explosions produce fragments of lava and lithics which can be categorised into three tephra size ranges; ash (<2 mm), lapilli (2-64 mm) and bomb/blocks (>64 mm). Due to their different sizes and bulk densities, tephra fall and ballistics are dispersed and deposited through vastly different physical processes. Their dispersion patterns strongly control their impacts on society (Wilson et al., 2015).

Dispersal of tephra fall

Tephra fall is the most frequently occurring volcanic hazard, with tephra fall produced in 90% of all eruptions (Newhall and Hoblitt, 2002). Tephra fall is a geographically widespread hazard with the potential to affect communities over hundreds of square kilometres depending on eruption magnitude, wind conditions, tephra density and grain size (Wilson et al., 2015). Volcanic tephra fall can be initially transported away from the volcano via two different transport processes. Tephra can travel in co-ignimbrite plumes formed by pyroclastic density currents, or larger volumes can be transported over more widespread areas in convective eruption plumes (Carey and Bursik, 2000).

The base of a convective eruption plume is called the jet thrust zone (Figure 62). Here tephra and gas are ejected into the atmosphere at high velocity by explosions. The jet thrust zone has a bulk density higher than that of the surrounding atmosphere but tephra continues to rise due its momentum from the explosion. As the plume rises it entrains air, leading to an increase in plume size but decrease in velocity and bulk density. The entrained air becomes heated, making the plume less dense than the surrounding atmosphere and allowing it to rise by convection in the aptly named, convection zone. The plume will continue to convect upwards until its density becomes equal to that of the surrounding atmosphere through continual entrainment and cooling. This area of the plume is called the umbrella zone and from here tephra can move laterally, sometimes up to thousands of kilometres (Carey and Sparks, 1986; Wilson et al., 2012).

After tephra reaches the umbrella zone, tephra fallout occurs in three stages (Rose et al., 2001). Coarse tephra fall closest to the source during the first stage which can last 1-2 hours. During the second phase, the fallout of aggregated tephra particles occurs, rapidly reducing the concentration of fine and very fine of grained ash particles over a period of up to 24 hours. In the third stage, the concentration of tephra in the umbrella zone has been depleted but the remainder of the plume can travel downwind of the source for thousands of kilometres. This pattern of fallout typically produces tephra fall deposits with thicknesses and grain sizes which decrease, either exponentially (Pyle, 1989), or according to a power-law trend (Bonadonna and Houghton, 2005).

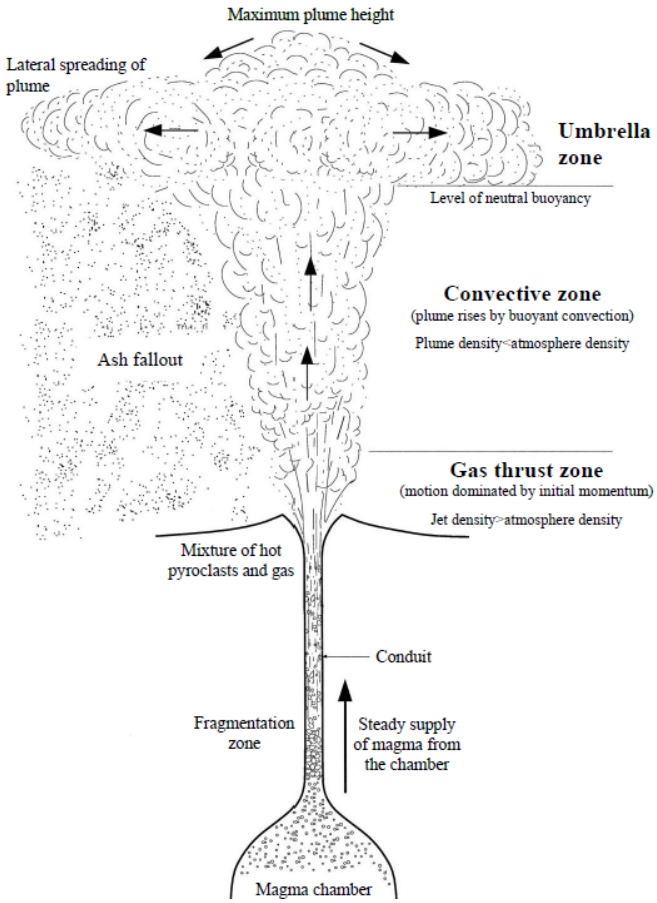

Figure 62: The typical structure of an eruption plume formed by fragmentation of silicic magma. After pyroclasts are ejected from the vent a plume develops with three distinct zones: the gas thrust zone; the convective zone; and the umbrella zone. Figure from Wilson(Wilson, 2011), originally modified from Carey and Bursik (2000).

Dispersal of ballistics

Compared to tephra fall, ballistics are a proximal hazard, typically landing within a 5-km radius of the vent and rarely landing >10 km (Blong, 1984). Unlike tephra fall,

ballistics do not remain suspended in an eruption plume after they are erupted. Following explosions, gas and fine ash in the jet phase of the plume quickly lose their initial momentum. Larger particles on the other hand have higher inertia, allowing them to maintain their momentum and become decoupled from the plume to be ejected with near parabolic, ballistic trajectories (Fagents and Wilson, 1993; Mastin, 2001; Harris et al., 2012). Ballistic size is typically measured by the clast's diameter and values can vary from a few centimetres to >10 metres in size (Figure 63). Ballistic clasts of different sizes will typically be normally laterally graded (i.e. average ballistic diameter will decrease with distance from the vent) (Fagents et al., 2013). However, in some eruptions the opposite has occurred (e.g. Asama Volcano, 1938 (Minakami, 1942); Ukinrek Maar, 1977 (Self et al., 1980) and Upper Te Maari, 2012 (Breard et al., 2014). Reverse lateral size grading is thought to occur due to the complex drag interactions between ballistics and the expanding pyroclastic mixture that surrounds them near the vent (Self et al., 1980; Capaccioni and Cuccoli, 2005; De'Michieli Vitturi et al., 2010).

Figure 63: Ballistics of various sizes distributed across the Abuta-Gunn highway after the 2000 eruption of Mount Usu. Scale stick in 25 cm increments. Photo credit Prof. H. Okada.

Another factor influencing the size distribution of ballistic particles is particle collision (Tsunematsu et al., 2014). The Tsunematsu study found that a ballistic's maximum range could be increased by a factor of two to six due to the energy transfer that occurs when a relatively small particle is struck by a larger particle, under the right conditions (Figure 64).

The style and magnitude of eruption also have a strong influence on ballistic distribution patterns. Some important aspects of ballistic hazard which are influenced by eruption style and magnitude include the number of ballistics ejected, the maximum distance they're ejected and what type of ballistic is ejected. Ballistics can occur as solid blocks or semi-molten bombs depending on eruption style. Ballistic blocks are made up of rocks which surround or overlay the vent before becoming fractured and ejected by explosions (Alatorre-Ibargüengoitia et al., 2016). Ballistic bombs are made up of clots of unsolidified lava, so they are only produced by eruption styles which have a magmatic component such as hawaiian, strombolian and phreatomagmatic eruptions (Fisher and Schmincke, 1984).

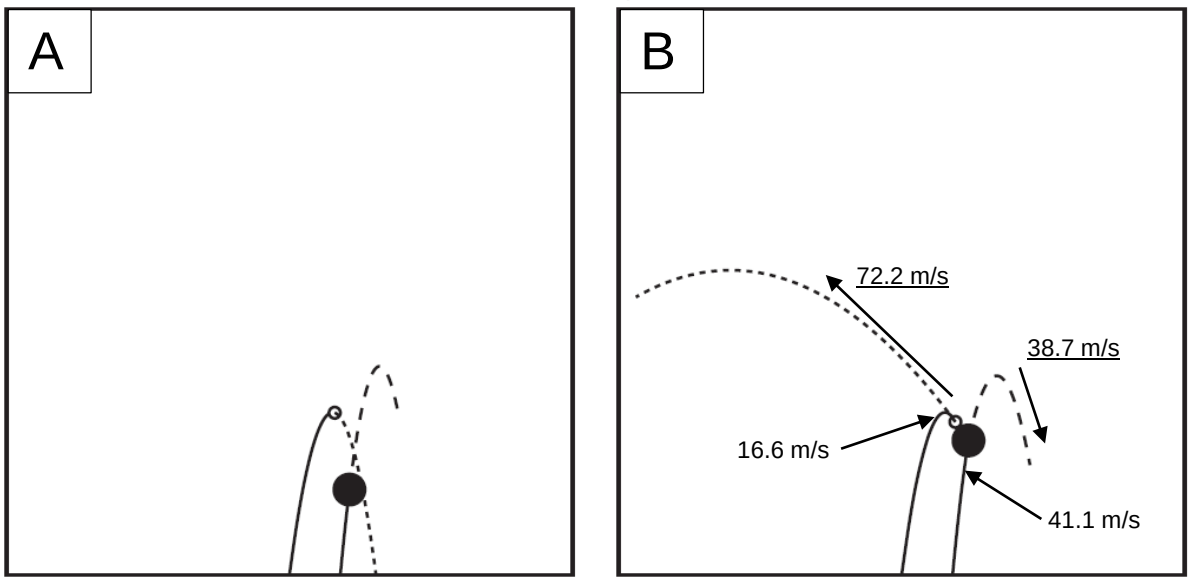

Figure 64: Illustration of modelled ballistic trajectories with and without particle collision. The small white circle represents a particle which has a mass of 3 kg. The larger black disk represents a particle that has a mass of 81 kg and was ejected 4.8 s after the white circle. (A) shows the trajectories that would be taken by particles if collision is ignored. (B) shows the particle positions at the moment of particle collision. Solid and dashed lines illustrate particle trajectories taken before and after collision respectively. The velocities of both particles, at the moments immediately before and after collision are shown. Adapted from Tsunematsu et al (2014).

The initial velocity of ballistics varies with different eruption types. The highest reported velocities for phreatic eruptions range up to 380-400 m/s for eruptions from Mount Ngauruhoe, New Zealand; Arenal Volcano, Costa Rica and Hole-in-the ground Maar, USA (Nairn and Self, 1978; Steinberg and Babenko, 1978; Fagents and Wilson, 1993). For Strombolian eruptions, the maximum initial velocities are generally lower than for phreatic eruptions. Velocities are typically below 100 m/s but speeds of 150 m/s and between 172-405 m/s have been calculated for Paricutin (Pioli et al., 2008) and Stromboli respectively (Taddeucci et al., 2012). The impact velocities of ballistics are typically much lower than their initial velocities due to drag as the particle moves through the air. However despite air drag causing ballistics to decelerate during flight, if a clast is ejected high enough to attain terminal velocity during its fall then it can still have a relatively high impact velocity (depending on its mass and density). Capaccioni and Cuccoli (2005) presented trajectory and velocity profiles for particles ejected under different conditions as part of their pyroclast cooling model (Figure 65). Figure 65 highlights how several different properties of a ballistic influence ballistic trajectory and in particular, it also illustrates the time taken for a particle of a certain size, shape and density to reach its terminal velocity.

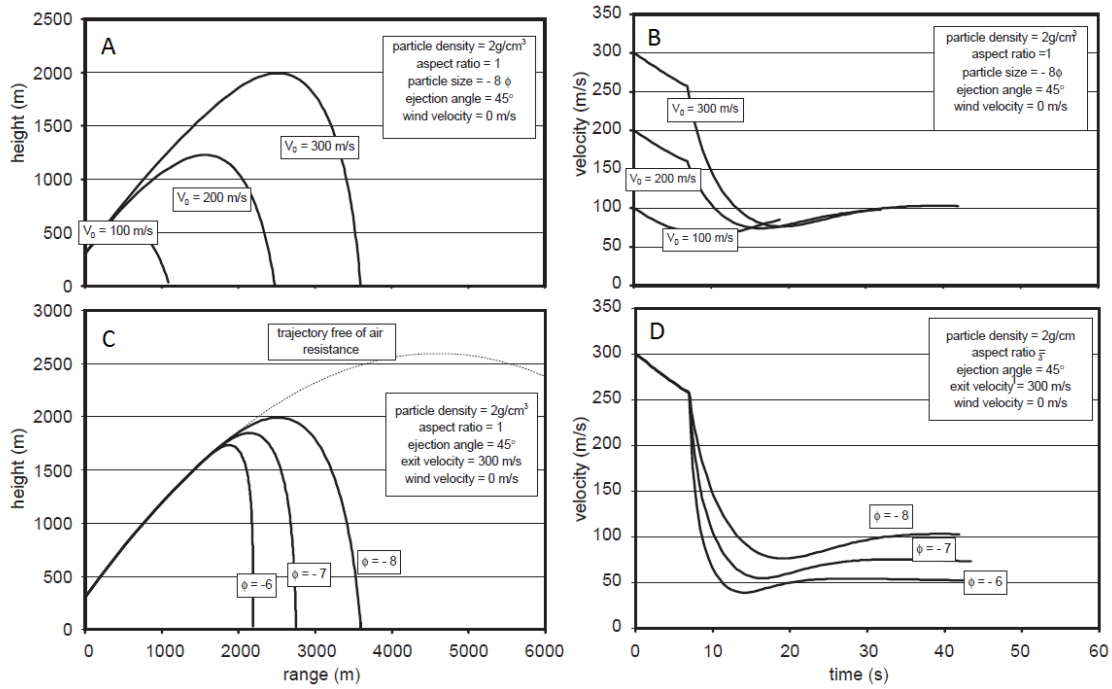

Figure 65: Trajectory and velocity profiles for different particles as a function of ejection velocity (A and B) and particle size (C and D). From A and B, note that the particle ejected at 100 m/s was not ejected high enough to attain terminal velocity during its fall. From C and D note that for highly

explosive eruptions (300 m/s initial velocity) even the smallest (64 mm diameter) ballistics can attain relatively high velocities of 50 m/s. Modified from Capaccioni and Cuccoli (2005).

The relatively high mass and final velocity of many ballistic projectiles means they have high kinetic energies when they land. Kinetic energies >80 joules impacting humans are considered lethal, from a study by Baxter and Gresham (1997) suggesting that a ballistic travelling at 6-13 m/s and weighing 10 kg carries a 90% probability of death. The authors made these suggestions after conducting autopsies on 5 of the 9 people killed in the 14 January, 1993 eruption of Galeras Volcano, Colombia. Autopsy reports found that “flying rocks” were responsible for all of the deaths. Common injuries to humans from the ballistic impacts included severe lacerations and destruction of the subject’s skull. The impact energy threshold for skull fracture causing death is ~100 J (Raymond et al., 2009), given that ballistic impacts have been observed to cause perforation of reinforced concrete slabs which have an estimated perforation threshold of 4000 – 10,000 joules (Blong, 1981; Spence et al., 2005a) ballistics constitute a significant hazard to buildings and building occupants.

Table 1: Literature review of ballistic model input parameters carried out by Rebecca Fitzgerald (90%) and the author (10%).

	Literature	
Input parameter	**Phreatic**	**Strombolian**
Initial velocity	400 m/s - Ngauruhoe (Nairn and Self 1978); 325-400 m/s - Arenal (Fudali and Melson 1972); 92-380 m/s - Hole-in-the-ground (Steinberg and Babenko 1978); 340 m/s - Shiveluch (Steinberg 1976); 130-212 m/s - Asama (Minakami 1942); 200 m/s - Arenal (Donnadieu et al. 2005); 54-168 m/s - Soufriere Hills (Formenti et al. 2003); 99-166 m/s - Big Hole Maar (Lorenz 1970); 110-230 m/s - Popocatepetl (Alatorre-Ibargüengoitia et al. 2012); 70 m/s - Montserrat (Druitt et al. 2002); 67-96 m/s - Tokachidake (Yamagishi and Feebrey 1994); 200 m/s - Upper Te Maari (Fitzgerald et al. 2014)	150 m/s - Paricutin (Pioli et al. 2008); max. 129 m/s, average 46 m/s - Stromboli (Harris et al. 2012); mean 50 m/s - Etna (McGetchin et al. 1974); 44-70 m/s - Stromboli (Hort et al. 2003); 10-40 m/s - Stromboli (Gouhier and Donnadieu 2011); max. velocity 70 m/s - Stromboli (Gurioli et al. 2013); mean 38-149 m/s, max. 172-405 m/s - Stromboli (Taddeucci et al. 2012); mean 48 m/s, 26-71 m/s range, standard deviation 9.51 - Stromboli (Vanderkluysen et al. 2012)
Particle density	1700-2000 kg/m³ - Auckland Volcanic Field (Houghton, Wilson and Smith 1999); 2000 - 2200 kg/m³ - Auckland country rock (Kereszturi et al. 2013)	1100-1500 kg/m³ - Auckland Volcanic Field (Houghton, Wilson and Smith 1999); 1260 kg/m³ - Paricutin (Pioli et al. 2008); 1350 kg/m³ - Stromboli (Aluppa et al. 2010); average 1810 kg/m³, range 1370-2300 kg/m³ - Stromboli (Gurioli et al. 2013)
Particle diameter	Mean 30 cm - Popocatepetl (Alatorre-Ibargüengoitia and Delgado Granados 2006); typically 1-2 cm but max 50 cm - Auckland Volcanic Field (Houghton, Wilson and Smith 1999); up to 1.5 m - Guagua Pichincha (Wright et al. 2006); average 20-60 cm - Popocatepetl (Alatorre-Ibargüengoitia et al. 2012); < 0.4 m to > 1 m - Montserrat (de'Michieli Viturri et al. 2010); 10 cm-3.5 m - Galeras (Artunduaga and Jimenez 1997); up to 1.2 m diameter - Soufriere Hills (Robertson et al. 1998); 20 cm - 20 m - Tokachidake (Yamagishi and Feebrey 1994); 50 cm-3 m - Ukinrek Maars (Self et al. 1980); Mean 36 cm, standard deviation 23 cm - Upper Te Maari (Fitzgerald et al. 2014)	-6 phi (up to 20 cm bombs) - Auckland Volcanic Field (Houghton, Wilson and Smith 1999); 50% of ejecta in 1969 between 10-40 cm in diameter - Mt. Etna (McGetchin et al. 1974); 7-459 cm, mean 48 cm - Stromboli (Gurioli et al. 2013); cm to metre - Stromboli (Taddeucci et al. 2012); 0.1-2 m - Eldjfell (Booth 1979)
Inclination angle		20° - Mt. Etna (Gouhier and Donnadieu 2010); 90% of particles ejected within 37° dispersion cone at Stromboli 1971 (Chouet et al. 1974)
Rotation angle	As low as 30° - Montserrat (de'Michieli Vitturi et al. 2010); 37-78° - Asama (Minakami 1942)	Majority vertical (around 72°) - Mt. Etna (Gouhier and Donnadieu 2011); 45° - Stromboli (Gurioli et al. 2013); within 5° from vertical - Stromboli (Chouet et al. 1974); 70-85° - Stromboli (Pistolesi et al. 2008); average 82°, 27-90° range, standard deviation 11.2° - Stromboli (Vanderkluysen et al. 2012)
Displacement of ejection points from vent centre		2.5 m - Stromboli (Taddeucci et al. 2012); 3 m - Stromboli (Chouet et al. 1974)
Number of particles	13200 - Upper Te Maari (Fitzgerald et al. 2014)	780 - Stromboli (Gurioli et al. 2013); 2594 - Stromboli (Chouet et al. 1974); 1249-4001 - Stromboli (Taddeucci et al. 2012)
Direction		South - Stromboli (Gurioli et al. 2013)
Flow velocity	197-230 m/s with 99-166 m/s ballistics - Big Hole Maar (Lorenz 1970); 125-128 m/s with 69-91 m/s ballistics - Ara Shatan (Wood and Dakin 1975;) max. 150 m/s - Stromboli (Gurioli et al. 2013); 175-200 m/s - Ukinrek Maars (Self et al. 1980); 150-350 m/s - Waiotapu (Hedenquist and Henley 1985); 150 m/s - Upper Te Maari (Fitzgerald et al. 2014)	100 m/s for paroxysmal gas jet flow from Stromboli (Aiuppa et al. 2010); 30 m/s with maximum 100 m/s - Stromboli (Patrick et al. 2007); mean 100 m/s - Mt. Etna (Steinberg and Babenko 1978); 70-110 m/s at Stromboli (Gouhier and Donnadieu 2011)
Flow velocity radius	300 m - Shinmoedake (Maeno et al. 2013)	50 m - Stromboli (Harris et al. 2012)

Appendix B – Electronic Appendix

Refer to the accompanying media for the following:

1. Cannon experiment photos
2. Cannon experiment spreadsheets
3. Cannon experiment graphs of raw data
4. Fragility function suites
5. StreetView window coverage analysis
6. Tephra impact assessment spreadsheets
7. Tephra impact assessment modelling limitations